SPECTRAL STRUCTURE AND GENERATION MECHANISM OF DUCTED VLF WHISTLER MODE SIDEBAND WAVES

A DISSERTATION

SUBMITTED TO THE DEPARTMENT OF ELECTRICAL ENGINEERING

AND THE COMMITTEE ON GRADUATE STUDIES

OF STANFORD UNIVERSITY

IN PARTIAL FULFILLMENT OF THE REQUIREMENTS

FOR THE DEGREE OF

DOCTOR OF PHILOSOPHY

By

Luiz Augusto Discher de Sá

December 1989

ABSTRACT

An accurate determination is made of the sideband structure of ducted VLF whistler mode waves transmitted from Siple Station and observed at Lake Mistissini, Quebec. Single- and double-frequency transmissions are analyzed. "Single-frequency" sidebands are shown to be due to interactions between the input wave and harmonics of 60 Hz present within the duct (assumed to be radiation from the Canadian power line system).

Sideband spectra are explained as due to wave-wave interactions occurring in the magnetosphere through electron cyclotron resonances, the line intensities required for such interactions being low. Resonances can be located outside (external resonances) or inside the wave potential wells (trapped resonances). External resonances produce radiation through bunching in essentially the same way as the incoming carriers do. Trapped resonances produce oscillatory disturbances in the potential well charge distributions that frequency modulate the carriers to produce the sidebands.

Application of the KAM theorem to the electron equations of motion shows the possible sideband radiation frequencies. Both external and trapped resonances generate the same radiation spectrum with frequencies given by a very simple formula. The carrier trapping frequencies do not affect the sideband wave frequencies, and do not impose sharp constraints on either the spectrum bandwidth, the sideband line separation, or the maximum interacting carrier frequency separation.

We find that the inhomogeneity of the magnetic field of the earth introduces phase shifts on the equilibrium positions of the resonances we discuss. Those phase shifts, whether time dependent or not, will be translated at the receiving station as frequency shifts in the observed sidebands. Since the phase shifts are dependent on $v_\perp$, the sideband waves should undergo an increase in width as they shift away from their nominal positions.

A strong enough inhomogeneity will destroy a resonance completely. We find that trapped resonances are much more resilient to the effects of the inhomogeneity than external resonances, this being the reason why extremely weak carriers can produce sizable and readily observable sidebands when they interact with stronger carriers.

ACKNOWLEDGMENTS

This research was supervised by Profs. R.A. Helliwell and U.S.Inan. I wish to thank them for their guidance and support. Special thanks are due to my principal advisor, Prof. Helliwell, for his encouragement, criticisms, and continuous suggestions of new research topics that did much to shape the content of the present work.

I thank Dr. T.F. Bell and Prof. D.L. Carpenter for valuable suggestions and for reading parts of the manuscript. Assistance from Mr. Jerry Yarbrough in selecting some of the data used in this research is gratefully acknowledged.

I want to thank my StarLab colleagues for their hospitality and friendship during my stay at Stanford, and my third reader, Prof. M.J. Flynn, for reviewing this manuscript.

This research was sponsored by the Division of Polar Programs of the National Science Foundation under grant DPP-86-13783.

CONTENTS

CONTENTS (Cont.)

ILLUSTRATIONS

1. Introduction

1.1. What This Dissertation Is All About

The purpose of this thesis is to explain the existence and properties of discrete frequency radiation produced by the magnetospheric plasma when excited by a set of monochromatic waves propagating in a duct. It can be extended to include non-ducted radiation received by satellites, and so called "natural" line formation effects, observed in ducts but apparently not related to the injection of discrete waves in the plasma.

The author had his attention first called to the subject when observing sideband radiation [*Park*, 1981] produced by single frequency transmissions made from Siple Station, Antarctica, and received at Lake Mistissini, Quebec, after ducted wave propagation (see Figure 1.1). He was impressed by the fact that the observed sideband wave separations were frequently an integer multiple of ten Hertz. Since the plasma in the ducts has its natural frequencies in the kilohertz range and above, those frequencies could not easily be related to plasma parameters, and since their numerical values seemed artificial, they should be due to plasma contamination. A candidate for that contamination already existed: harmonics of 60 Hz radiated into the duct from the Canadian power distribution system or, maybe, from the Siple transmitter generators. Such power line radiation (PLR) was, however, not considered important at the time, since its levels were so low that the harmonics could barely be seen when compared to the amplitudes of other waves propagating in the plasma. Additionally, it was not easy to justify sideband spacings of 10 Hz or 20 Hz when the frequency difference between harmonics was known to be 60 Hz.

Some theories existed at the time to explain sideband formation:

"Trapping" theories explained single carrier[1] sidebands by stating that a strong enough carrier would create a potential well in which the plasma electrons would oscillate [*Nunn*, 1974; *Nunn*, 1973; *Brinca*, 1972; *Helliwell and Crystal*, 1973; *Das*, 1968; etc.]. Radiation from the oscillating electrons would then produce the sidebands. There were doubts, however, that real carriers would have amplitudes large enough to "trap" the electrons in the required way.

Two-carrier sidebands were explained as coming from distortions of the injected waveforms due to wave growth in the plasma. Such an explanation, however, was phenomenological, no fundamental reason for the effect being given [*Helliwell et al.*, 1986].

The absence of a well defined and successful formalism to describe sideband effects, a lack of knowledge of basic physical parameters such as the interacting carrier amplitudes, and the absence of a detailed knowledge of the sideband spectral structure, prompted the author to do this work. It begins with an accurate determination of the sideband spectra for one and two transmitted carriers, and continues by making a rigorous study of the equations describing the motion of an electron under the influence of several waves. The equations are formally solved, and the calculations taken as far as possible without making specific assumptions about the physical systems under study. As a result, sidebands come out as a necessary consequence of the equations of motion, single frequency

[1] In this manuscript, "carrier" means a single frequency wave transmitted from Siple Station.

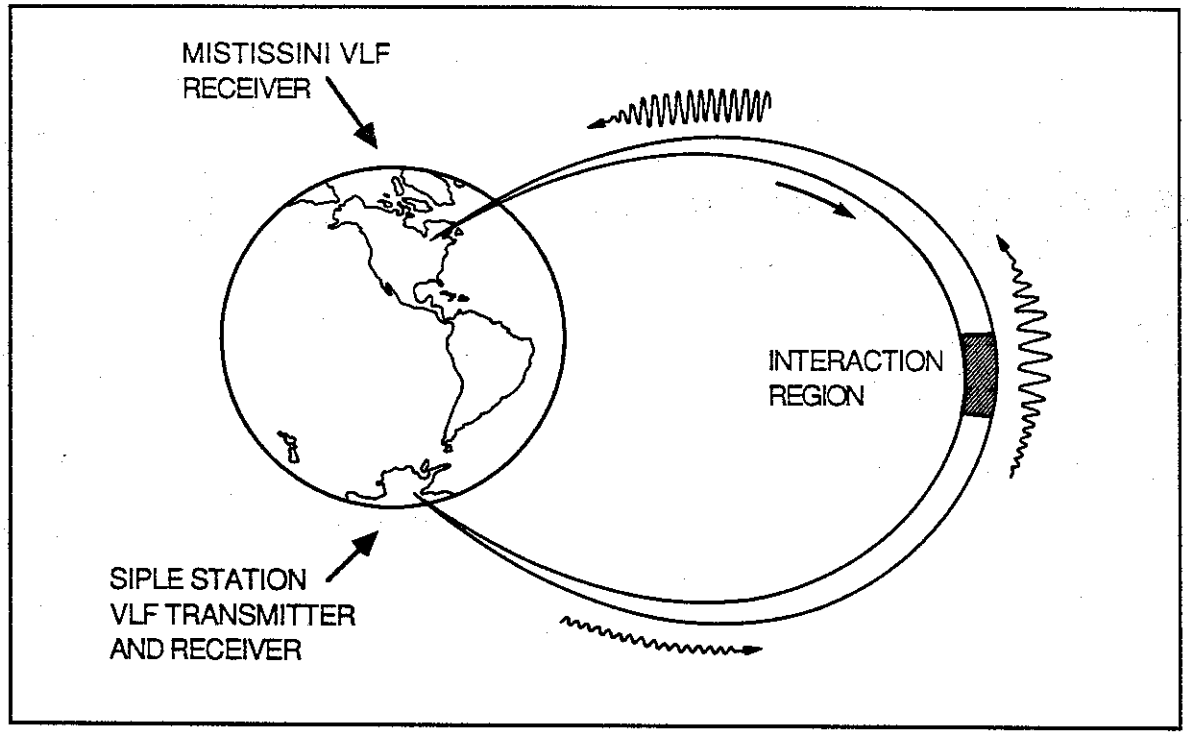

Fig. 1.1. VLF transmissions are made from Siple Station, Antarctica, and received at Lake Mistissini, Quebec. The waves propagate within ducts because of their higher index of refraction. In a region around the Equator, where the geomagnetic field goes through a minimum, the waves interact with counterstreaming electrons producing additional radiation in the form of wave growth, sidebands, triggered emissions, etc.

sidebands are seen not to exist, and PLR effects are found to be almost omnipresent. Although the effects of PLR are found in almost all spectra studied, they are indirect: sideband wave spacings are almost never equal to 60 Hz and the amplitudes of PLR harmonics are never large enough to permit a direct determination of their presence.

The theoretical part of this work is not an effort to produce quantitative results to be compared with experiment, but is aimed at those who want to understand the sideband formation process. The mathematics used is not a computational tool, but a language used to describe and explain the several physical phenomena relevant to sideband formation and, as such, cannot be stripped away from the main body of the work. The work, as a whole, forms an infrastructure, firmly founded on the equations of motion, from which extensions should be made to obtain specific quantitative results for each case under study. Such extensions, of course, are not part of the present work.

1.2. Outline of the Dissertation

In chapter 2, an accurate determination is made of the sideband structure of ducted VLF whistler mode waves transmitted from Siple Station and observed at Lake Mistissini, Quebec. Single- and double-frequency experiments are studied. It is shown that sideband spectra can be explained by interactions between two or more waves in the magnetosphere, the wave intensities required for such interactions being low. When one of the waves is a transmitted carrier, the other wave can be as much as 40 dB lower in amplitude, implying that power line radiation (PLR) can be an important

factor in sideband generation. It is shown that "single-wave" sidebands are consistently explained by interactions between the input wave and harmonics of 60 Hz present within the duct (assumed to be PLR), and that two-wave spectra are affected by their position relative to the same 60-Hz system of waves. A study of two-wave spectra as a function of wave frequency separation and wave amplitude ratio is made.

Chapter 3 of the dissertation introduces the reader to the physical and mathematical aspects of the problem of sideband formation associated with VLF whistler mode waves propagating in ducts in the magnetosphere. It starts with an introduction to the general problem of charge distribution in the duct and looks at the effect of monochromatic electromagnetic waves acting on such distributions. It describes sidebands as due to wave-wave interactions occurring in the magnetosphere through electron cyclotron resonances, and concentrates on sideband radiation coming from resonances formed outside the wave potential wells (external resonances). It also presents a general solution to the electron equation of motion, based on the KAM theorem [*Rasband*, 1983], that lists the possible sideband radiation frequencies. Both an analytical treatment, based on Lie Transform perturbation theory, and a numerical treatment, based on phase plots, are used in the detailed part of the analysis. Effects of the inhomogeneity of the magnetic field of the Earth are mainly neglected in this chapter.

Chapter 4 of the dissertation presents an analytical and numerical treatment of cyclotron resonances formed inside the potential wells of a set of monochromatic carriers propagating in a duct in the magnetosphere. It is found that those resonances produce oscillatory disturbances in the potential well charge distribution that frequncy modulate the carriers to produce sidebands. The frequency spectrum is the same as the one generated by the external resonances defined in chapter 3. It is shown that the carrier trapping frequencies do not affect the sideband wave frequencies and do not impose sharp constraints on the spectrum bandwidth, on the sideband wave separation, or on the maximum interacting carrier frequency separation. When not highly distorted by wave growth, a two-carrier sideband spectrum should have an approximately exponential profile.

Chapter 5 addresses the effects of the inhomogeneity of the magnetic field of the earth on the resonances studied previously. We find that the inhomogeneity introduces phase shifts on the equilibrium positions of both types of resonance we have treated. Those phase shifts are time dependent if either the main carrier in the case of internal resonances, or the interacting carriers in the case of external resonances have time dependent amplitudes. The time dependent phase shifts will translate into sideband wave frequency shifts. If the carriers have constant amplitudes, the phase shifts are locally constant. However, frequency shifts observable at the end of the interaction region can still be produced if the amplitude of the radiated sidebands are locally time dependent. Since the phase shifts are dependent on $v_\perp$, the sideband waves should undergo an increase in linewidth as they shift away from their nominal positions. A strong enough inhomogeneity will destroy a resonance completely. It is found that trapped resonances are much more resilient to the effects of the inhomogeneity than external resonances, this being one of the main reasons why we can experimentally observe the creation of sizable sidebands by extremely weak carriers.

Chapter 6, the last chapter, contains the conclusions and suggestions for future work.

1.3. Previous work on Sideband Formation

Before the present work, "single-frequency" sidebands were thought to come solely from the interaction between a single carrier and the magnetospheric plasma. From that point of view, several theoretical papers were published [*Nunn*, 1974; *Nunn*, 1973; *Brinca*, 1972; *Helliwell and Crystal*, 1973; *Das*, 1968; etc.]. Since the present analysis indicates that such sidebands come in reality from interactions with PLR, the conclusions of those papers appear doubtful. It is important, however, to remark that in our opinion none of them succeeded in presenting a complete and conclusive mechanism for sideband creation, indicating that maybe not even in principle single frequency sidebands can exist in the magnetosphere. *Park* [1981] described and analyzed such papers, and already pointed out that they could not describe the data available at the time. The following paragraphs repeat and complement some of his observations.

All of the above authors, with the exception of *Helliwell and Crystal*, tried to explain "single-frequency" sidebands as radiation from electrons oscillating inside the single carrier potential well. This approach has several flaws:

a. The electron oscillation frequency depends on its pitch angle, and since pitch angles have a continuous distribution, the radiated sidebands should not have sharply defined frequencies, as seen in the data.

b. The electron oscillation frequencies are dependent on the carrier amplitudes. A variable amplitude carrier should produce shifting sidebands with shifts proportional to the square root of the carrier amplitude. This is not observed in the data.

c. The carrier amplitude must have a minimum value to overcome the effect of the magnetic field of the earth and "trap" the electrons. There is no conclusive evidence that the wave amplitudes in the Siple experiments are always strong enough to do that.

Helliwell and Crystal are an exception to the above group of authors: their sideband frequencies are a function of the propagation time of waves going from one end to the other of the interaction region, added to the transit time of electrons moving in the opposite direction. This approach is also flawed: to obtain well defined delays, the ends of the interaction region are made artificially sharp, and all electrons in the duct are given the same $v_{\parallel}$ and the same pitch angle. As an additional radical feature, particles are created and injected at the beginning of the interaction region and suddenly destroyed at the end, in contradiction to the continuity equation. A more realistic model [*Carlson*, 1987] that injects electrons at the beginning of the duct, takes into consideration the "fuzzy" ends of the interaction region and a consequent spread in electron and wave time delays, does not exhibit sidebands: the amplified wave shows only some ripples, due to an artificial sharpness still present in the electron distribution (*Carlson*, personal communication).

Helliwell et al. [1986] explained two-wave sidebands as distortions of the two-wave beat envelope due to the interaction of the electromagnetic field with the plasma. To justify harmonic sideband generation, a phenomenological argument was given to explain why the distorted envelope still had the same period as the original beat envelope. Such a fact is in reality only an approximation: in this thesis it is shown that as the sidebands become stronger, the period of the envelope decreases, approaching zero and defining an asymptotically chaotic electromagnetic field.

Chang et al. [1980] did not explain sidebands, but tried to give a mechanism for the wave-wave interactions observed in their data. The paper suffers from a typical flaw: although wave-wave interactions are highly non-linear, the explanation they provided assumes linearity. According to the authors, each wave, independently, is capable of accelerating electrons moving within a certain frequency range called the coherence bandwidth. Two waves will interact only when their coherence bandwidths overlap. The reader, after going over the present work, will realize that such a condition is not necessary: two-wave interactions are much more complex and general, occurring through cyclotron resonances, and are possible even when the waves are much farther apart than estimated by the above authors.

Nunn [1986] studied sideband growth. In this paper he still explained "single-frequency" sidebands as coming from a single carrier and tried to find support for his hypothesis in the data shown by *Park* [1981]. In the main body of his work, however, sidebands were simply assumed to exist without worrying about their possible cause.

1.4. Contributions of the Present Work

In general, this work shows the importance and necessity of a formal mathematical treatment, coupled with data analysis to illustrate theoretical points, when the data originally available to describe a physical system are incomplete, important physical parameters are unknown, and contradictory explanations have been put forward.

Some of the main results are:

1. Magnetospheric sidebands are due to the interaction of two or more waves propagating in the plasma. Radiation comes from resonant electron motion produced by such an interaction. "Single-frequency" sidebands come from the interaction of a single carrier with PLR harmonics present in the duct.
2. Sideband wave frequencies are given by a simple formula. Although the formula is simple, it is recurrent, allowing for the generation of extremely complex spectral structures.
3. Sideband waves do not have constant frequencies, but shift and increase their linewidths when the interacting waves have time dependent amplitudes. Such shifts are a perturbative correction to the sideband frequencies, proportional to the degree of inhomogeneity of the magnetic field of the earth, and should not be confused with the larger shifts mentioned in 1.3.b.
4. Carrier amplitudes involved in sideband formation are not critical. In particular, it is not necessary that any of the carriers be strong enough to "trap" the electrons in the plasma. If, in a set of interacting carriers, some have large enough amplitudes (say, 30dB above noise level), the others can be vanishingly small (at least 40dB lower in amplitude) and still participate in the generation of sizable sidebands (comparable in size to the large carriers).
5. Sophisticated mathematical techniques are indispensable: without the help of Lie Transform Perturbation Theory, most of the analytical calculations would not have gone beyond their initial steps. The study of radiation frequency shifts, where the inhomogeneity of the magnetic field of the earth plays a very important role, or the calculation of high order sidebands, could not have been carried out.

2. Experimental Determination of the Sideband Spectra

2.1. Introduction

Whistler mode sidebands generated by the Siple Station transmitter have been the subject of several papers, some of them mainly descriptive, such as *Park* [1981], others, such as *Helliwell et al.* [1986], also presenting a mechanism for the observed sidebands. A shortcoming noted in those papers was the lack of a unifying idea that could shed some light on the cause and structure of all observed spectra, indicating relevant variables and suggesting experiments in which the mechanism of spectra formation could be investigated. As a result of such a lack, only for the case of double carrier transmissions [*Helliwell et al.*, 1986], where the sideband spectra consist mainly of harmonics of the carrier frequency separation, was it possible to arrive at a successful description of the line structure together with a possible mechanism for its creation.

In this chapter,[1] such a unifying idea is put forward, together with a set of experimental data showing its plausibility. In the following chapters the same idea will be justified from a mathematical viewpoint, and many of its consequences will be further explored.

2.2. Sideband Generation Mechanism

The basic assumption used to analyze the data in this chapter is a property common to many nonlinear dynamical systems, being mentioned and discussed, for instance, by *Chirikov* [1979]. In the present chapter, we quote this property without proof and justify it simply by the accurate way in which it describes the data. (Such a property is nothing but the KAM theorem. A detailed explanation of it, and of other statements made in this section, is found in the subsequent chapters.) It may be stated as follows:

If several lines with frequencies $\Omega_i, i = 1 \ldots n$, measured from one of the carriers, are present in the magnetosphere, they are able to interact with one another, and a new line can be created at a frequency Ω, given by

$$m\Omega = m_1\Omega_1 + \cdots + m_n\Omega_n \tag{2.1}$$

where m and m_i are arbitrary integers ($m \neq 0$). The likelihood of a line being created depends partly on the underlying electron distribution and incoming line intensities, but is higher the smaller the integers in question are and the smaller the number of lines involved in the interaction is.

As an example we can look at the two-line case: If only two lines are initially present, one of the frequencies will be zero, and the other will be the frequency separation between the lines, $\Delta\Omega$. Then

$$q\Omega = p\Delta\Omega \tag{2.2}$$

This means that a line can be created at any rational point between the original two lines, small values for p and q being more likely to occur. Equation (2.2) predicts the occurrence of harmonics ($q = 1$, any p), half harmonics ($q = 2, p = 1$), one-third harmonics ($q = 3, p = 1, 2$), etc.

[1] The present chapter is a close reproduction of *Sá and Helliwell* [1988].

For three lines, with subscripts 1, 2, 3, an interesting result is obtained for a particular choice of the smallest nonzero values of the integer coefficients:

$$\Omega = \Omega_2 - \Omega_3 \tag{2.3}$$

For $\Omega_2 \geq \Omega_3$ this implies the creation of a mirror image of line 3, within the interval defined by lines 1 and 2, as shown in Figure 2.1.

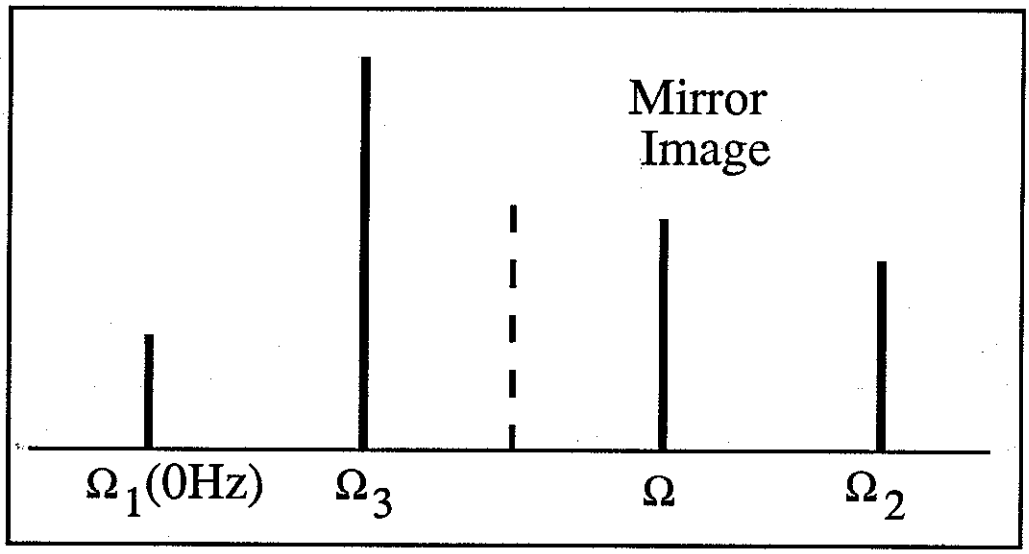

Fig. 2.1. Mirror image sideband creation. Dashed line marks symmetry axis.

Other sign combinations in (2.3) are possible, but lead to rarely found lines. For instance, a plus instead of a minus sign in (2.3) will describe an intermodulation effect:

$$\Omega = \Omega_2 + \Omega_3 \tag{2.4}$$

Although infrequently seen, an example of this effect is found in Figure 2.4*h*, and is described in section 2.4.

2.3. Description of Experimental Methods

Most of the data discussed in this chapter came from the CISP (carrier interaction with simulated power line) program,[2] transmitted from Siple Station and received at Lake Mistissini, Quebec, after ducted whistler mode propagation. Its format consists of a sequence of 3-s pulses, 10 s apart, each one

[2] The author gratefully acknowledges the help of Prof. R.A. Helliwell in designing and implementing the CISP program.

made up of a pair of single-frequency carriers with defined amplitude ratio and frequency separation, as shown in Figure 2.2. The position of the upper carrier is fixed at a power line harmonic frequency, its amplitude being a variable parameter. The amplitude of the lower carrier is kept constant, but its position below the upper carrier can be varied. The transmitted upper to lower carrier amplitude ratio can be set to -20 dB, -30 dB, -40 dB, or minus infinity. The carrier frequency separation can be 20 Hz, 23 Hz, 30 Hz, 37 Hz, 40 Hz, and 60 Hz.

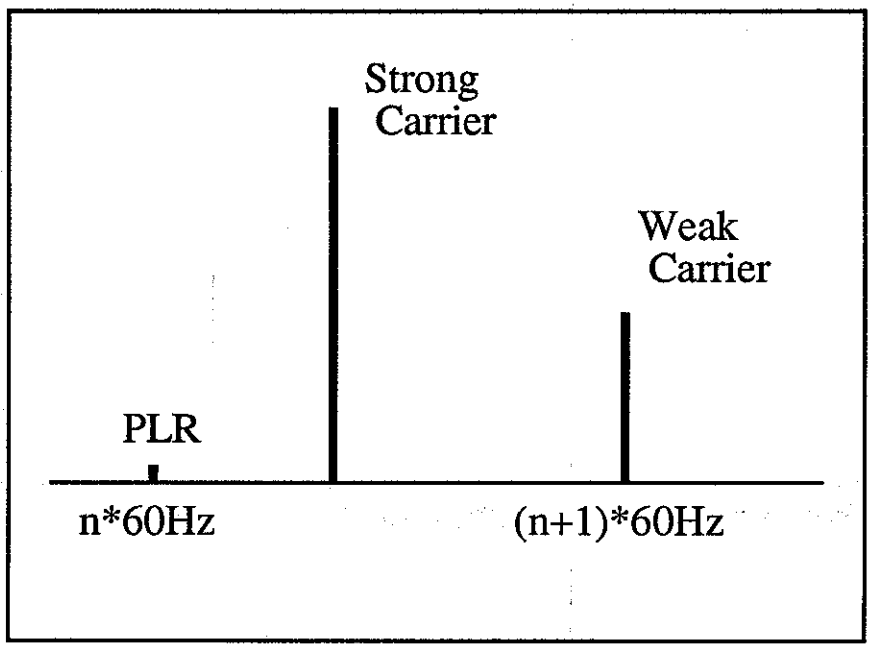

Fig. 2.2. CISP format used in sideband structure analysis described in this chapter.

Those frequency and amplitude ratio values are chosen with power line radiation (PLR) effects in mind. The reason for choosing such amplitude ratios is that PLR levels in the magnetosphere are believed to be 30 dB or more below the carrier amplitude levels. Since signals with such low amplitudes are not directly detectable, a possible PLR presence, together with its effects, must be verified by studying the effects produced on the spectra by weak lines radiated by the transmitter together with the main carrier.

The frequency separations consist of two groups: The first group, 20 Hz, 30 Hz, 40 Hz, 60 Hz, consisting of submultiples of 60 Hz, is chosen such that the carrier frequency separation is a rational function of the PLR line separation. This allows for the establishment of a resonance condition between the transmitted radiation and the one present in the duct. Under those circumstances, both systems can excite essentially the same lines, creating an easily understood spectrum. The second group, 23 Hz, 37 Hz, is chosen such that the carrier frequency separation is either the most irrational function of 60 Hz possible, the golden mean of 60 Hz [see *Berry*, 1978], or its complement with respect to 60 Hz. This choice does not allow easy excitation of the rational modes described

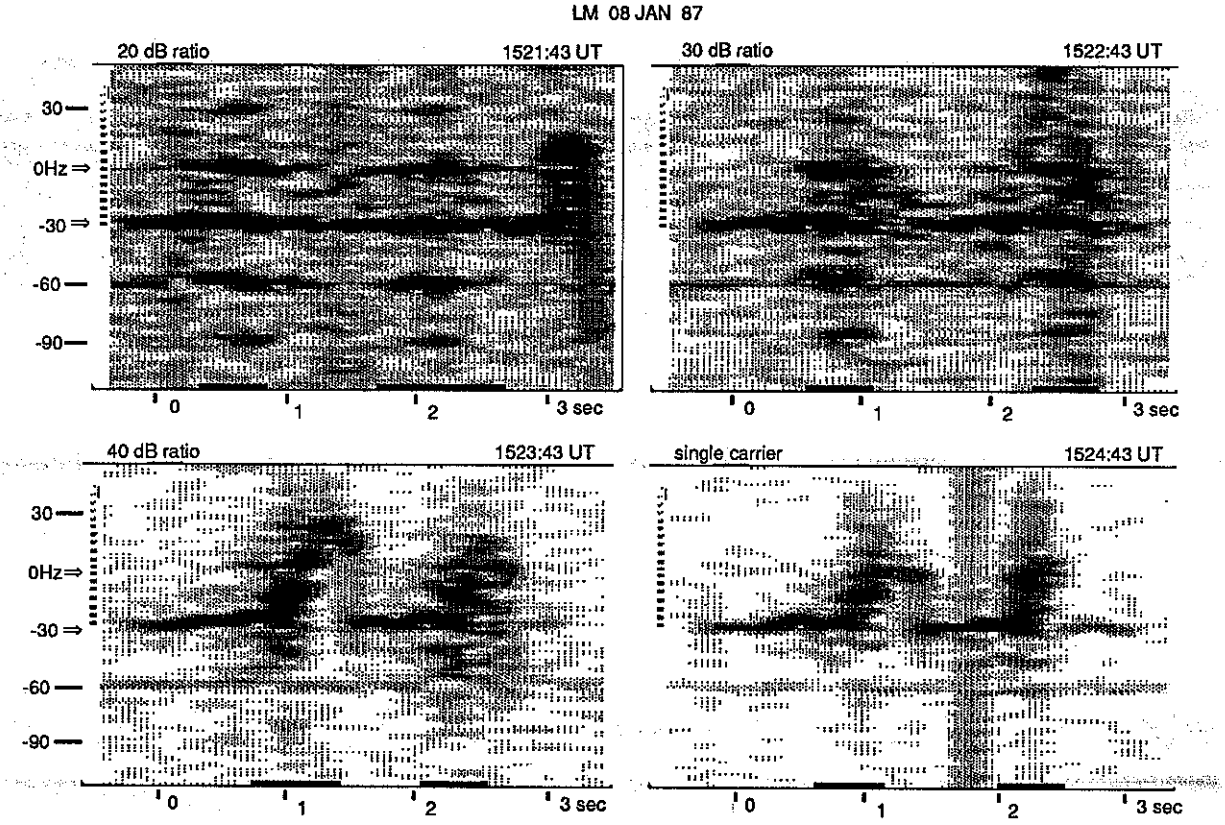

Fig. 2.3. Sequence of 3-s pulses with carrier separation equal to 30 Hz. 0 Hz in those pictures corresponds to 2220 Hz. The arrows point to the location of the two carriers. The horizontal bars at the bottom of each picture indicate the time intervals over which the average spectra shown in Figure 2.4 were taken. In all spectra the filter bandwidth was 1.56 Hz.

above, resulting in the appearance of more complex line interactions such as the one responsible for the creation of mirror image sidebands.

2.4. Description of Data

Figure 2.3 shows a sequence of transmissions made with a constant line separation of 30 Hz, a very rational function of 60 Hz, and amplitude ratio varying from -20 dB to minus infinity. It can be seen that, as the upper carrier becomes weaker, the two carrier spectra blend in smoothly with the single carrier spectrum shown at the bottom right. For this particular set of transmissions it can also be seen that the line intensities in each pulse exhibit two maxima. Although the reason for the existence of such maxima will not be discussed in this manuscript, their presence provides a way of testing the reproducibility of the sideband structures, as described below.

Figure 2.4 displays the same sequence of pulses in a way that allows for easy and accurate measurements of frequency separations and relative line amplitudes. Each picture shows a 0.5s (or more) average of the spectrum. In each row, the first plot (A scan) comes from an average over the

first, and the second plot over the second maximum in the pulse. The averages are taken over the time intervals marked by solid horizontal bars at the bottom of each picture shown in Figure 2.3. Comparison of two A scans in the same row shows how reproducible the spectra are. The vertical lines in each plot locate multiples of 60 Hz where low-intensity PLR may be present. Figures 2.4*a* and 2.4*b* show the 20 dB ratio spectrum. The structure is almost what should ideally be expected. The two carriers create harmonics, which in turn create several half harmonics between them. Frequency distortion is minimal, all lines being at their theoretical positions within one filter bandwidth (1.56 Hz). Figures 2.4*c* and 2.4*d* show the 30 dB spectrum. Because of enhanced growth at the upper carrier, frequency distortion increases both for harmonics and sub harmonics. The bandwidth of each spectrum is also slightly decreased. Figures 2.4*e* and 2.4*f* show the 40 dB spectrum. The upper carrier would not be seen in this plot without the help of large temporal and differential growth with respect to the lower carrier (32 dB average). The lower carrier also goes through a pronounced growth process, adding to frequency distortion effects. Since growth is a function of the instantaneous electron distribution, reproducibility of the spectrum decreases (Figures 2.4*e* and 2.4*f* are fairly different). Increased initial amplitude asymmetry between the carriers encourages the appearance of sub harmonics different from the simple half harmonic. The harmonics initially seen in the 20 dB and 30 dB transmissions have now all but disappeared, more closely spaced harmonics being seen instead.

A detailed analysis of Figure 2.4*e* reveals the following line configuration: Line 2 is a harmonic of 5 and 7. Line 4 is a harmonic of 5 and 6. Line 3 is a half harmonic of 2 and 4. Line 9 is a one-third harmonic of 7, the upper carrier, and 10, a PL harmonic. Line 8 is a half harmonic of 7 and 9. Line 6 is simultaneously a one-fourth harmonic of 1 and 7, and a one-third harmonic of 5 and 7.

Lines such as line 9 are strongly excited because the sequence of sidebands behaves in this case as an incipient triggered emission. Energy is transferred upward from the carrier, is reflected at line 9, lingers around line 8, and is partly returned to the lower carrier, as shown in Figure 2.3.

Figure 2.4*f* has approximately the same structure as Figure 2.4*e* with some lines missing. Line 6 in Figure 2.4*f* is a half harmonic of 4 and 7.

Figures 2.4*g* and 2.4*h* show the single carrier spectrum. All sidebands now are coming from interactions between the carrier and the residual PLR present in the duct. Since PLR forms a system of harmonic lines, we should expect the presence of multiple lines to influence the spectra.

In Figure 2.4*g*, line 4 is a half harmonic of 3 and the adjacent PL harmonic (not numbered in the picture). Line 7 is a one-third harmonic of the same PL with line 8 which also is a PL harmonic. Line 5 is simultaneously a half harmonic of 3 and 7, and a one-fourth harmonic of 3 and 8. Line 6 is a half harmonic of 5 and 7. Line 2 is simultaneously a harmonic of 4 and 6, and a one-third harmonic of the two PL harmonics immediately above and below it.

In Figure 2.4*h*, lines 4 and 5 are one-third harmonics of 3 and 7. Lines 2 and 8 are harmonics of 3 and 5. Line 6 is simultaneously a half harmonic of 5 and 7, and a one-fourth harmonic of 3 and the next PL harmonic above 7. Line 1 is a case of intermodulation: line 6 interacting with two PLs (theory requires them to be line 7 and the PL immediately above it), creates a line below itself at a distance of 60 Hz, the PLs' frequency separation.

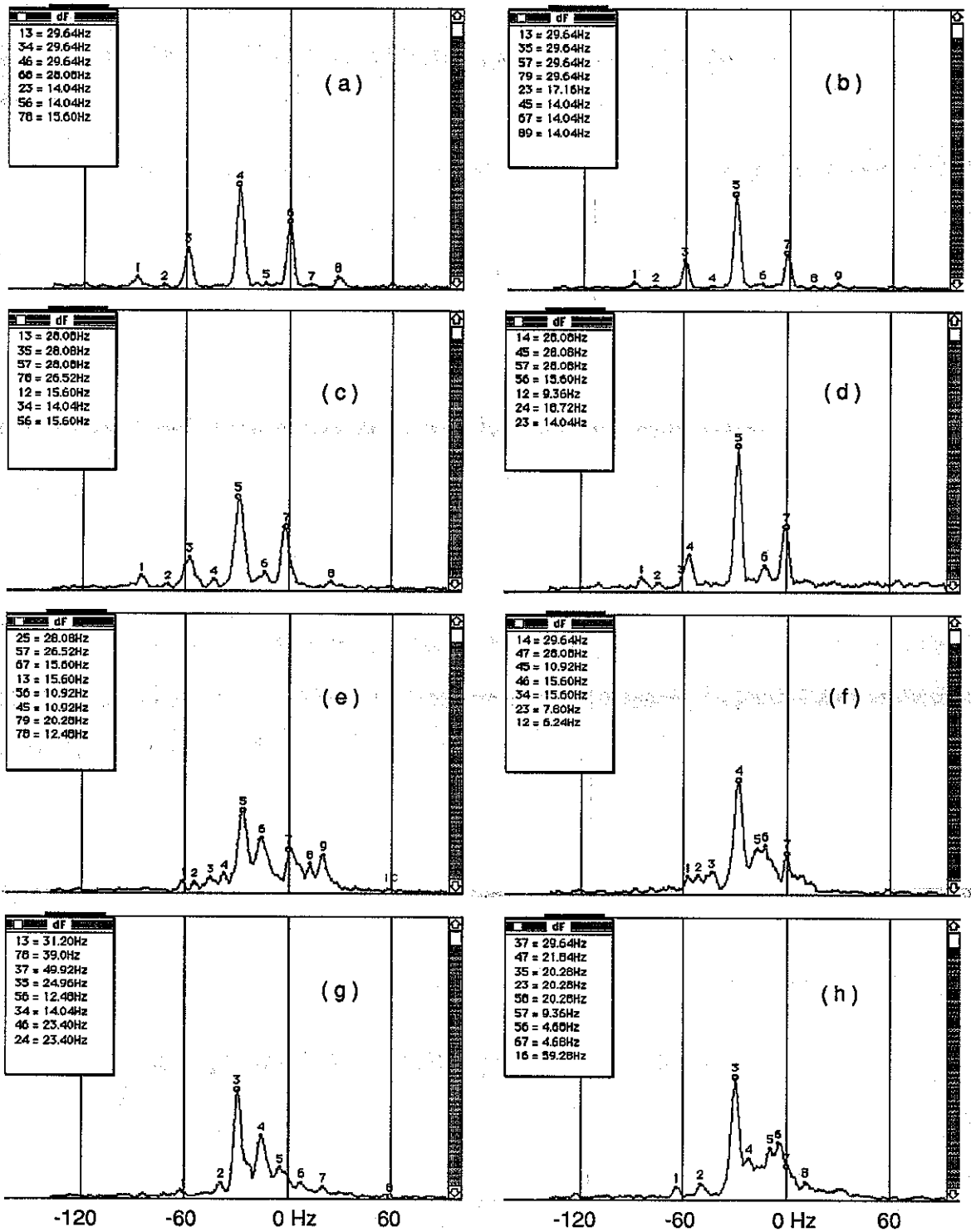

Fig. 2.4. Average spectra obtained from pulses shown in Figure 2.3: (*a*) and (*b*) 20 dB ratio, (*c*) and (*d*) 30 dB ratio, (*e*) and (*f*) 40 dB ratio, and (*g*) and (*h*) single carrier pulse. The first picture represents the first average; the second picture, the second average over each pulse. The vertical scale is linear and arbitrary. 0 Hz in those pictures corresponds to 2220 Hz absolute frequency. The carriers are denoted by small circles at the maxima. The windows in each picture contain a table of frequency differences: at the left of each equal sign are two digits representing two spectral lines; at the right is their frequency difference.

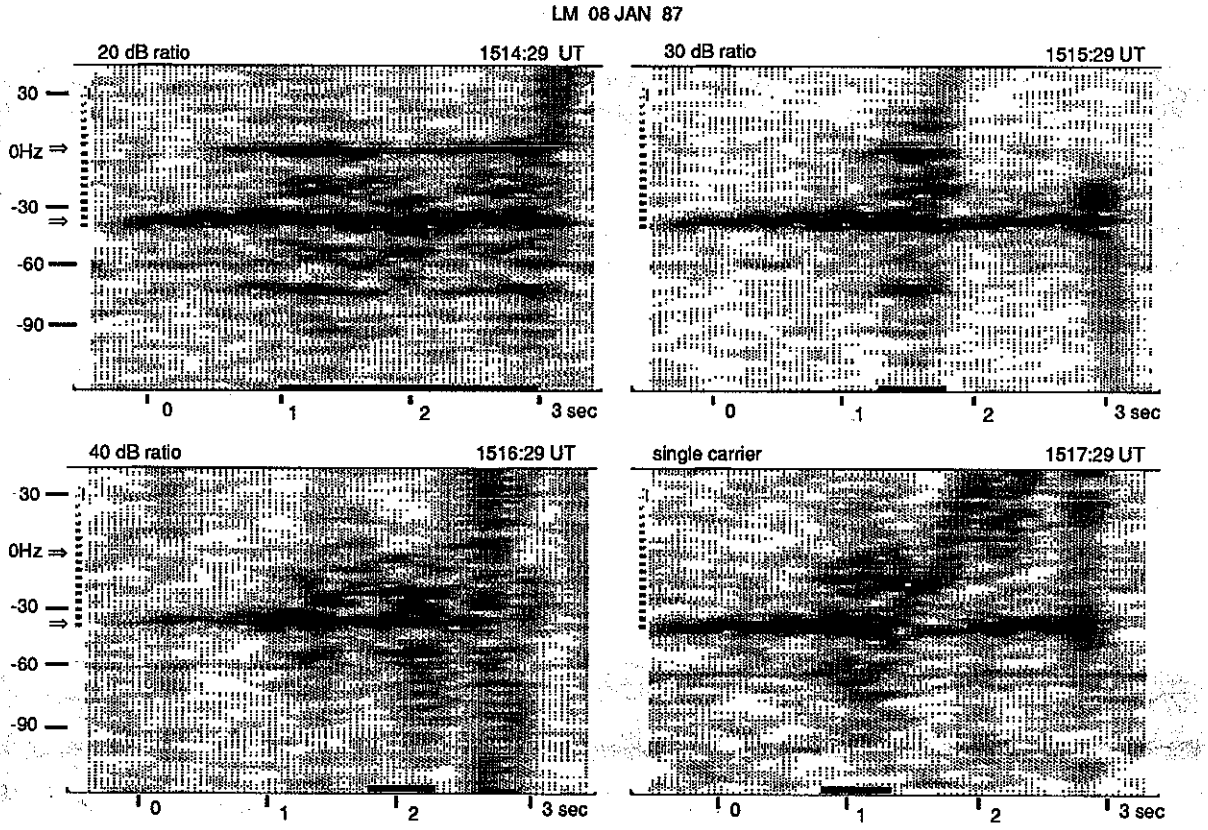

Fig. 2.5. Sequence of 3-s pulses with carrier separation equal to 37 Hz. 0 Hz in those pictures corresponds to 2460 Hz. The arrows point to the location of the two carriers. The horizontal bars at the bottom of each picture indicate the time intervals over which the average spectra shown in Figure 2.6 were taken. In all spectra the filter bandwidth was 1.56 Hz.

Figure 2.5 shows a sequence of pulses with carrier separation kept at 37 Hz, the most irrational possible function of 60 Hz, with amplitude ratios varying from -20 dB to minus infinity. Figure 2.6 shows the corresponding sequence of A scans from which average frequencies and amplitudes are measured. Due to the irrationality of the frequency ratios involved, few rational sub harmonics are excited, allowing for the creation of a particularly simple and repeatable spectrum. For each pulse there is now a single average made over the region where sidebands are present.

Figure 2.6*a* shows the basic structure which is approximately repeated in Figures 2.6*b* and 2.6*c*. Line 1 is simply a harmonic of 4 and 7. Line 5 is special: it is the mirror image of 4 in the interval defined by 2 and 7 (it is therefore a three-line effect involving two carriers and one PL harmonic). Line 3 is a harmonic of 4 and 5. Line 6 is simultaneously a harmonic of 2 and 4, and the mirror image of 5 in the interval defined by 4 and 7.

Figure 2.6*b* shows essentially the same structure as in Figure 2.6*a*, with two added lines. Line 7 is the harmonic of 5 and 6, and line 8 is the harmonic of 4 and 6.

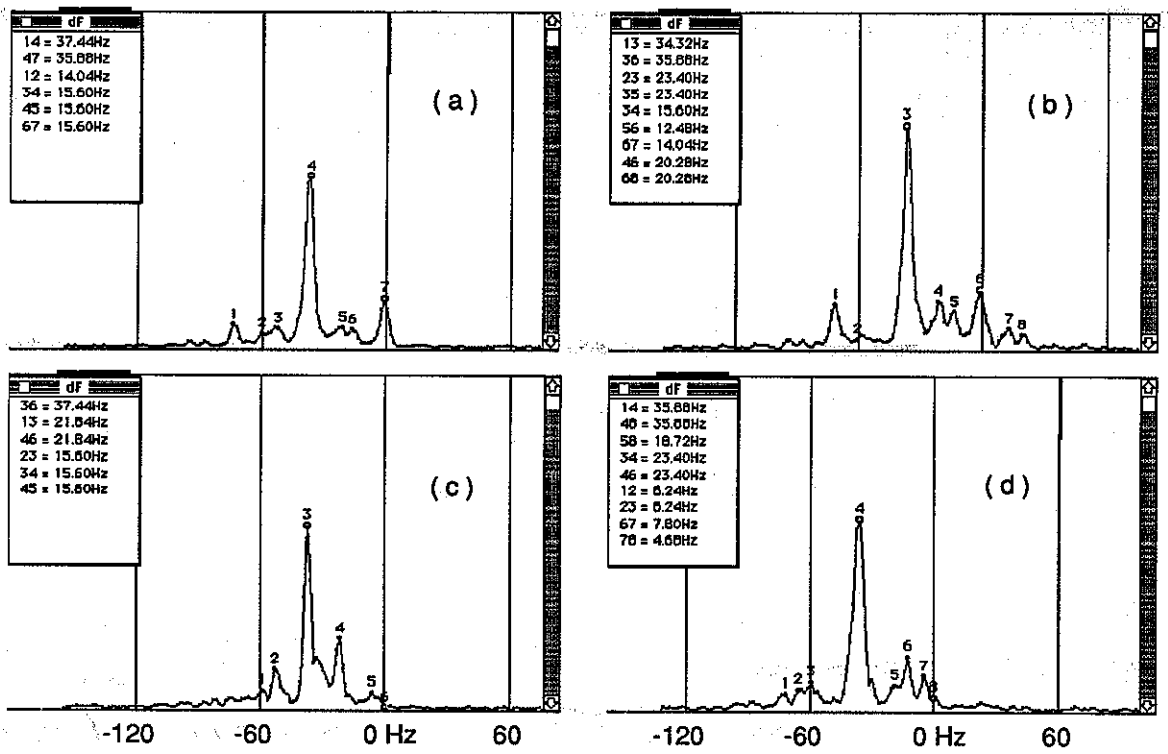

Fig. 2.6. Average spectra obtained from pulses shown in Figure 2.5: (*a*) 20 dB ratio, (*b*) 30 dB ratio, (*c*) 40dB ratio, and (*d*) single carrier pulse. The vertical scale is linear and arbitrary. 0 Hz in those pictures corresponds to 2460 Hz absolute frequency. The carriers are denoted by small circles at the maxima. The windows in each picture contain a table of frequency differences: at the left of each equal sign are two digits representing two spectral lines; at the right is their frequency difference.

Figure 2.6*c* shows that carriers can influence the spectrum even when they are too weak to be seen. Line 6, which is the upper carrier, does not appear in the spectrum. Nevertheless, its effect, which is the creation of mirror image line 4 in the interval defined by 1 and 6, is readily apparent. Lines 2 and 5 are harmonics of 3 and 4.

Figure 2.6*d* shows the single carrier spectrum. Due to the weakness of the PLR lines, three-line effects are not seen, a series of harmonics and half harmonics making up the spectrum, instead. Line 1 is a harmonic of 4 and 8. Line 2 is a half harmonic of 1 and 3. Line 6 is a harmonic of 3 and 4. Line 7 is a half harmonic of 6 and 8. It is far-fetched to think of line 5 as the mirror image of 4, since its position is almost 5 Hz off from what would be required for that interpretation. Line 5 is almost exactly halfway between lines 4 and 8, and should therefore be thought of as a half harmonic of those two lines .

2.5. Summary

The sideband spectra described above can be summarized as follows:

1. Sideband spectra are a consequence of the interaction of two or more lines. No real single-frequency sidebands have yet been identified.
2. Lines which are not readily seen in the measured spectra (30 dB or more below the stronger lines) can have an appreciable effect in sideband formation.
3. PLR is involved in virtually all sideband spectra. Its presence is fundamental in the creation of "single carrier" sidebands.
4. If several lines with frequencies $\Omega_i, i = 1 \ldots n$, measured from one of the carriers, interact creating a new line, its frequency Ω will be given by equation (2.1):

$$m\Omega = m_1\Omega_1 + \cdots + m_n\Omega_n$$

   where m and m_i are arbitrary integers ($m \neq 0$).
5. New line amplitudes depend on the combined effects of parent line intensities, frequency separations, and the electron distribution. The instability of the latter is thought to be the main cause for the imperfect reproducibility of the sideband spectra observed and described in this chapter.

2.6. Concluding Remarks

In this chapter, spectral data were presented together with an equation from which the observed frequencies in the spectra can be derived. The striking results are that vanishingly small lines can contribute to spectra formation, with no such thing as a single-frequency sideband spectrum being ever found in the data analyzed. This may explain why theories for single-frequency sidebands have not met with success when applied to sidebands observed in ducted radiation received from Siple Station.

Theories, such as the ones put forward by *Nunn* [1974], *Brinca* [1972], *Das* [1968], etc., describe sidebands as coming from interactions between a single carrier and the underlying continuous electron distribution present in the magnetosphere. Their predictions do not match the data in two main respects: First, the resulting expressions for the sideband-carrier frequency separation depend on $v_\perp$, the projection of the electron velocity in the direction perpendicular to the magnetic field of the Earth. This velocity has a continuous distribution, and after integration, should create a hump next to the carrier, instead of a sideband. This does not agree with the observed data, which show very well defined lines with widths comparable to the carrier line width. Second, such theories have as their only frequency parameter the trapping frequency of the carrier, dependent on its amplitude. This implies that any calculable frequency in those theories will be a function of the carrier amplitude, making impossible the description of sidebands that do not shift when the carrier oscillates in amplitude as seen in the data in this chapter or in papers such as *Park* [1981].

The approach presented in this chapter, describing sidebands as coming from a line-line interaction, does not suffer from any of the mentioned drawbacks and is in good agreement with the data. The following chapters describe its theoretical roots and implications in a systematic and general manner.

3. Description of External Resonances

3.1. Introduction

The purpose of the next three chapters is to provide a comprehensive description of the processes leading to the formation of sideband waves associated with discrete frequency transmissions originated in the VLF transmitter located at Siple Station - Antarctica and received at Lake Mistissini - Canada after ducted wave propagation. Those sidebands are found both in single- and double-frequency transmissions. In the preceding chapter we have shown that "single-frequency" sidebands are due to the combined effect of a transmitted wave from Siple and radiation present in the duct at multiples of 60 Hz probably, but not certainly, coming from the Canadian power distribution system. This allowed us to understand the VLF sideband process as being always caused by the effect on the magnetospheric electrons of several discrete frequency carriers, that disturbing the electron motion, change the electron distribution in such a way that radiation always occurs at certain well defined frequencies, given by a simple formula (see equation (3.34)).

The reader will notice that the next three chapters rely heavily on nonlinear mechanics formalism and methods uncommon to the VLF field. They are, however, essential to the problem we will treat, as can be shown by some simple considerations: The sideband process in the magnetospheric plasma is a combined effect of accelerated charge radiation, regulated by Maxwell's equations, and charge acceleration, described by the Lorentz force equation. Maxwell's equations are linear and predict radiation only at the frequencies at which charges oscillate. (Following *Feynman* [1964], we write Maxwell's equation in a vacuum, and include in the source densities all charges present in the plasma.) Sidebands clearly contain radiation at frequencies different from the incoming wave frequencies. Nonlinear forces, therefore, must be at play, producing accelerations at frequencies different from those present in the incoming wave field. The solution of the Lorentz force equation, that describes such an effect, is an exercise in mechanics, and is the main effort of the following three chapters. An understanding of the radiation coming from the accelerated charge distributions, complements the effort. The results are fruitful: the main aspects of the radiation described in the previous chapter are easily obtained. The reader that wants an overview of nonlinear oscillator systems together with references to recent research on the subject, should consult *Lichtenberg and Lieberman* [1983].

In section 3.2 of this chapter we will show how some simple symmetry properties of the duct in the absence of an external wave field imply the existence of a non-radiating electron distribution. In section 3.3 we show how an injected electromagnetic field, breaking the symmetry, creates radiation. In section 3.4, the equations governing the electron motion under the influence of one or more RHCP whistler mode waves are introduced and an interpretation of their solutions is made. In section 3.5, the equations of motion are solved numerically and the solutions are displayed with the help of phase plots. Emphasis is put on effects occurring outside the potential well of each incoming wave and, more specifically, on the occurrence of resonances of the electron motion at the frequencies where radiation is observed (external resonances). An example of "bunching" produced by those

resonances is presented. Section 3.6 begins the analytical treatment of the wave interaction process, with the application of the KAM theorem for nonlinear systems to the interaction we are describing. As a result we obtain an extremely general and simple expression for the possible frequencies of the sideband waves. Section 3.7 describes a perturbative method based on Lie transforms which is used for a detailed study of the electron motion. Section 3.8 applies the Lie perturbation method to non-resonant electrons. Section 3.9 describes the lowest order resonance, the half harmonic, a second order effect produced by the interaction of any wave pair in the incoming wave system. Section 3.10 describes third order effects associated with two or three interacting waves. Section 3.11 contains a description of higher order effects and section 3.12, the conclusions.

3.2. Duct Symmetries and Non-Radiating Electron Configurations

We will assume that in the absence of outside incoming radiation the hot electron distribution is so stirred up that all points in a perpendicular cross section of the duct will have the same electron density. Moreover, we will assume that this local electron distribution is isotropic, that is, the number of electrons observed moving in any direction of the cross section is the same, independent of the direction chosen. At each point, the observed electrons will also have different velocities of motion in the direction parallel to the axis of the duct, $v_\parallel$. We will have to assume that the distribution is homogeneous and isotropic for each $v_\parallel$, otherwise by selecting a specific $v_\parallel$ we would be able to define a specific direction in the duct, contrary to the assumption that all directions are equally important. This assumption of homogeneity and isotropy will provide us with the means to build the electron distribution in the duct.

Figure 3.1 shows a perpendicular cross section of the duct with some electrons singled out. Those electrons will be moving in a helical orbit due to the presence of the magnetic field of the Earth. Let the projected motion of all electrons be counterclockwise. We will show that every electron in the distribution belongs to a DC current loop. Suppose that at point P_1 we consider a volume element $dAdl$ of electrons moving in the direction and sense defined by the arrow in the picture. Let the circle in the picture be the projection of their helical orbit on the plane of the cross section. At another point P_2, arbitrarily located on that circumference, we draw a volume element identical to $dAdl$. Due to the homogeneity of the duct the number of electrons in this volume, dN_2, will be equal to dN_1. If we now draw a third volume element $dAdl$ with dl tangential to the circumference, the number of electrons, dN_3, moving in it and having the circumference as their projected trajectory will be equal to dN_2 due to the isotropy of the duct. Therefore, $dN_1 = dN_3$. Since P_2 is arbitrary, we conclude that the circumference we have drawn is uniformly populated by electrons, and moves as a rigid body in the direction of the Earth's magnetic field with velocity $v_\parallel$.

If we assume that the duct is in stationary equilibrium (the distribution is translationally invariant in time), the plane of the cross section will be continually crossed by those DC loops, identical to each other, indicating that the distribution is in reality made up of cylinders with constant charge density on their surfaces and moving with velocity $v_\parallel$ as in figure 3.2. Such a charge configuration will not radiate due to its rotational symmetry. Symmetry considerations, however, cannot constrain the value of the surface charge density to be the same for cylinders with different

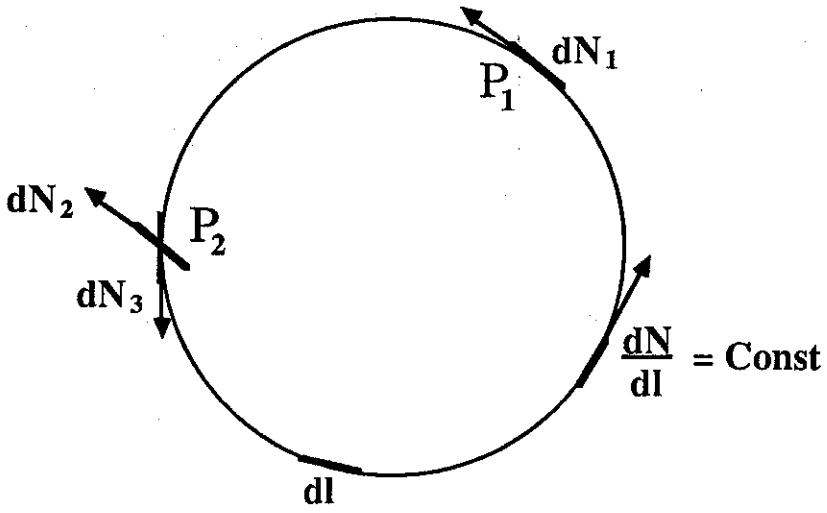

Fig. 3.1. Duct isotropy and homogeneity. Due to symmetries in the duct geometry, the electron distribution in a perpendicular cross-section of the duct can be broken down into a set of DC current loops.

$v_\parallel$, or different radii. In reality, in a real electron distribution, the cylinders will have surface charge varying as a function of their radii and $v_\parallel$. This is a very important fact since we will see that a gradient in the surface charge density as a function of $v_\parallel$ is necessary for the radiation due to the sum of all cylinders to be different from zero when an electromagnetic wave interacts with the electron distribution. As electromagnetic radiation reaches each cylinder, the isotropy of the forces will be broken by the vector fields of the wave, the electron distribution will lose its isotropy and radiate.

3.3. Effect of Radiation on the Electron Distribution

To simplify our analysis of the radiation generation process, we assume that the interaction between the electron distribution and the incoming waves occur in a region with sharply defined boundaries, and that the incoming electromagnetic radiation is a superposition of monochromatic whistler mode waves. The region of interaction, located around the equator, will have dimensions such that inside it, the inhomogeneity of the magnetic field of the Earth can be neglected. It will be extremely convenient to observe the interaction from a reference system with no translational motion, rotating around the axes of the charge cylinders with an angular velocity ω_1, equal to the frequency of one of the waves, and having its z axis pointing in the direction opposite to $v_\parallel$, the velocity of the electrons resonating with the electromagnetic field.

Figure 3.3 shows the described situation, and our approach to the analysis of the problem: We imagine each cylinder to be composed, outside the interaction region, of a sequence of DC loops. As each of those current loops enters and propagates through the interaction region, it will be

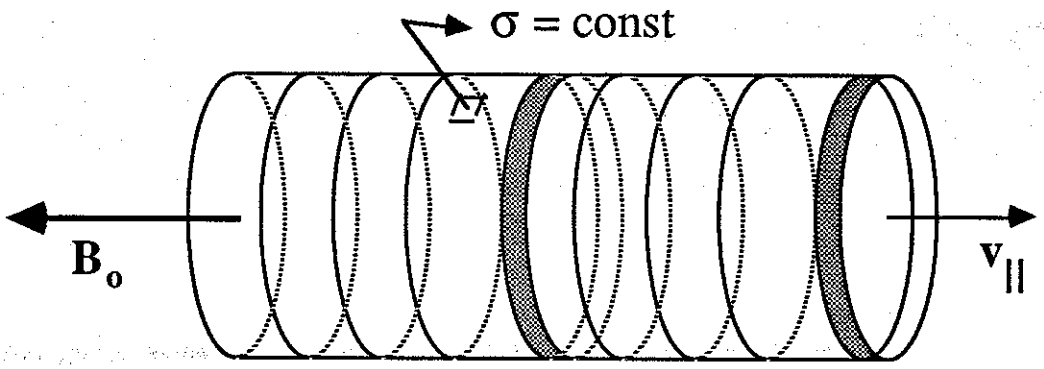

Fig. 3.2. Undisturbed electron distribution. Because the duct is in stationary equilibrium, each loop belongs to a cylinder with constant surface charge density, σ, which propagates along $-z$ with velocity $v_{\|}$.

deformed by the forces of the incoming electromagnetic waves acting on it. Since vector fields define preferred directions in space, the distortions will be such that the isotropy of the cylindrical charge distribution will be lost. As a consequence, each cylinder will now be made up of a sequence of AC current loops, and radiation will start to be emitted. (An accurate analysis shows that, due to the way the electrons and the electromagnetic field interact, each loop is distorted in the z direction as it propagates along the interaction region. The AC loops that make up the distorted cylinder are not simply individually distorted DC loops, but a combination of parts of several of them, each one having entered the interaction region at a slightly different time.)

If the incoming radiation is monochromatic, with frequency ω_1, and if the reference system rotates with the same frequency ω_1, the whistler-mode wave will have a static configuration. All current loops will see the same forces and will have the same distortions as they reach the same points in the interaction region. The distorted charge configuration will be independent of time, will behave as a rigid body with an asymetrical charge distribution rotating with angular velocity ω_1, and will radiate at the same frequency as the incoming monochromatic radiation. The emitted radiation will in general have variable phase and variable amplitude (especially in the initial transient stage when the wave first meets the electron distribution). This might give rise to some spectral broadening, but no well defined sidebands.

For two or more waves, even after we adjust our reference system to rotate with one of them, the resultant electromagnetic field will be explicitly time dependent. Each loop as it penetrates the interaction region will see a different electromagnetic field configuration. At each point the charge densities on the surface of the cylindrical electron distribution will be time dependent, and as the cylinder rotates, frequencies different from ω_1 will be generated. The problem of sideband formation will be reduced to the study of radiation created by the rotation of this time dependent cylindrical charge distribution. For that purpose a cylinder is divided into loops fixed in space (at

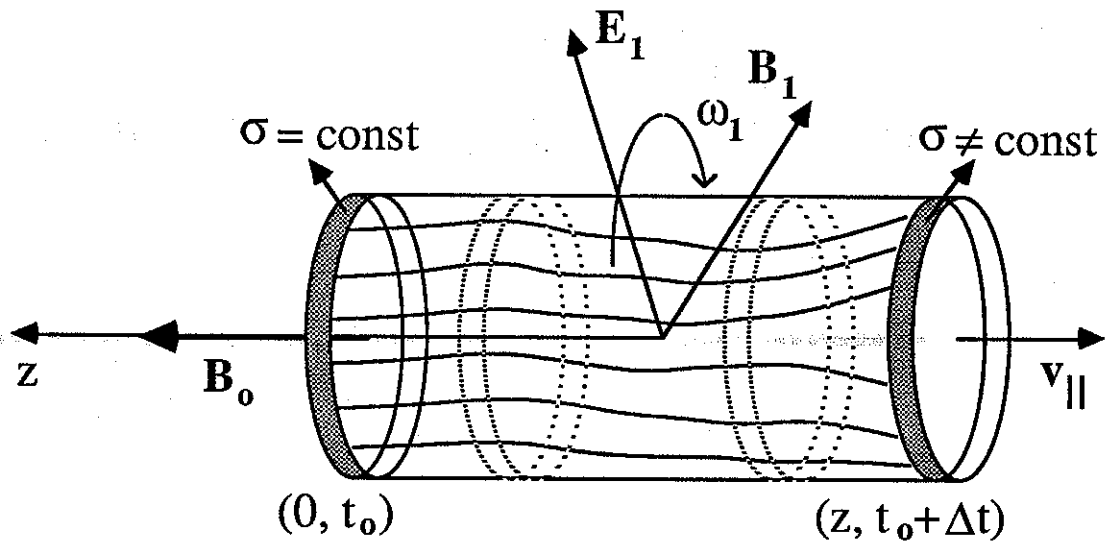

Fig. 3.3. Effect of electromagnetic field on electron distribution. As each cylinder penetrates the interaction region, forces due to the electromagnetic field, change its charge distribution, breaking its rotational symmetry and creating radiation. A ring obtained by slicing the cylindrical charge at $z = 0$ will have constant charge density, another one at $z \neq 0$, will not. The wavy horizontal lines represent schematically the electron streams into which the cylindrical charge distribution can also be decomposed. With the conventions used in this dissertation, z is negative in the picture.

a constant z), and the radiation that comes from each of them is studied. The total radiation is obtained by integrating all loops over different values of $\mathbf{v}_{\|}$, for the same z, then integrating over different z values, over cylinders with different radii, and over different locations of the symmetry axis. The charge configuration in each loop is obtained from the electron's equation of motion under the influence of the incoming electromagnetic field. The solution of this equation, a function of $(z, \mathbf{v}_{\|})$, can be obtained either numerically, through the use of phase plots, or analytically, with the help of perturbation theory.

3.4. Equations for Electron Motion Under the Influence of Several Monochromatic Waves

Figure 3.4 shows an electron at a point P, moving with velocity $\mathbf{v} = v_{\|}\mathbf{u}_{\|} + v_{\perp}\mathbf{u}_{\perp}$. $\mathbf{u}_{\|}$ is a unit vector pointing in the direction opposite to $\mathbf{B}_o$, the Earth's magnetic field, and $\mathbf{u}_{\perp}$ is a unit vector pointing along the projection of the electron velocity on the plane (x, y), perpendicular to $\mathbf{B}_o$. $(\mathbf{E}_1, \mathbf{B}_1)$ represents the electric and magnetic fields of one of the N waves in the incoming radiation singled out as a reference for the electron motion.

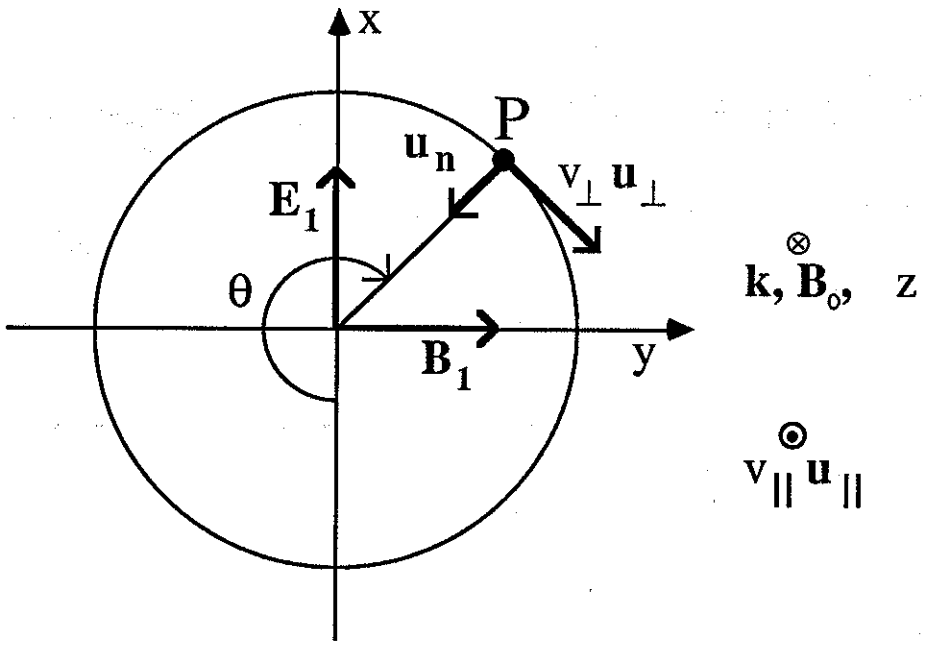

Fig. 3.4. Diagram of relevant field and electron variables. Notice that the waves propagate in the $+z$, and the electrons, in the $-z$ direction.

If we define

$$\mathbf{E}_t = \sum_{i=1}^{N} \mathbf{E}_i \tag{3.1}$$

$$\mathbf{B}_t = \mathbf{B}_o + \mathbf{B}_w = \mathbf{B}_o + \sum_{i=1}^{N} \mathbf{B}_i \tag{3.2}$$

The equation of motion can be written as:

$$\dot{\mathbf{v}} = \dot{v}_{\|}\mathbf{u}_{\|} + \dot{v}_{\perp}\mathbf{u}_{\perp} + v_{\perp}\dot{\mathbf{u}}_{\perp} = -\frac{e}{m}(\mathbf{v} \wedge \mathbf{B}_t + \mathbf{E}_t) \tag{3.3}$$

It is possible to show that

$$\dot{\mathbf{u}}_{\perp} = (\dot{\theta} + \omega_1 + k_1 v_{\|})\mathbf{u}_n \tag{3.4}$$

where ω_1 and k_1 are the angular frequency and wave number of the reference whistler-mode wave, and $\dot{\theta}$ is the angular velocity of the electron referred to the same wave field. It should be noted that $\dot{\theta}$ is a convective derivative. Its value takes into account the change in relative wave-electron position due not only to the electron rotation as it moves along its path, but also to the different orientations of the wave field at different points in space and different instants of time. From the last two equations we get, neglecting terms important only for very small pitch angles,

$$\dot{\theta} = -\omega_1 - k_1 v_{\|} + \frac{\dot{\mathbf{v}} \cdot \mathbf{u}_n}{v_{\perp}} = -k_1 v_{\|} - \omega_1 + \frac{eB_o}{m} = -k_1(v_{\|} - v_{res}) \tag{3.5}$$

If $v_{\|} = v_{res}$, we say that the electron is in resonance with the wave. This implies $\dot{\theta} \equiv 0$.

From (3.3), the Lorentz Force equation, we get

$$\dot{v}_{\parallel} = \dot{\mathbf{v}} \cdot \mathbf{u}_{\parallel} = \frac{ev_{\perp}}{m}(\mathbf{u}_n \cdot \mathbf{B}_w) \tag{3.6}$$

which can be simplified to

$$\dot{v}_{\parallel} = \frac{ev_{\perp}}{m} \sum_{i=1}^{N} B_i sin(\theta + \Delta\theta_i) \tag{3.7}$$

with

$$\Delta\theta_i = \Delta k_i z - \Delta\omega_i t + \Delta\phi_i \tag{3.8}$$

where the Δ operation means taking the difference between a parameter of wave i and the same parameter of reference wave 1. Putting in $z = -v_{\parallel}(t - t_o)$, where t_o is the time the electron enters the interaction region, we get after some manipulation,

$$\Delta\theta_i = -\Omega_i t + \phi_i \tag{3.9}$$

with

$$\Omega_i = (\frac{v_{\parallel}}{v_g} + 1)\Delta\omega_i \tag{3.10}$$

and

$$\phi_i = (\Omega_i - \Delta\omega_i)t_o + \Delta\phi_i \tag{3.11}$$

where v_g is the wave group velocity at the average radiation frequency, and Ω_i is the Doppler shifted frequency difference between waves i and 1.

Finally, from (3.5), (3.7) and (3.9),

$$\ddot{\theta} = -\sum_{i=1}^{N} \Omega_{ti}^2 \sin(\theta - \Omega_i t + \phi_i) \tag{3.12}$$

where $\Omega_{ti}^2 = ev_{\perp}k_1 B_i/m$ is the square of the trapping frequency associated with wave i. Reminding ourselves that

$$\frac{d^2}{dt^2} = v_{\parallel}^2 \frac{d^2}{dz^2} \tag{3.13}$$

we can also write

$$\theta'' = -\sum_{i=1}^{N} \left(\frac{\Omega_{ti}}{v_{\parallel}}\right)^2 \sin\left[\theta + \left(\frac{\Omega_i}{v_{\parallel}}\right) z - \Delta\omega_i t_o + \Delta\phi_i\right] \tag{3.14}$$

The last equation emphasizes that the variation in angular position of the electron depends on how far it has traveled inside the interaction region, that the electron oscillations to be discussed in the following sections do not occur at a fixed point in space as function of time but are spread in space as the electron travels along the z axis, and that their periods do not modulate the electromagnetic waves in any direct way. The solution to the equation will be

$$\theta = \theta(\theta_o, \theta_o', z, t_o) \tag{3.15}$$

The trajectory described by the electron will depend on θ_o, its initial orientation, θ_o', which is related to the initial value of $v_{\parallel}$, and on t_o, the time the electron arrives at the interaction region. If only one

wave is present, all $\Delta\omega_i$ will be equal to zero, there will be no dependence on t_o, and the trajectories will be the same for all electrons starting with the same initial angular positions and same $v_\parallel$. As stated in section 3.3, the charge distribution will behave as a rotating rigid body radiating at the single wave frequency. If more than one wave is present, the equation predicts the existence of a set of trajectories, with initial point and derivative given by θ_o and θ'_o, which are slowly (compared with ω_1, the frequency of the reference wave) being distorted in time. The electron distribution can be decomposed into a sum of loops rotating with velocity ω_1 and having time dependent charge distributions. This charge distribution can be obtained by studying the solution θ at a fixed point in space, z_o, as a function of the initial angular position, initial $v_\parallel$, and moment of entrance in the interaction region.

For actual calculations, it will be more convenient to use the time dependent form of the equation of motion, keeping in mind that observation of the motion at a fixed position in space is equivalent to an observation at a time $t_{z_o} = |z_o|/v_\parallel + t_o$, a function of the electron travel time and instant of arrival at the interaction region. We assume in that expression that $v_\parallel$ is aproximately constant over the electron trajectory.

3.5. Phase Plots

To study the evolution of the electron distribution, we assume initially that all electrons arrive at time t_o at the interaction region, having a random distribution in θ_o and $\dot{\theta}_o$ with constant probability density in each variable. This distribution will not give rise to radiation because its gradient as a function of $\dot{\theta}_o$ (initial $v_\parallel$) is zero. However, if we follow the evolution of each electron trajectory in space and plot its projection in the $(\theta, \dot{\theta})$ plane, we will arrive at a clear qualitative understanding of the radiation process.

Figure 3.5 shows the resulting phase plots for the case of two equal amplitude waves separated by a frequency Ω. Different values for t_o were chosen in each plot so that the waves in the beginning of the interaction region are rotated relatively to each other by an additional 60° from one plot to another. They are in phase in the first plot.

To create the plots, for a given initial time t_o, several trajectories are started at random values of $(\theta_o, \dot{\theta}_o)$. The time evolution of each trajectory is calculated and the electron position $(\theta, \dot{\theta})$ is plotted as a point in the plane at times

$$t = t_o + \frac{2n\pi}{\Omega}, \quad n = 1, 2, \ldots \infty \tag{3.16}$$

This must be done because, as seen by looking at the different plots, all trajectories posses a continuous upwards motion which would blur the pictures, if all moments in time were plotted. The choices of t given by the above equation are such that the waves' relative angular position is always the same and the trajectories are always at the same position. A complete description of the motion would consist of the set of all phase plots for all values of t_o.

The plots show various resonances. Those are sets of electron trajectories which have been strongly affected by the presence of the two waves. The trajectories have been changed from vertical straight lines to sets of concentric distorted ovals, defining regions from which we should expect

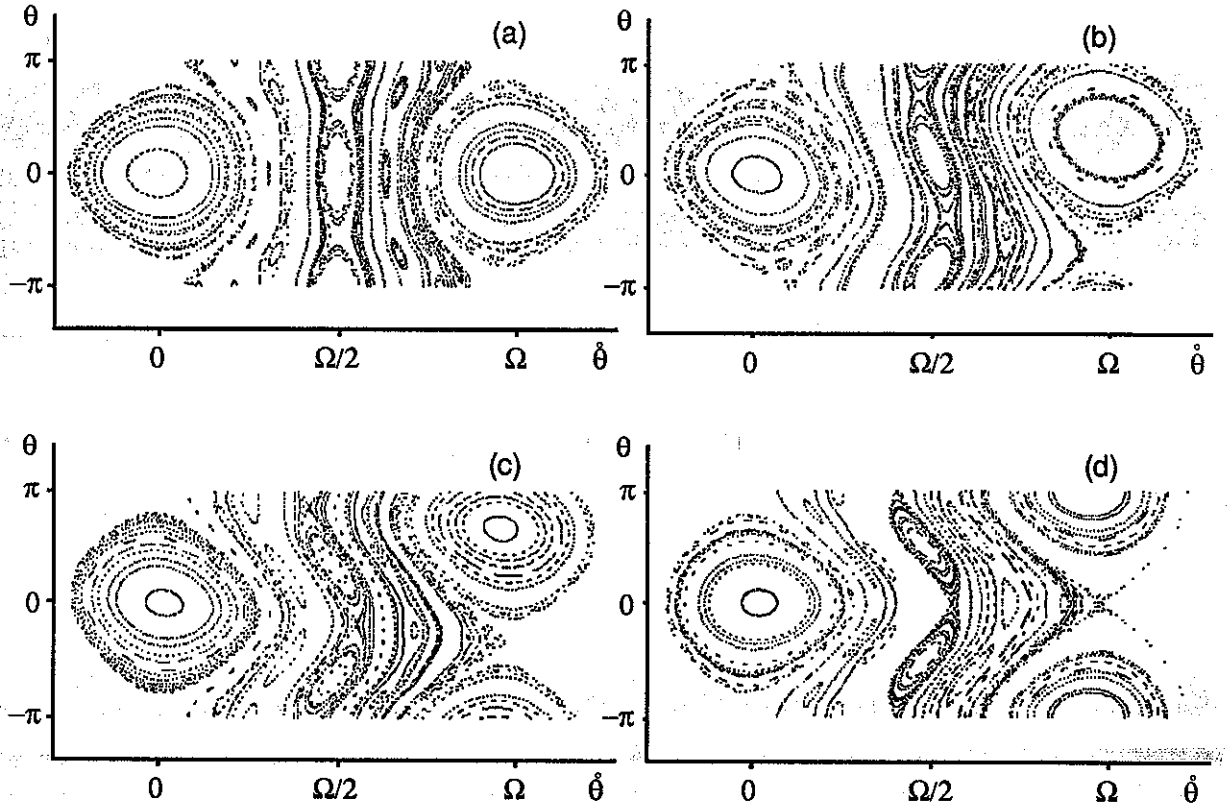

Fig. 3.5. Resonances created by two equal intensity carriers. The presence of each carrier resonance at $\dot{\theta} = 0$, Ω is readily apparent, together with additional resonances at $\dot{\theta} = \Omega/3$, $\Omega/2$, and $2\Omega/3$. As the carriers rotate relatively to each other, the additional resonances are seen to rotate and radiate at frequencies $\omega/3$, $\omega/2$, and $2\omega/3$. Their distortions, created by the presence of the carriers, will modulate their radiations, modifying the spectrum as described in the text: (a) Relative carrier phase = 0°. (b) Relative carrier phase = 60°. (c) Relative carrier phase = 120°. (d) Relative carrier phase = 180°.

most of the radiation to come. There is one resonance at each incoming wave frequency, one halfway between them (half harmonic), two at one third of the distance from one wave to another, and many more, that would be seen if the plots were more accurate.

Figure 3.6 shows a phase plot of the same two waves after their amplitudes are increased by a factor of 12.5 (22 dB growth). Due to the greater amplitude values, the previously seen resonances have been destroyed, chaotic electron motion being present, instead. However, outside the chaotic region, two resonances are present. They are separated from the main waves by a frequency Ω and will radiate at their first harmonic frequencies.

Figure 3.7 shows plots for a more realistic situation. The region of phase space chosen for observation is located, as shown in plot 3.7*a*, around the half harmonic resonance. The chosen electron distribution is constant in θ at $z = 0$ but has a constant gradient in $\dot{\theta}$ (that is, in $v_{\parallel}$), as shown in plot 3.7*b*. Plot 3.7*c* shows the effect of the waves on the electron distribution at a point z_o

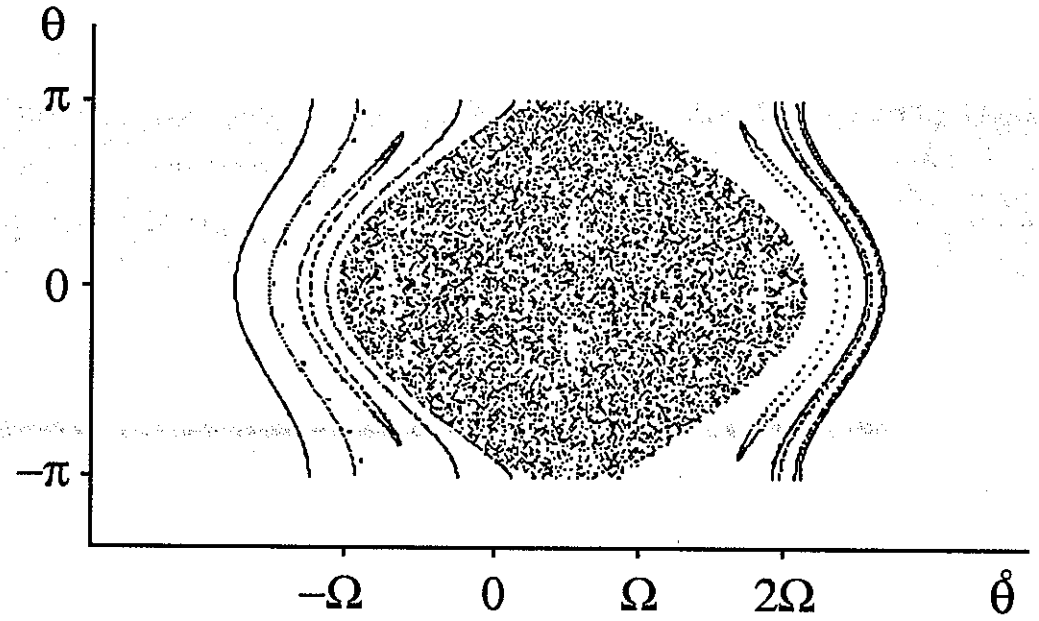

Fig. 3.6. Chaotic motion and first harmonics created by two strong waves. The carriers are at 0 and Ω, and their relative phase is 0°. Their common trapping frequency is $\Omega/2$. The first harmonics are at $-\Omega$ and 2Ω. Due to the high intensity of the carriers, organized electron motion in a large region containing the carrier potential wells is completely destroyed and replaced by chaotic motion, where wave growth cannot take place. The first harmonic resonances would be destroyed only if they were wide enough to overlap the chaotic region. Chaotic motion is believed by the author to be one of the main causes of triggered emissions observed in magnetospheric data.

well into the interaction region. The gradient in $\dot{\theta}_o$ has been partially transformed into a gradient in θ. The gradient in θ is equivalent to an inhomogeneous charge loop at z_o, rotating with the average frequency of the two waves, and giving rise to radiation at the same frequency. We see that not all bunching comes from inside the resonance. Plot 3.7*d* shows the wave effect on a distribution with zero gradient. In this case there is no bunching, indicating that an initial density gradient is necessary for radiation to be generated.

3.6. General Solution of the Equation of Motion - KAM Theorem

When writing the equation of motion

$$\ddot{\theta} = -\sum_{i=1}^{N} \Omega_{ti}^2 \sin(\theta - \Omega_i t + \phi_i) \tag{3.17}$$

we have assumed that the reference wave has been wave 1 and that all $\Delta\omega_i$ are measured relative to it. It will be convenient in our next considerations, to measure frequencies from an arbitrary origin. With that in mind, we will shift our origin to an infinitesimally weak wave having an arbitrary frequency, ω_r, which will serve only as a frequency reference, being ignorable for all other purposes. This will imply $\Delta\omega_1 \neq 0$ and that all $\Delta\omega_i$ will be defined up to an overall additive constant.

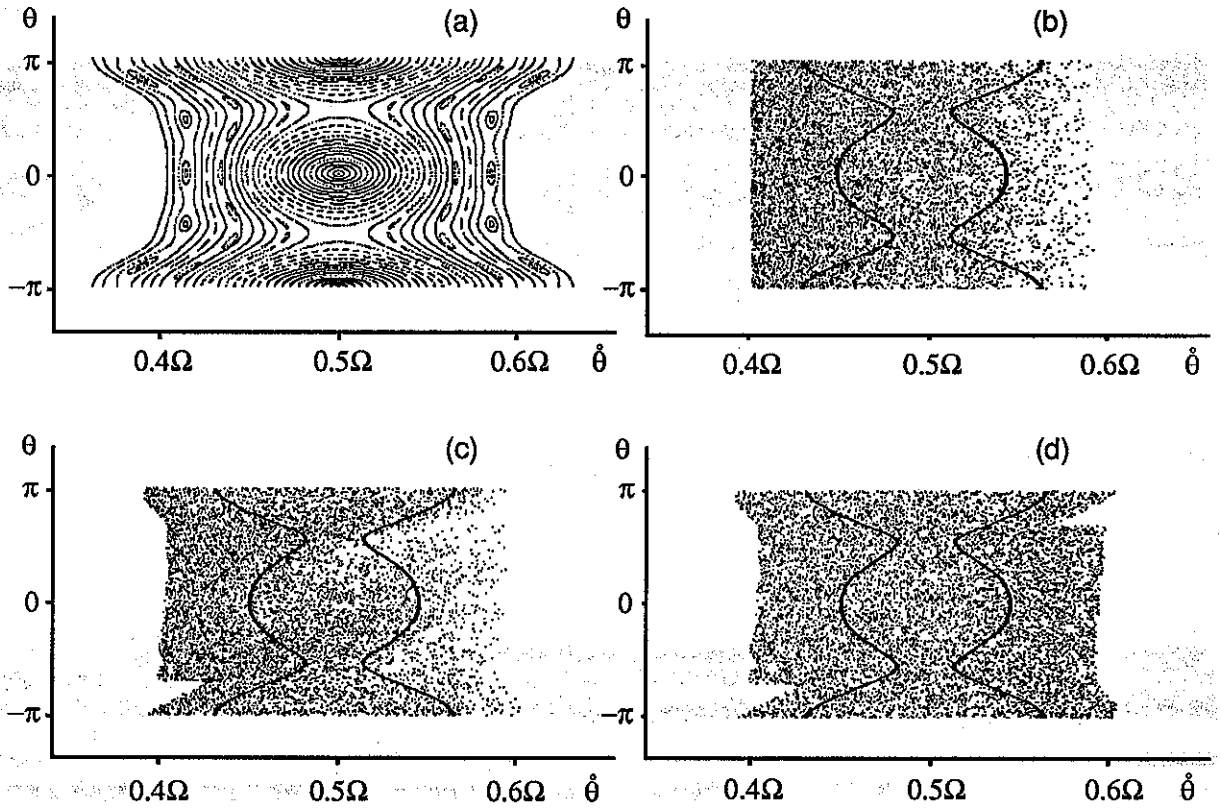

Fig. 3.7. "Bunching" of electron distributions created by half harmonic resonance. The carriers are at frequencies 0 and Ω. The dark lines in (b), (c) and (d) are the approximate two branches of the separatrix of resonance (a): (a) Phase plot of half harmonic resonance which produces the "bunching" effect in the following pictures. (b) An initial electron distribution with constant gradient in the $\dot{\theta}$ direction. (c) Effect of resonance (a) on electron distribution (b) after it has propagated for some distance along the interaction region. It can be seen that "bunching", when it occurs, is as pronounced outside as inside a resonance. The charge rarefactions at $\approx \pi/2$ and $\approx -\pi/2$ are slightly different from each other due to distortions in the resonance, as mentioned in section 3.9. Because of it, a net amount of radiation will be created. (d) Effect of resonance (a) on an electron distribution with zero gradient. It is null, as shown by this picture made at the same z position as in (c).

The above equation of motion is equivalent to the Hamiltonian

$$H(q,p,t) = p^2/2 - \sum_{i=1}^{N} \Omega_{ti}^2 \cos(q - \Omega_i t + \phi_i) \tag{3.18}$$

as can be seen by Hamilton's equations:

$$\dot{q} = \frac{\partial H}{\partial p} = p \tag{3.19}$$

$$\dot{p} = -\frac{\partial H}{\partial q} = -\sum_{i=1}^{N} \Omega_{ti}^2 \sin(q - \Omega_i t + \phi_i) \tag{3.20}$$

The system we are studying has $N+1$ degrees of freedom: the phase of the N waves, and the electron angular position. This is explicitly shown by the fact that it can be described by the $N+1$ dimensional Hamiltonian,

$$H(q_i, p_i) = p_{N+1}^2/2 + \sum_{i=1}^{N} \Omega_i p_i - \sum_{i=1}^{N} \Omega_{ti}^2 \cos(q_{N+1} - q_i + \phi_i) \tag{3.21}$$

which has the following equations of motion:

$$\dot{q}_{N+1} = \frac{\partial H}{\partial p_{N+1}} = p_{N+1} \tag{3.22}$$

$$\dot{p}_{N+1} = -\frac{\partial H}{\partial q_{N+1}} = -\sum_{i=1}^{N} \Omega_{ti}^2 \sin(q_{N+1} - q_i + \phi_i) \tag{3.23}$$

$$\dot{q}_i = \frac{\partial H}{\partial p_i} = \Omega_i \tag{3.24}$$

and

$$\dot{p}_i = -\frac{\partial H}{\partial q_i} = \Omega_{ti}^2 \sin(q_{N+1} - q_i + \phi_i) \tag{3.25}$$

The p_i are dummy variables and can be ignored. The equations for the q_i give:

$$q_i = \Omega_i t \tag{3.26}$$

Substituting those values in equations (3.22) and (3.23), eliminating p_{N+1}, and making $q_{N+1} = \theta$, we get the original equation of motion. If we now define

$$H_o(p_i) = p_{N+1}^2/2 + \sum_{i=1}^{N} \Omega_i p_i \tag{3.27}$$

and

$$H_1(q_i, p_i) = -\sum_{i=1}^{N} \Omega_{ti}^2 \cos(q_{N+1} - q_i + \phi_i) \tag{3.28}$$

we can write

$$H(q_i, p_i) = H_o(p_i) + H_1(q_i, p_i), \quad i = 1 \ldots (N+1) \tag{3.29}$$

where $H_1(q_i, p_i)$ is periodic in all q_i, and $H_o(p_i)$ depends only on the p_i. Under those circumstances, the KAM (Kolmogoroff, Arnold, Moser) Theorem for nonlinear systems states that the motion described by H_o (free electron motion) will be apreciably affected by H_1 only if the following relationship holds for the variables describing the free motion:

$$\sum_{i=1}^{N+1} n_i \dot{q}_i = 0, \tag{3.30}$$

n_i being arbitrary integers. Making $\dot{q}_{N+1} = \dot{\theta} = \Omega$, we will have:

$$n\Omega = \sum_{i=1}^{N} n_i \Omega_i \tag{3.31}$$

Now, the interaction between the electron and the system of electromagnetic waves should not be dependent on the chosen origin of coordinates. Therefore, if we make a shift $\delta\Omega$ in the coordinate system, the new equation obtained should also be a valid description of the interaction:

$$n(\Omega + \delta\Omega) = \sum_{i=1}^{N} n_i(\Omega_i + \delta\Omega) \tag{3.32}$$

Since $\delta\Omega$ is arbitrary, the two equations can be true only if

$$n = \sum_{i=1}^{N} n_i \tag{3.33}$$

Since $\omega_i = \omega_r + \Delta\omega_i = \omega_r + \Omega_i(v_\parallel + v_g)/v_g$, the formula that gives the frequencies for strong electron-wave interaction, that is, the resonant frequencies, is:

$$\omega = \frac{\sum_{i=1}^{N} n_i\omega_i}{\sum_{i=1}^{N} n_i} \tag{3.34}$$

where $\omega = \omega_r + \Omega(v_\parallel + v_g)/v_g$ is both the frequency of a wave resonant with an electron of $\dot{\theta} = \Omega$, and the frequency at which such an electron would radiate. The allowed resonance frequencies are just the weighted averages, with arbitrary integer weights, of the incident wave frequencies. This simple formula, independent of the detailed form of the Hamiltonian describing the motion, and mentioned in the introduction of this chapter, was the one succesfully used in the previous chapter to describe the Siple sideband spectra.

3.7. Analytical Solution - Lie Transform Perturbation Method

To study specific resonances, a more sophisticated mathematical treatment is required. We choose the Lie Transform Perturbation Method, applicable to any Hamiltonian system, which has the following advantages: It does not use mixed variables in its formalism, allowing the perturbation expansion to be extended to arbitrarily high orders. It does not generate secular terms or small denominators if a judicious choice of the associated generating function is made. Its formalism, being based on Poisson brackets series, is canonical and invariant in form under any canonical change of coordinates.

The method has been described in several places. Here we follow the notation used by *Cary* [1981] (Deprit perturbation series), and summarize it as follows:

We assume that the known Hamiltonian, h, is expressible as a power series for a small quantity ϵ:

$$h(q,p,t) = \sum_{n=0}^{\infty} \epsilon^n h_n(q,p,t) \tag{3.35}$$

and we look for a new and simpler hamiltonian, K:

$$K(Q,P,t) = \sum_{n=0}^{\infty} \epsilon^n K_n(Q,P,t) \tag{3.36}$$

through a change in coordinates

$$Q = T(q,p,t)q \tag{3.37}$$

$$P = T(q,p,t)P \tag{3.38}$$

where T is an unknown operator expressible in powers of ϵ:

$$T(q,p,t) = \sum_{n=0}^{\infty} \epsilon^n T_n(q,p,t) \tag{3.39}$$

The solution is found with the help of a generating function

$$W(q,p,t) = \sum_{n=0}^{\infty} \epsilon^n W_{n+1}(q,p,t) \tag{3.40}$$

and a sequence of operators L_n defined by

$$L_n f(q,p,t) = \{W_n, f\}, \quad n = 1 \ldots \infty \tag{3.41}$$

where the curly brackets represent the Poisson bracket operation.

The new Hamiltonian, expressed in the new variables (Q,P), can be obtained up to third order from the following set of equations:

$$K_o = h_o \tag{3.42}$$

$$\frac{\partial W_1}{\partial t} + \{W_1, h_o\} = K_1 - h_1 \tag{3.43}$$

$$\frac{\partial W_2}{\partial t} + \{W_2, h_o\} = 2(K_2 - h_2) - L_1(K_1 + h_1) \tag{3.44}$$

$$\frac{\partial W_3}{\partial t} + \{W_3, h_o\} = 3(K_3 - h_3) - L_1(K_2 + 2h_2) - L_2(K_1 + h_1/2) - L_1^2 h_1/2 \tag{3.45}$$

and the inverse transformation, to return to the original (q,p) pair is

$$q = T^{-1}Q \tag{3.46}$$

$$p = T^{-1}P \tag{3.47}$$

$$T^{-1}(Q,P,t) = \sum_{n=0}^{\infty} \epsilon^n T_n^{-1}(Q,P,t) \tag{3.48}$$

where

$$T_o^{-1} = I \tag{3.49}$$

$$T_1^{-1} = L_1 \tag{3.50}$$

$$T_2^{-1} = L_2/2 + L_1^2/2 \tag{3.51}$$

$$T_3^{-1} = L_3/3 + L_1 L_2/6 + L_2 L_1/3 + L_1^3/6 \tag{3.52}$$

We see that the set of functions W_n defines the change of coordinates completely. Since the set of equations defining the new Hamiltonian has $2n$ unknowns, up to order n, we are free to choose the W_n as we please, defining the change of coordinates arbitrarily. After a choice is made, the K_n can be calculated together with the T_n^{-1} that define the inverse transformation. The choice of the W_n

should be made judiciously, however, since they have to be bounded for the perturbation expansion to be valid. The equation for the W_n can be written in the form:

$$\frac{\partial W_n}{\partial t} + \{W_n, h_o\} = nK_n(Q,P,t) - f_n(Q,P,t) = g_n(Q,P,t) \tag{3.53}$$

Assuming we are solving the equations recursively, f_n is known because it depends on $h_n \ldots h_1$, which are given, and on $W_{n-1} \ldots W_1$ and $K_{n-1} \ldots K_1$, which are found at a lower order. The solution to such an equation is given by *Cary* [1981]:

$$W_n = \int^t d\tau \; g_n \left[Q + \Omega(\tau - t), P, \tau\right] \tag{3.54}$$

with

$$\Omega = \frac{\partial h_o}{\partial P} \tag{3.55}$$

It seems clear that if g_n has terms which are slowly varying in time, as, for example, a constant or a resonance for a certain value of P, W_n will vary approximately linearly in time, will be unbounded, and the perturbation expansion will fail. This gives us the guidelines for choosing K_n, and implicitly, the desired change of coordinates: K_n must absorb all constant terms present in f_n together with any term representing a resonance in the neighborhood of the P we are interested in. This will make W_n a bounded function and, at the same time, will transfer to K_n the resonances we intend to study.

The process of solution of our equations is therefore defined: Starting with K_o, and proceeding to successively higher orders, we put in the K_n all constants present in the functions f_n of our equations. At the same time, we inspect each f_n for a resonance of interest. If we do not find it, we calculate W_n and proceed to a higher order. If we do find it, we add it to K_n and stop the search. The new Hamiltonian, K, will be composed of constant terms plus a single, higher order, term describing a resonant process, and will be valid for all values of P away from resonances skipped and incorporated in the lower order W_n's. Expressions for the (q,p) can be obtained by calculating the operator T^{-1} and applying it to (Q,P).

3.8. Electron Motion for Non-Resonant Values of $v_\parallel$

If we use the explicitly time-dependent form of the Hamiltonian, and put $\Omega_{ti}^2 = \epsilon A_i$, we have

$$h(q,p,t) = h_o(q,p,t) + \epsilon h_1(q,p,t) \tag{3.56}$$

with

$$h_o = p^2/2, \quad h_1 = -\sum_{i=1}^{N} A_i \cos(q - \Omega_i t + \phi_i) \tag{3.57}$$

To study non-resonant terms, we ignore all resonances, and put in the K_n only constant terms. To get the simplest non-trivial transformation of coordinates we have to go up to second order in the perturbation expansion. Doing this, we get $K_o = h_o$ and $K_1 = 0$ (because h_1 has no constant terms).

This implies

$$W_1 = -\int^t d\tau\ h_1\left[Q+\Omega(\tau-t),P,\tau\right] = \sum_{i=1}^{N}\frac{A_i}{(P-\Omega_i)}\sin(Q-\Omega_i t+\phi_i) \tag{3.58}$$

since $\Omega = P$ for our h_o.

We then choose

$$2K_2 = \langle L_1 h_1\rangle = \langle\{W_1,h_1\}\rangle \tag{3.59}$$

where the pointed bracket operation means that the constant part of the function enclosed in brackets should be taken. A straightforward calculation shows that

$$\begin{aligned}\{W_1,h_1\} &= -\frac{\partial W_1}{\partial P}\frac{\partial h_1}{\partial Q}\\ &= -\sum_{i,j=1}^{N}\frac{A_iA_j}{2(P-\Omega_i)^2}\{\cos\left[2Q-(\Omega_i+\Omega_j)t+\phi_i+\phi_j\right]-\cos\left[(\Omega_i-\Omega_j)t-(\phi_i-\phi_j)\right]\}\end{aligned} \tag{3.60}$$

Therefore,

$$K_2 = \frac{1}{2}\langle\{W_1,h_1\}\rangle = \frac{1}{4}\sum_{i=1}^{N}\frac{A_i^2}{(P-\Omega_i)^2} \tag{3.61}$$

and

$$K = \frac{P^2}{2}+\frac{\epsilon^2}{4}\sum_{i=1}^{N}\frac{A_i^2}{(P-\Omega_i)^2} \tag{3.62}$$

The trasformation back to (q,p) is given by

$$q = Q+\epsilon\{W_1,Q\}+\frac{\epsilon^2}{2}\{W_1,\{W_1,Q\}\}+\ldots \tag{3.63}$$

$$p = P+\epsilon\{W_1,P\}+\frac{\epsilon^2}{2}\{W_1,\{W_1,P\}\}+\ldots \tag{3.64}$$

Keeping only first order terms and constant second order terms,

$$q = Q-\epsilon\frac{\partial W_1}{\partial P}-\frac{\epsilon^2}{2}\langle\{W_1,\frac{\partial W_1}{\partial P}\}\rangle \tag{3.65}$$

$$p = P+\epsilon\frac{\partial W_1}{\partial Q}+\frac{\epsilon^2}{2}\langle\{W_1,\frac{\partial W_1}{\partial Q}\}\rangle \tag{3.66}$$

and

$$q = Q+\epsilon\sum_{i=1}^{N}\frac{A_i}{(P-\Omega_i)^2}\sin(Q-\Omega_i t+\phi_i) \tag{3.67}$$

$$p = P-\frac{\epsilon^2}{2}\sum_{i=1}^{N}\frac{A_i^2}{(P-\Omega_i)^3}+\epsilon\sum_{i=1}^{N}\frac{A_i}{(P-\Omega_i)}\cos(Q-\Omega_i t+\phi_i) \tag{3.68}$$

Hamilton's equations of motion for K can be solved :

$$\dot{P} = -\frac{\partial K}{\partial Q} = 0 \tag{3.69}$$

$$\dot{Q} = \frac{\partial K}{\partial P} = P - \frac{\epsilon^2}{2}\sum_{i=1}^{N}\frac{A_i^2}{(P-\Omega_i)^3} = \Omega \tag{3.70}$$

The solution is

$$P = P_o \approx \Omega \tag{3.71}$$

$$Q = \Omega t + Q_o \tag{3.72}$$

The meaning of Ω (and Q_o) can be obtained by noting that $Q \to q$ as $\epsilon \to 0$. For a free electron, q represents the angular position of the electron measured from the reference wave as the electron propagates along the $-z$ direction. We will consider electrons with a $v_\parallel$ such that its motion is in resonance with an infinitesimally weak wave of frequency $\Delta\omega$ above the reference wave frequency (this imposes no constraint on the motion). If the electron is in resonance with such a wave, their relative angular position will be constant, and the electron's angular position with respect to the reference wave will be the difference in phase between the two waves, $\Delta\theta$. This expression is known from equations (3.9) and (3.11), allowing us to write

$$Q = q = \Delta\theta = \Omega(t - t_o) + \Delta\omega t_o - \Delta\phi = \Delta\omega t_o + q_{z_o} \tag{3.73}$$

We see that Ω is the Doppler shifted frequency difference of the two waves seen by the electron as it moves along. $(t - t_o)$ is the constant time it takes each electron to go from the beginning of the interaction region to the point of observation, z_o. Substituting those values in the expressions for q and p,

$$q = \Delta\omega t_o + q_{z_o} + \epsilon\sum_{i=1}^{N}\frac{A_i}{(\Omega-\Omega_i)^2}\sin\left[(\Delta\omega - \Delta\omega_i)t_o + \phi_{z_o}\right] \tag{3.74}$$

$$p = \Omega + \epsilon\sum_{i=1}^{N}\frac{A_i}{(\Omega-\Omega_i)}\cos\left[(\Delta\omega - \Delta\omega_i)t_o + \phi_{z_o}\right] \tag{3.75}$$

where $\phi_{z_o} = (\Omega - \Omega_i)(t - t_o) - (\Delta\phi - \Delta\phi_i)$ and q_{z_o} are arbitrary but constant phases at the point of observation z_o. The equations state that a stream of electrons starting with a constant phase relative to the infinitesimally weak wave of frequency $\Delta\omega$ will in the limit $\epsilon \to 0$, have an intersection with the plane $z_o = -v_\parallel(t - t_o)$ which turns, as t_o varies, with angular velocity $\omega = \omega_r + \Delta\omega$. If those streams are initially equally distributed in phase, the resulting intersection will form a DC current loop and will not radiate, as expected. If $\epsilon > 0$, the equations predict conditionally periodic changes away from constant frequency rotation. Those distortions are the first order approximation to the bunching created by the incoming waves outside their potential wells. Each term in the summation represents the effect on the electron of one wave, and will produce radiation at the perturbing wave frequency. Because we have kept only the first order terms, the effects add up linearly, and the bunching from one wave does not affect the bunching created by the others.

An important effect, here due to the adiabatic invariance of P, must also be noted: If we average away the oscillatory terms, and assume that a certain particle has $p = P = \Omega_o$ for $\epsilon = 0$, and that the wave fields are adiabatically turned on, then P will remain constant, and p will vary as:

$$p = \Omega_o - \frac{\epsilon^2}{2}\sum_{i=1}^{N}\frac{A_i^2}{(\Omega_o - \Omega_i)^3} \tag{3.76}$$

The particle will be shifted due to the presence of the waves, the forces being such that each wave tends to pull the particle towards it. The combination of such an effect with the natural fall-off of the electron distribution density with increasing $v_{\|}$ (that is, increasing ω), can explain why sideband growth is more pronounced on the upper frequency side of a carrier. Figure 3.8 shows the effect of a single wave on the electron distribution. The electron shift flattens it on the low frequency side, and steepens it on the high frequency side. Since wave growth increases with the electron density gradient, growth will be expected to be more noticeable on the high frequency side of the carrier as is seen in most Siple data.

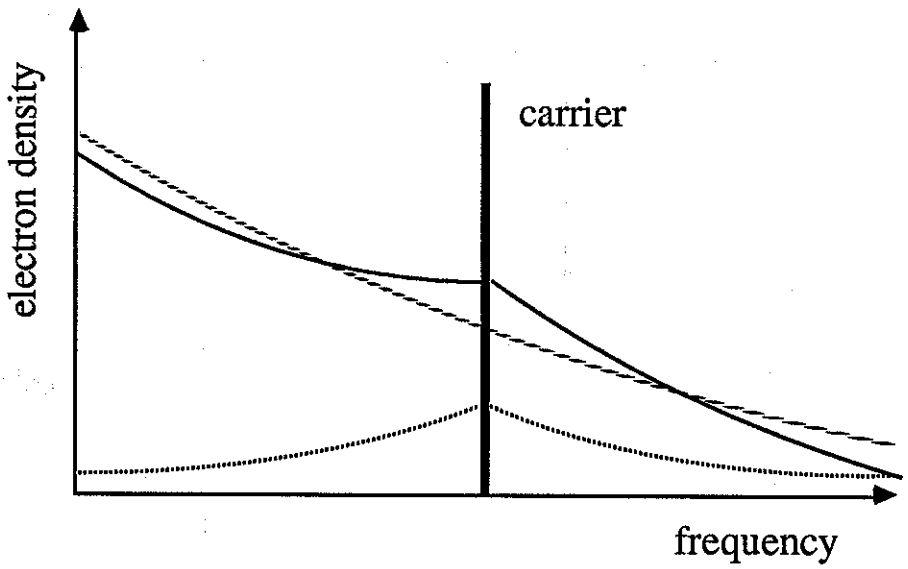

Fig. 3.8. Distortion of electron distribution by electromagnetic wave. The dotted line shows the effect of the carrier on an otherwise constant electron distribution. The dashed line represents a typical unperturbed distribution. The continuous line shows the resulting flattening at lower frequencies and steepening at the higher frequencies present on the final electron distribution as a consequence of the wave forces.

3.9. Half Harmonic Resonance

If we look for resonances using the perturbation expansion up to second order, we will get first :

$$K_o = h_o \tag{3.77}$$

We will have then to put

$$K_1 = 0 \tag{3.78}$$

because h_1 has resonances only for $\dot{Q} \approx \Omega_i$. Those are resonances at the incoming waves' frequencies which we do not intend to study now. They will be focused in chapter 4 with the help of different canonical variables.

With those choices, W_1 will be the same as for the non-resonant case. The possible second order resonances will come from the term $L_1 h_1$. This term was already calculated (equation (3.60)), and is made up of two sums. The second sum contains, among other things, a constant term which we must include in K_2. The first, has several resonances, all of the same form. We will study one such resonance for a pair of waves $(i,j), i \neq j$. (For $i = j$ the resonance again falls on one of the incoming carriers). By choosing

$$2K_2 = \frac{1}{2}\sum_{i=1}^{N} \frac{A_i^2}{(P-\Omega_i)^2} - \left[\frac{A_i A_j}{2(P-\Omega_i)^2} + \frac{A_i A_j}{2(P-\Omega_j)^2}\right] \cos\left[2Q - (\Omega_i + \Omega_j)t + \phi_i + \phi_j\right] \quad (3.79)$$

and defining $\Omega_{\frac{1}{2}} = (\Omega_i + \Omega_j)/2$, we get,

$$K = \frac{P^2}{2} + \frac{\epsilon^2}{4}\sum_{i=1}^{N} \frac{A_i^2}{(P-\Omega_i)^2} - \frac{\epsilon^2 A_i A_j}{4}\left[\frac{1}{(P-\Omega_i)^2} + \frac{1}{(P-\Omega_j)^2}\right] \cos(2Q - 2\Omega_{\frac{1}{2}}t + \phi_i + \phi_j) \quad (3.80)$$

Hamilton's equations applied to K, will give:

$$\dot{Q} = \frac{\partial K}{\partial P} = P - \frac{\epsilon^2}{2}\sum_{i=1}^{N} \frac{A_i^2}{(P-\Omega_i)^3} + \mathcal{O}(P - \Omega_{\frac{1}{2}}) \quad (3.81)$$

$$\dot{P} = -\frac{\partial K}{\partial Q} = -\frac{\epsilon^2 A_i A_j}{2}\left[\frac{1}{(P-\Omega_i)^2} + \frac{1}{(P-\Omega_j)^2}\right] \sin(2Q - 2\Omega_{\frac{1}{2}}t + \phi_i + \phi_j) \quad (3.82)$$

Since we are considering only points close to the resonance,

$$P \approx \dot{Q} \approx \Omega_{\frac{1}{2}} \quad (3.83)$$

and the equation of motion will be

$$\Delta\ddot{Q} = -\frac{8\epsilon^2 A_i A_j}{(\Omega_i - \Omega_j)^2} \sin(\Delta Q) \quad (3.84)$$

with

$$\Delta Q = 2Q - 2\Omega_{\frac{1}{2}}t + \phi_i + \phi_j \quad (3.85)$$

This is the familiar pendulum equation, describing a resonance region of width (in the variable Q)

$$\Gamma_{\frac{1}{2}} = \frac{4\sqrt{2}\epsilon\sqrt{A_i A_j}}{|\Omega_i - \Omega_j|} \quad (3.86)$$

The equilibrium points are given by $\Delta Q = 2n\pi$, or:

$$Q = \Omega_{\frac{1}{2}}t - \frac{\phi_i + \phi_j}{2} + n\pi, \; n = 0, 1 \quad (3.87)$$

Substituting ϕ_i and ϕ_j for their values, and defining:

$$\Delta\omega_{\frac{1}{2}} = (\Delta\omega_i + \Delta\omega_j)/2 \quad (3.88)$$

$$\phi_{ij} = \Omega_{\frac{1}{2}}(t - t_o) - \frac{\Delta\phi_i + \Delta\phi_j}{2} \quad (3.89)$$

we have,

$$Q = \Delta\omega_{\frac{1}{2}} t_o + \phi_{ij} + n\pi, \quad n = 0, 1 \tag{3.90}$$

ϕ_{ij} is a constant phase, dependent, however, on the point of observation z_o. The equation describes two resonances oppositely located in phase, which rotate in the Q direction with velocity $\Delta\omega_{\frac{1}{2}}$. Because the two branches are oppositely phased in the (Q, P) plane, we see that to obtain net radiation we will have to depend on the existence of different electron populations in each resonance branch. Expressed in terms of the original variables,

$$q = \Delta\omega_{\frac{1}{2}} t_o + \frac{\Delta Q}{2} + \phi_{ij} + \epsilon \sum_{k=1}^{N} \frac{A_k}{(\Omega_{\frac{1}{2}} - \Omega_k)^2} \sin\left[(\Delta\omega_{\frac{1}{2}} - \Delta\omega_k)t_o + \frac{\Delta Q}{2} + \phi_{ijk}\right] \tag{3.91}$$

$$p = \Omega_{\frac{1}{2}} + \frac{\Delta\dot{Q}}{2} + \epsilon \sum_{k=1}^{N} \frac{A_k}{(\Omega_{\frac{1}{2}} - \Omega_k)} \cos\left[(\Delta\omega_{\frac{1}{2}} - \Delta\omega_k)t_o + \frac{\Delta Q}{2} + \phi_{ijk}\right] \tag{3.92}$$

where ϕ_{ijk} does not depend on time. The $\Delta Q/2$ term in q, shows that the relative position of any two electrons can be changed by as much as π, making bunching effects appreciable.

The radiation from each charge can be obtained if we go to configuration space. Each charge is obtained by the intersection of the electron stream with the plane $z = z_o$. In that plane, each charge will be rotating with an angular velocity, ω, given by:

$$\omega = \frac{\partial q}{\partial t_o} + \omega_r \tag{3.93}$$

(Note that p is irrelevant for this calculation, since it describes each individual electron motion as it moves in the $-z$ direction, and we are interested in the stream at a fixed point). The radiation will be circularly polarised. To obtain the frequency spectrum, we will project the motion in the (x, z) plane. If we define

$$\omega_{\frac{1}{2}} = \omega_r + \Delta\omega_{\frac{1}{2}} = (\omega_i + \omega_j)/2, \tag{3.94}$$

$$\Delta\omega_{ijk} = \Delta\omega_{\frac{1}{2}} - \Delta\omega_k, \tag{3.95}$$

$$b_k = \frac{A_k}{(\Omega_{\frac{1}{2}} - \Omega_k)^2}, \tag{3.96}$$

and

$$\theta_1 = \sum_{k=1}^{N} b_k \sin(\Delta\omega_{ijk} t_o + \eta_k), \tag{3.97}$$

we can write

$$\theta = \omega_{\frac{1}{2}} t_o + \frac{\Delta Q}{2} + \phi_{ij} + \epsilon\theta_1. \tag{3.98}$$

To first order the electron's acceleration along x will be

$$\ddot{x} = -r\omega_{\frac{1}{2}}^2 \cos\theta = -r\omega_{\frac{1}{2}}^2 \cos(\omega_{\frac{1}{2}} t_o + \frac{\Delta Q}{2} + \phi_{ij}) + \epsilon\theta_1 r\omega_{\frac{1}{2}}^2 \sin(\omega_{\frac{1}{2}} t_o) \tag{3.99}$$

or

$$\ddot{x} = -r\omega_{\frac{1}{2}}^2 \cos(\omega_{\frac{1}{2}} t_o + \frac{\Delta Q}{2} + \phi_{ij}) + \epsilon r\omega_{\frac{1}{2}}^2/2 \sum_{k=1}^{N} b_k \{\sin[(\omega_i + \Delta\omega_j - \Delta\omega_k)t_o + \eta_k] + \sin[\omega_k t_o - \eta_k]\} \tag{3.100}$$

The equation shows that radiation will be mainly produced at the frequency $\omega_{\frac{1}{2}}$, as should be expected by the location of the resonance in frequency space, but that there are smaller contributions at the frequencies ω_k and $\omega_i + \Delta\omega_j - \Delta\omega_k$, $k = 1 \ldots N$. Those are radiation on top of wave k and at the mirror image position of k in the interval defined by i and j. We will see that radiation at those frequencies is generated by other resonances in a more efficient way, and will therefore neglect those small corrections. With this approximation, we can consider all radiation coming from the half harmonic resonance as being located at the frequency $\omega_{\frac{1}{2}}$.

If both resonance branches are equally populated in the (Q,P) plane, for each particle with position ΔQ it is always possible to find an equivalent particle with position $\Delta Q + \pi$. Those particles have opposite accelerations and cancel each other's radiation in the z-direction. However, at the beginning of the interaction region the two branches will be located at slightly different positions in the (q,p) plane due to the distortion effects created by the incoming waves. If the electron distribution has a gradient in p different from zero, the population of the two branches will not be the same and a net amount of radiation will be produced (see Figure 3.7*c*). We note, also, that all points in the resonance radiate at the same frequency $\omega_{\frac{1}{2}}$, despite the resonance finite width, and that the 2-branch resonance structure is inconsistent with the presence of radiation. As soon as radiation starts, it will form an additional resonance, rotated by $-\pi/2$ from the radiating resonance, changing the initial electron motion and resonance configuration.

3.10. Third-Order Resonances

3.10.1. General Expressions

To look for third-order resonances, we choose K_o, K_1, W_1, and K_2 the same as in the non-resonant case. This implies

$$W_2 = \sum_{i,j=1}^{N} \frac{A_i A_j}{2(P-\Omega_i)^2\,[2P-(\Omega_i+\Omega_j)]} \sin\left[2Q-(\Omega_i+\Omega_j)t+\phi_i+\phi_j\right] - \sum_{\substack{i,j=1 \\ i\neq j}}^{N} \frac{A_i A_j}{2(P-\Omega_i)^2(\Omega_i-\Omega_j)} \sin\left[(\Omega_i-\Omega_j)t-(\phi_i-\phi_j)\right] \tag{3.101}$$

Among the third order terms, $L_1 K_2$ can be ignored for it contains resonances only at the incoming carriers' frequencies. Third order resonances must come, then, from the terms $L_2 h_1$ and $L_1^2 h_1$. After a straightforward but rather lengthy calculation they are found to be:

$$L_2 h_1 = \sum_{i,j,k=1}^{N} \frac{b_{ijk}}{2} \cos\left[3Q-(\Omega_i+\Omega_j+\Omega_k)t+\phi_i+\phi_j+\phi_k\right] + \sum_{i,j,k=1}^{N} \frac{a_{kji}-a_{ikj}-b_{ijk}}{2} \cos\left[Q-(\Omega_i+\Omega_j-\Omega_k)t+\phi_i+\phi_j-\phi_k\right] \tag{3.102}$$

$$L_1^2 h_1 = \sum_{i,j,k=1}^{N} \frac{c_{ijk}-d_{ijk}}{2} \cos\left[3Q-(\Omega_i+\Omega_j+\Omega_k)t+\phi_i+\phi_j+\phi_k\right] + \sum_{i,j,k=1}^{N} \frac{c_{ijk}-c_{kji}-c_{ikj}+d_{ijk}}{2} \cos\left[Q-(\Omega_i+\Omega_j-\Omega_k)t+\phi_i+\phi_j-\phi_k\right] \tag{3.103}$$

with

$$a_{ijk} = \frac{A_i A_j A_k}{(P-\Omega_i)^3(\Omega_i-\Omega_j)} \tag{3.104}$$

$$b_{ijk} = -\frac{A_i A_j A_k \left(3P-(2\Omega_i+\Omega_j)\right)}{(P-\Omega_i)^3\left[2P-(\Omega_i+\Omega_j)\right]^2} \tag{3.105}$$

$$c_{ijk} = \frac{A_i A_j A_k}{(P-\Omega_i)^3(P-\Omega_k)} \tag{3.106}$$

$$d_{ijk} = \frac{A_i A_j A_k}{(P-\Omega_i)^2(P-\Omega_k)^2} \tag{3.107}$$

K_3 will have to be chosen from the terms in

$$\begin{aligned}\frac{L_2 h_1 + L_1^2 h_1}{6} = &\sum_{i,j,k=1}^{N} \alpha_{ijk}\cos\left[3Q-(\Omega_i+\Omega_j+\Omega_k)t+\phi_i+\phi_j+\phi_k\right]+ \\ &\sum_{i,j,k=1}^{N} \beta_{ijk}\cos\left[Q-(\Omega_i+\Omega_j-\Omega_k)t+\phi_i+\phi_j-\phi_k\right]\end{aligned} \tag{3.108}$$

For $i=j=k$ all terms in the above expression are resonant at the incoming carriers' positions and are not of interest. We must pick terms with at least one index different from the other remaining two. They will provide the third order resonances we are looking for.

3.10.2. Two-Wave Resonances

One-Third Subharmonic.

For $i=j\neq k$, the term symmetrical under permutation of the three indices gives:

$$K_3 = (\alpha_{iik}+\alpha_{kii}+\alpha_{iki})\cos\left[3Q-(2\Omega_i+\Omega_k)t+2\phi_i+\phi_k\right] \tag{3.109}$$

Defining $\Omega_{\frac{2}{3}} = (2\Omega_i+\Omega_k)/3$, and calculating the α's:

$$K_3 = -\frac{243A_i^2A_k}{16(\Omega_i-\Omega_k)^4}\cos\left(3Q-3\Omega_{\frac{2}{3}}t+2\phi_i+\phi_k\right) \tag{3.110}$$

The Hamiltonian will be:

$$K = \frac{P^2}{2}+\frac{\epsilon^2}{4}\sum_{i=1}^{N}\frac{A_i^2}{(P-\Omega_i)^2}-\epsilon^3\frac{243A_i^2A_k}{16(\Omega_i-\Omega_k)^4}\cos\left(3Q-3\Omega_{\frac{2}{3}}t+2\phi_i+\phi_k\right) \tag{3.111}$$

which will give the equation of motion:

$$\Delta\ddot{Q} = -\epsilon^3 9\frac{243A_i^2A_k}{16(\Omega_i-\Omega_k)^4}\sin(\Delta Q) \tag{3.112}$$

with

$$\Delta Q = 3Q-3\Omega_{\frac{2}{3}}t+2\phi_i+\phi_k \tag{3.113}$$

The motion will have three points of equilibrium for $\Delta Q = 2n\pi$, indicating a three-lobed resonance in Q:

$$Q = \Omega_{\frac{2}{3}}t-\frac{2\phi_i+\phi_k}{3}+\frac{2n\pi}{3},\ n=0,1,2 \tag{3.114}$$

In terms of t_o,

$$Q = \Delta\omega_{\frac{2}{3}} t_o + \Omega_{\frac{2}{3}}(t - t_o) - \frac{2\Delta\phi_i + \Delta\phi_k}{3} + \frac{2n\pi}{3},\ n = 0, 1, 2 \tag{3.115}$$

with $\Delta\omega_{\frac{2}{3}} = (2\Delta\omega_i + \Delta\omega_k)/3$. Observed at a fixed point in space, the resonance will rotate and radiate at:

$$\omega_{\frac{2}{3}} = \omega_r + \Delta\omega_{\frac{2}{3}} = \frac{(2\omega_i + \omega_k)}{3} \tag{3.116}$$

and will create a line in the frequency axis 2/3 of the way from wave i towards j. Since the labeling of the waves is arbitrary, there will be another resonance, identical to this one, but with wave indices permutated. It will be a resonance creating a sideband wave at a frequency 1/3 of the way from i to j. The full width of the first resonance in the (Q, P) plane will be:

$$\Gamma_{\frac{2}{3}} = 9\sqrt{3}\frac{\epsilon^{\frac{3}{2}} A_i \sqrt{A_k}}{(\Omega_i - \Omega_k)^2} \tag{3.117}$$

and of the second one,

$$\Gamma_{\frac{1}{3}} = 9\sqrt{3}\frac{\epsilon^{\frac{3}{2}} A_k \sqrt{A_i}}{(\Omega_i - \Omega_k)^2} \tag{3.118}$$

The different dependence of each resonance on the variables A_k and A_i is clearly very important when one of the carriers in the interacting pair is much weaker than the other.

First Harmonic Resonance

Again assuming $i = j \neq k$ in equation (3.108), we find from the term asymmetrical in i, j, k the following resonance:

$$K_3 = \beta_{iik} \cos\left[Q - (2\Omega_i - \Omega_k)t + 2\phi_i - \phi_k\right] \tag{3.119}$$

If we define $\Omega_{1h} = (2\Omega_i - \Omega_k)$, and calculate β_{iik},

$$K_3 = -\frac{A_i^2 A_k}{16(\Omega_i - \Omega_k)^4} \cos\left(Q - \Omega_{1h} t + 2\phi_i - \phi_k\right) \tag{3.120}$$

The full Hamiltonian will be:

$$K = \frac{P^2}{2} + \frac{\epsilon^2}{4}\sum_{i=1}^{N} \frac{A_i^2}{(P - \Omega_i)^2} - \epsilon^3 \frac{A_i^2 A_k}{16(\Omega_i - \Omega_k)^4} \cos\left(Q - \Omega_{1h} t + 2\phi_i - \phi_k\right) \tag{3.121}$$

In a way similar to the one-third subharmonic, we get the equation of motion:

$$\Delta\ddot{Q} = -\epsilon^3 \frac{A_i^2 A_k}{16(\Omega_i - \Omega_k)^4} \sin(\Delta Q) \tag{3.122}$$

with

$$\Delta Q = Q - \Omega_{1h} t + 2\phi_i - \phi_k \tag{3.123}$$

There is only one equilibrium point, $\Delta Q = 0$, and only one lobe in this resonance (making it a more efficient radiation source). For the equilibrium point, as a function of t_o, we have:

$$Q = \Delta\omega_{1h} t_o + \Omega_{1h}(t - t_o) - (2\Delta\phi_i - \Delta\phi_k) \tag{3.124}$$

where $\Delta\omega_{1h} = (2\Delta\omega_i - \Delta\omega_k)$. The resonance has width

$$\Gamma_{1h} = \frac{\epsilon^{\frac{3}{2}} A_i \sqrt{A_k}}{(\Omega_i - \Omega_k)^2} \tag{3.125}$$

and rotates with frequency

$$\omega_{1h} = \omega_r + \Delta\omega_{1h} = \omega_i + (\omega_i - \omega_k) \tag{3.126}$$

The radiation will be a first harmonic of the two wave frequency separation, located next to wave i. Again, because the labeling is arbitrary, there will be another first harmonic resonance next to wave k, rotating with frequency $\omega_k + (\omega_k - \omega_i)$ and having width $\epsilon^{\frac{3}{2}} A_k \sqrt{A_i}/(\Omega_i - \Omega_k)^2$.

3.10.3. Three-Wave Effects

Arithmetic Mean

Assuming $i \neq j, j \neq k, k \neq i$ we get from the symmetrical term a single type of interaction:

$$K_3 = (\alpha_{ijk} + \alpha_{jik} + \alpha_{ikj} + \alpha_{kij} + \alpha_{kji} + \alpha_{jki}) \cos\left[3Q - (\Omega_i + \Omega_j + \Omega_k)t + \phi_i + \phi_j + \phi_k\right] \tag{3.127}$$

which can be calculated to give:

$$K_3 = -\frac{3^5}{2} \frac{A_i A_j A_k (\Delta_{ij}^2 + \Delta_{ij}\Delta_{jk} + \Delta_{jk}^2)}{(2\Delta_{ij} + \Delta_{jk})^2 (2\Delta_{jk} + \Delta_{ij})^2 (\Delta_{ij} - \Delta_{jk})^2} \cos\left[3Q - (\Omega_i + \Omega_j + \Omega_k)t + \phi_i + \phi_j + \phi_k\right] \tag{3.128}$$

where $\Delta_{ij} = \Omega_i - \Omega_j$ and $\Delta_{jk} = \Omega_j - \Omega_k$. This resonance has a three lobe structure similar to the one-third subharmonic, and radiates at the frequency

$$\omega = \frac{\omega_i + \omega_j + \omega_k}{3} \tag{3.129}$$

that is, at the average frequency of the three waves. The resonance width will be

$$\Gamma_{arith} = 2\sqrt{2}\epsilon^{\frac{3}{2}} \left[\frac{3^5 A_i A_j A_k (\Delta_{ij}^2 + \Delta_{ij}\Delta_{jk} + \Delta_{jk}^2)}{(2\Delta_{ij} + \Delta_{jk})^2 (2\Delta_{jk} + \Delta_{ij})^2 (\Delta_{ij} - \Delta_{jk})^2} \right]^{\frac{1}{2}} \tag{3.130}$$

The denominator is divergent, effectively increasing the resonance width up to second order when one of the two waves is approximately halfway between the other two. The perturbation expansion will break down (due to the formation of chaotic motion) when the resonances associated with any two waves begin to overlap. This imposes a minimum displacement of the sideband location away from wave j: $P \approx \Omega_j + 2\sqrt{\epsilon A_j}$. This implies $\Delta_{ij} - \Delta_{jk} \approx 6\sqrt{\epsilon A_j}$, and $|\Delta_{ij}| \approx |\Delta_{ik}|/2$. The resonance width will be under those conditions approximately equal to

$$\Gamma_{arith} \approx \frac{2\epsilon\sqrt{2A_i A_k}}{|\Delta_{ik}|} \tag{3.131}$$

which is of the order of the half harmonic resonance width.

Intermodulation Effects

For $i \neq j, j \neq k, k \neq i$, we get from the asymmetrical term in equation (3.108):

$$K_3 = (\beta_{ijk} + \beta_{ijk}) \cos[Q - (\Omega_i + \Omega_j - \Omega_k)t + \phi_i + \phi_j - \phi_k] \tag{3.132}$$

which gives, when the coefficients are calculated:

$$K_3 = -\frac{1}{2} \frac{A_i A_j A_k}{\Delta_{ik}\Delta_{jk}(\Delta_{ik} + \Delta_{jk})^2} \cos[Q - (\Omega_i + \Omega_j - \Omega_k)t + \phi_i + \phi_j - \phi_k] \tag{3.133}$$

The above term creates three different resonances, depending on the wave that is singled out as wave k. All resonances have a single lobe and, therefore, are efficient radiators. Figure 3.9 shows the three possible radiation frequencies. The effect is equivalent to the intermodulation of one wave by the frequency difference of the other two, either sign being possible. The frequencies of radiation will be

$$\omega = \omega_i + (\Delta\omega_j - \Delta\omega_k) = \omega_i + (\omega_j - \omega_k) \tag{3.134}$$

and the resonance widths will be :

$$\Gamma_{int} = \frac{2\epsilon^{\frac{3}{2}}\sqrt{2A_iA_jA_k}}{\sqrt{|\Delta_{ik}||\Delta_{jk}|}|\Delta_{ik} + \Delta_{jk}|} \tag{3.135}$$

When wave k is approximately halfway between the other two interacting waves, the resonance width increases without bounds. If wave k is specially weak, the observed phenomenon will be similar to an amplification of the said wave with a slight shift in its frequency. The limiting position of the resonance is given by $P \approx \Omega_k - 2\sqrt{\epsilon A_k}$. This implies $\Delta_{ik} + \Delta_{jk} \approx -2\sqrt{\epsilon A_k}$, and $\Delta_{ik} \approx \Delta_{kj} \approx \Delta_{ij}/2$.

The resonance width will be approximately

$$\Gamma_{int} \approx \frac{2\epsilon\sqrt{2A_iA_j}}{|\Delta_{ij}|} \tag{3.136}$$

which is of the order of the half harmonic resonance width. Under those conditions, and due partly to its single-lobe structure, this resonance will be the most efficient radiator among all we have seen in this chapter.

3.11. Higher Order Effects

It can be seen from the lower order terms and from the way they are generated that the general expression for the resonance frequencies of order n will be given by equation (3.34) with $\sum_{i=1}^{N} |n_i| = n$ as a constraining condition. This shows that an nth order effect can involve at most n different waves.

The expression for the frequency of the second harmonic resonance of a pair of waves (i, j) is $\Omega = \Omega_i + 2(\Omega_i - \Omega_j)$. The order of this term will be $n = |3| + |-2| = 5$. The second harmonic is, therefore, a 5^{th} order effect, and very likely will not produce directly observable radiation. Its creation through the present mechanism can be possible only through a two step process in which the first harmonic is created, grows, and then interacts with one of the carriers to produce another first harmonic which is the second harmonic we are looking for.

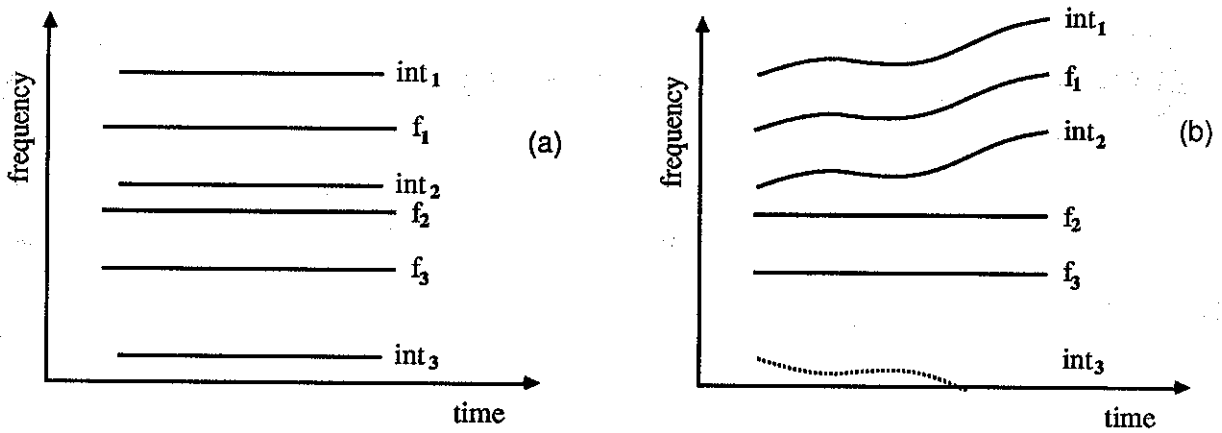

Fig. 3.9. Frequency distribution of sidebands created by third order intermodulation process: (a) f_1, f_2, and f_3 are incoming carriers and int_1, int_2, and int_3 are the three different sideband waves produced by the intermodulation process. For the spacings shown in the picture, int_2 is always greater in amplitude than int_1 and int_3. (b) Intermodulation is a non-local effect. If f_1 has variable frequency, the sideband waves created by the interaction are able to follow its shift in frequency, despite the fact that f_2 and f_3 remain fixed. int_3 is represented by a dotted line because it weakens as f_1 moves up.

3.12. Conclusions

As main features of the sidebands just studied, we can quote:

1. Sidebands are created only by a line-line interaction process. No single-line sidebands appear in the formalism.
2. Sidebands can be created only at certain specific frequencies given by

$$\omega = \frac{\sum_{i=1}^{N} n_i \omega_i}{\sum_{i=1}^{N} n_i} \tag{3.34}$$

3. Sidebands can be created only if the electron distribution has a non-zero gradient in $v_{\parallel}$.
4. Each sideband wave is associated with a resonance of the electron motion which, in an adequate system of coordinates, is always described by the pendulum equation.
5. Radiated sideband frequencies do not depend on $v_{\perp}$, only the amplitudes do. Integration over different pitch angles will not smear out the resonances increasing the radiation linewidth.
6. The frequency of individual electron oscillations ("trapping" oscillations) does not directly affect the observed sideband frequencies in any way. Those oscillations are convective, occurring as the electrons, as part of a stream, move along the interaction region. Although each electron oscillates, the stream as a whole constitutes a DC current line and will not radiate unless

distorted or accelerated by some additional cause. The overall emitted radiation will be a combined result from the acceleration of all such current lines, and its spectrum will reflect the frequency structure of the externally accelerating forces.

7. Growth will affect line amplitudes appreciably. The resonance widths calculated in this chapter will give only an order of magnitude estimate of the observed relative radiation intensities.
8. Due to its recurrent law of formation, the sideband system has a fractal structure, exhibiting many properties associated with randomness. Only for cases where the recurrence process of new wave formation stops due to limited wave growth, do we obtain spectra with a clearly recognizable order in the frequency distributions.
9. Chaos, present when the potential wells of different waves start to overlap, as seen in Figure 3.6, is an important factor in the formation of the final radiation spectra. This author believes that, combined with inhomogeneity effects, chaos is the cause for the triggered emissions frequently associated with Siple, and other narrow bandwidth, signals as they propagate through the magnetosphere (see section 6.2 for some conjectures on the subject).

In this chapter we have focused on resonances created outside the potential wells of a set of single-frequency carriers interacting with the ionospheric plasma. Those resonances are narrower than the ones directly associated with each carrier, and are, therefore, more susceptible to disruption by forces coming from the inhomogeneity of the Earth's magnetic field. In chapter 4, we will see that radiation, at the same frequencies as the ones we have studied in this first part, can also be created by resonances inside each carrier potential well. Those resonances are more protected from inhomogeneity effects and should produce radiation over a longer interaction length than the ones considered here.

4. Description of Internal ("Trapped") Resonances

4.1. Introduction

In this chapter we will concentrate on the study and classification, together with an analysis of the sideband radiation they produce, of cyclotron resonances created by the electromagnetic fields of an incoming set of carriers acting on plasma electrons inside the carriers' own potential wells ("trapped" resonances). A previous reading of chapter 3 is recommended, since the same analytical methods are used to solve the equations describing the electron motion and the same type of phase plots are used for displaying numerical results. Most of the notation used in this chapter is identical to the one used and defined in chapter 3.

We begin chapter 4 by displaying, in section 4.2, "trapped" resonances with the help of phase plots, and discussing qualitatively the process of radiation formation. In section 4.3, as a preparation for the work to follow, the equations describing the electron motion are rewritten using action-angle variables which are more adequate for the study of motion inside the potential wells. The KAM theorem is applied in section 4.4 to the Hamiltonian expressed in action-angle variables and general expressions for the resonant frequencies of motion and associated radiation frequencies are obtained. In section 4.5, the Lie perturbation method is applied to solve the equation of motion for non-resonant electrons. Section 4.6 describes analytically an infinite set of first order resonances coming from the interaction of any wave pair in the incoming wave packet and radiating mainly at their first harmonic frequencies. Weaker radiation at the subharmonic frequencies is also obtained. Section 4.7 describes two- and three-wave second order effects. Two-wave effects consist of the second harmonic and a series of subharmonics. Three-wave effects contain intermodulation effects, together with the infinite series of their associated subharmonics. Section 4.8 describes sideband interference effects due to the direct interaction of resonances located inside a same wave potential. Section 4.9 looks at higher order effects, and section 4.10 contains the conclusions.

4.2. Phase Plots and the Process of Radiation Formation

Figure 4.1 shows the time evolution of one of the trapped resonances we are going to study, seen by an observer at a fixed point in space. The resonance is created by a main wave, inside whose potential well it oscillates, and by a weaker wave not visible in the plot. The resonance motion is phase-locked to the weaker perturbing carrier and its rotation is at twice the carrier-carrier frequency difference as is indicated by the vector diagrams at the corner of the pictures (it is a second harmonic resonance). The trapping frequency of the main carrier is slightly higher than twice the two-carrier frequency difference, as should be expected, since the average rotation frequency of the resonant electrons is undisturbed by the presence of the resonance. A band of chaotic motion is seen around the resonance, and will be present in all cases where internal resonances are formed. Electrons in this chaotic band cannot be bunched, and its presence will contribute to the main carrier saturation by limiting its growth. We will see in the following sections that radiation from this trapped resonance will fall mainly outside the carrier potential well. Those two facts imply that, for this value of the

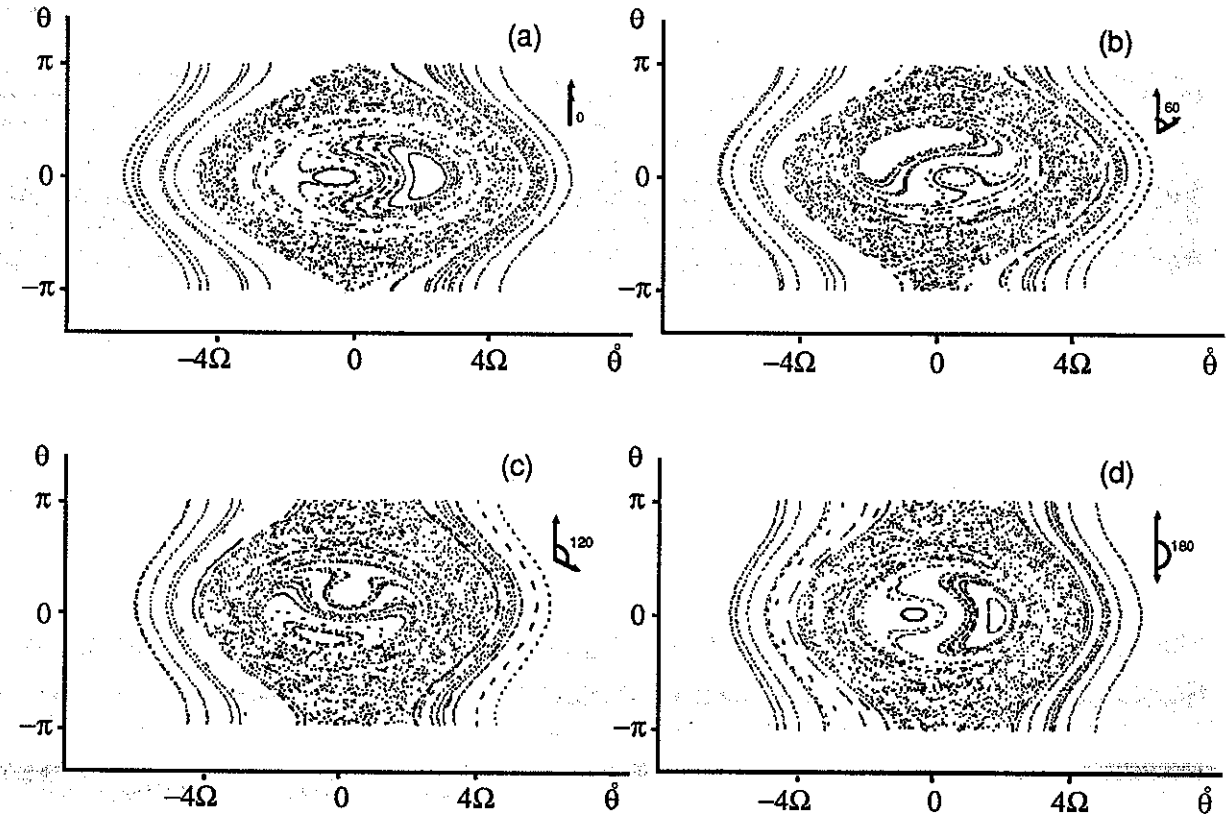

Fig. 4.1. Trapping resonance created by two interacting carriers. The main carrier is located at $\dot{\theta} = 0$ and the weaker, perturbing one, at $\dot{\theta} = \Omega$. The main carrier trapping frequency is $\approx 2\Omega$, and the weak to main carrier amplitude ratio is 0.2. As the carriers rotate relatively to each other, the internal resonance rotates at twice their frequency separation: (a) Relative carrier phase = 0°. (b) Relative carrier phase = 60°. (c) Relative carrier phase = 120°. (d) Relative carrier phase = 180°.

trapping frequency, few of the electrons that are directly affected by the main wave will radiate at its frequency. In other words, for this electron population, the main wave has practically saturated due to the presence of the weaker perturbing carrier. On the other hand, the weaker carrier is located inside the main carrier potential well, one quarter of the way from the center to the separatrix, but no resonance directly associated with its presence is seen. This means that the weaker carrier is not able to bunch electrons on its own and grow. We say that, under those circumstances, the weak carrier growth has been suppressed by the strong carrier.

The radiation process can be understood if we remind ourselves, from chapter 3, that resonances, coupled to the existence of an electron concentration gradient in $v_{\parallel}$ at all points in space, can cause bunching when they act on the convective motion of the electrons moving along the duct. Observed at a fixed point in space, the trappped resonance will exhibit some bunching causing a localized perturbation inside the potential well. Now, the resonance is phase-locked to the weak carrier, and,

as time flows, its position, together with the perturbation in electron concentration associated with it, will oscillate inside the main carrier potential well. This oscillation will modulate in frequency the radiation produced by the main carrier, creating sidebands. An important fact to be noticed is that the radiation process is a collective phenomenon coming from oscillations of distorted electron concentrations inside the potential well, occurring as a function of time at a fixed point in space, independently of the existence of full oscillations for individual electrons as they move along the duct.

Figures 4.2.a and 4.2.b have a pictorial description of the resonance radiation mechanism. We assume that the internal resonance, due to the disturbances it creates in the electron concentration, constitutes a localized source of radiation, with a periodically varying frequency. If the carrier has frequency ω_1 and the resonance turns inside the carrier wave potential with frequency $\Delta\omega$, radiation will be observed at frequencies $\omega = \omega_1 \pm n\Delta\omega,\ 0 \leq n < \infty$ as a consequence of the frequency modulation process.

Figures 4.2.c and 4.2.d show the case when the internal resonance has two lobes. Each lobe will radiate the same frequency spectrum shifted in phase by 180°. The modulation around the carrier frequency will now repeat itself twice as fast, creating a spectrum of lines separated from each other by the frequency $2\Delta\omega$ if the perturbations in electron concentration are exactly the same for the two lobes. If some difference occurs, due e.g. to variable distortions caused by the perturbing carrier, the spectrum will also have odd multiples of $\Delta\omega$ which will show up as weak half harmonics between the main even multiples of $\Delta\omega$.

4.3. Electron Equation of Motion in Action-Angle Variables

From chapter 3, we know that the equations describing the electron motion under the influence of N waves are

$$\ddot{\theta} = -\sum_{i=1}^{N} \Omega_{ti}^2 \sin(\theta - \Omega_i t + \phi_i) \tag{4.1}$$

$$\Omega_i = (\frac{v_\parallel}{v_g} + 1)\Delta\omega_i, \tag{4.2}$$

$$\phi_i = (\Omega_i - \Delta\omega_i)t_o + \Delta\phi_i \tag{4.3}$$

where $\Omega_{ti}^2 = ev_\perp k_1 B_i/m$ is the square of the trapping frequency associated with wave i, Ω_i is the Doppler shifted frequency difference between wave i and reference wave 1, and v_g is the wave group velocity at the average radiation frequency.

For the study of internal resonances created by the wave-wave interaction process, it will be extremely convenient to single out one of the waves, that can always be wave 1 by an appropriate labeling of the carriers, and rewrite the equation of motion using (j, ϕ), action-angle variables for electron motion under the influence of that single wave. The meaning of (j, ϕ) can be seen from Figure 4.3 and the defining equations:

$$j = \frac{1}{2\pi} \oint \dot{\theta} d\theta = \frac{2\theta_{MAX}}{\pi} \langle \dot{\theta} \rangle \tag{4.4}$$

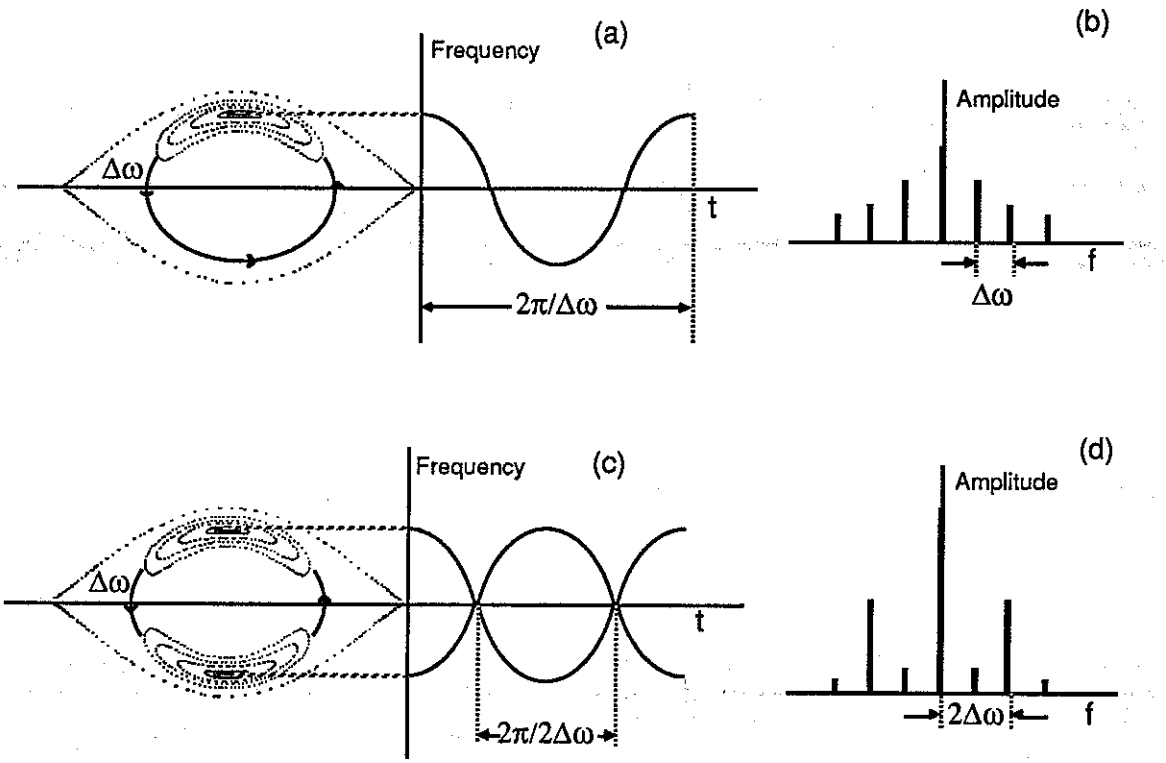

Fig. 4.2. Radiation from oscillating trapped resonance: (a) As the resonance oscillates with frequency $\Delta\omega$ in the potential well, it creates variable frequency radiation with period $2\pi/\Delta\omega$. (b) Demodulation shows a spectrum of lines separated by $\Delta\omega$. (c) If the resonance is two-lobed, the radiation will have a period of $2\pi/(2\Delta\omega)$. (d) Demodulation will show lines separated by a frequency $2\Delta\omega$. Since the two resonance populations are not identical, weak half harmonics will be found between any two main harmonics.

j is proportional to the average value of $\dot{\theta}$ over the electron phase space trajectory and equal to the area enclosed by the trajectory divided by 2π. ϕ is defined from the main wave trapping oscillation frequency:

$$\phi = \Omega_t(j)(t - t_o) \tag{4.5}$$

ϕ goes through one cycle in the same time the electron goes through one oscillation inside the potential well, and can be thought of as describing the phase of the motion. By an appropriate choice of t_o, the relation between θ and ϕ is:

$$\theta = 2\sin^{-1}\left[\kappa \,\mathrm{sn}\left(\frac{2K(\kappa)\phi}{\pi}\right)\right] \tag{4.6}$$

with sn the Jacobian sine function and K the complete elliptic integral of the first kind. κ is defined by

$$\kappa^2 = (1 + h_o/\Omega_{t1}^2)/2, \tag{4.7}$$

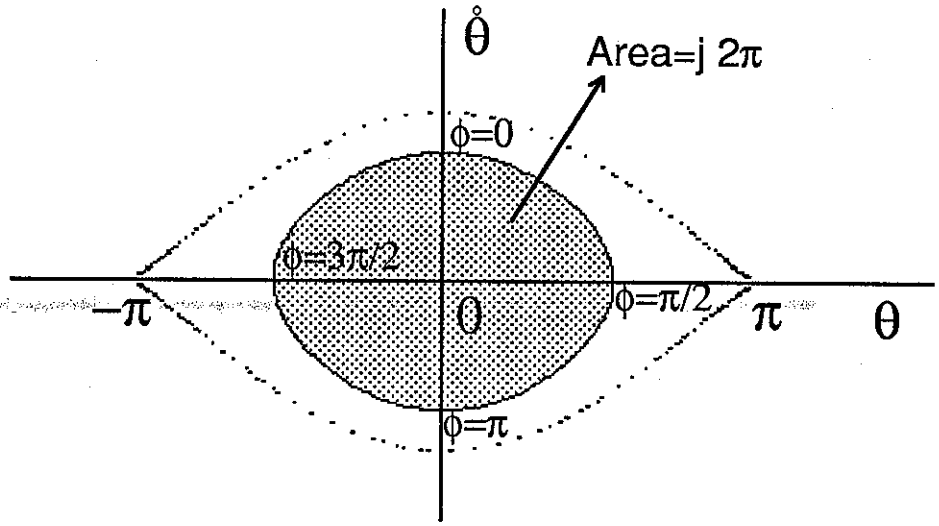

Fig. 4.3. Action-angle variables used for description of trapped resonances. $2\pi j$ is the area enclosed by the phase trajectory and ϕ is the phase of the motion. Although $\dot{\phi}$ is a constant, $\dot{\theta}$ has a complex dependence on time.

h_o being the energy of the motion. j is given by

$$j = \frac{8\Omega_{t1}}{\pi}\left[E(\kappa) - (1-\kappa^2)K(\kappa)\right] \tag{4.8}$$

where E is the complete elliptic integral of the second kind. The trapping frequency can be expressed as

$$\Omega_t(j) = \frac{\Omega_{t1}\pi}{2K(\kappa)}, \quad 0 \le \Omega_t(j) \le \Omega_{t1} \tag{4.9}$$

Written in Hamiltonian form the equation of motion becomes:

$$h = \dot{\theta}^2/2 - \Omega_{t1}^2\cos\theta - \sum_{i=2}^{N}\Omega_{ti}^2\cos(\theta - \Omega_i t + \phi_i) \tag{4.10}$$

As a function of (j,ϕ), it can be rewritten as:

$$h(j,\phi) = h_o(j) - \sum_{i=2}^{N}\Omega_{ti}^2\cos\left[\theta(\phi) - \Omega_i t + \phi_i\right] \tag{4.11}$$

The cos terms inside the summation can be explicitly written as a function of (j,ϕ). This was done in *Smith and Pereira* [1978] and the result is reproduced here:

$$\cos\left[\theta(\phi) - \Omega_i t + \phi_i\right] = \sum_{n=-\infty}^{\infty} V_n(j)\cos(n\phi - \Omega_i t + \phi_i) \tag{4.12}$$

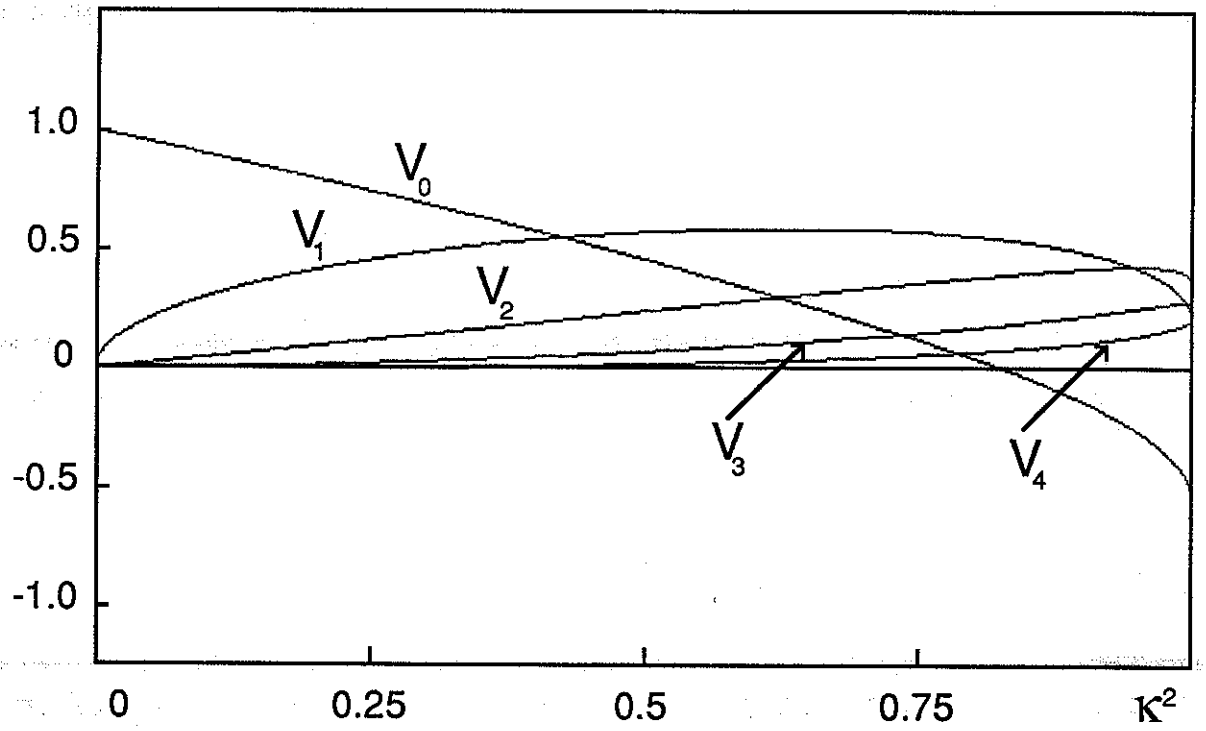

Fig. 4.4. Plots of the potential V_n as a function of κ^2 for $n = 0 \ldots 4$. Negative values of n can be obtained by noticing that $V_{-n}(j) = (-1)^n V_n(j)$.

with

$$V_n(j) = \left(\frac{\pi}{K(\kappa)}\right)^2 \frac{nq^{n/2}}{1-(-q)^n}, \quad (n \neq 0), \tag{4.13}$$

$$V_o(j) = 2E(\kappa)/K(\kappa) - 1, \tag{4.14}$$

and $q = \exp\left[-\pi K(\sqrt{1-\kappa^2})/K(\kappa)\right]$. An important symmetry property of the $V_n(j)$, is that $V_n(j) = (-1)^n V_{-n}(j)$. Figure 4.4 contains plots of V_n as a function of κ^2 for a few values of n.

The Hamiltonian can be finally written as:

$$h(j,\phi) = h_o(j) - \sum_{i=2}^{N} \sum_{n=-\infty}^{\infty} \Omega_{ii}^2 V_n(j) \cos(n\phi - \Omega_i t + \phi_i) \tag{4.15}$$

4.4. General Solution of the Equation of Motion - KAM Theorem

As in chapter 3, the system we are studying has $N+1$ degrees of freedom: the phase of the N waves, and the electron angular position. But since we have arbitrarily defined the origin of frequencies as being wave 1, we are left with only an N-degree of freedom system that can be described by the N

dimensional Hamiltonian:

$$h_N(q_i,p_i) = h_o(p_1) + \sum_{i=2}^{N} \Omega_i p_i - \sum_{i=2}^{N} \sum_{n=-\infty}^{\infty} \Omega_{ti}^2 V_n(p_1) \cos(nq_1 - q_i + \phi_i) \tag{4.16}$$

with the following equations of motion:

$$\dot{q}_1 = \frac{\partial h_N}{\partial p_1} = \frac{\partial h_o}{\partial p_1} - \sum_{i=2}^{N} \sum_{n=-\infty}^{\infty} \Omega_{ti}^2 V_n'(p_1) \cos(nq_1 - q_i + \phi_i) \tag{4.17}$$

$$\dot{p}_1 = -\frac{\partial h_N}{\partial q_1} = -\sum_{i=2}^{N} \sum_{n=-\infty}^{\infty} n\Omega_{ti}^2 V_n(p_1) \sin(nq_1 - q_i + \phi_i) \tag{4.18}$$

$$\dot{q}_i = \frac{\partial h_N}{\partial p_i} = \Omega_i \quad (i \neq 1) \tag{4.19}$$

and

$$\dot{p}_i = -\frac{\partial h_N}{\partial q_i} = \sum_{n=-\infty}^{\infty} \Omega_{ti}^2 V_n(p_1) \sin(nq_1 - q_i + \phi_i) \quad (i \neq 1) \tag{4.20}$$

The p_i for $i \neq 1$ are dummy variables and can be ignored. The equations for the q_i give:

$$q_i = \Omega_i t \tag{4.21}$$

Substituting those values in equations (4.17) and (4.18), making $p_1 = j$, and $q_1 = \phi$, we get the right equation of motion. If we now define

$$H_o(p_i) = h_o(p_1) + \sum_{i=2}^{N} \Omega_i p_i \tag{4.22}$$

and

$$H_1(q_i,p_i) = -\sum_{i=2}^{N} \sum_{n=-\infty}^{\infty} \Omega_{ti}^2 V_n(p_1) \cos(nq_1 - q_i + \phi_i) \tag{4.23}$$

we can write

$$h_N(q_i,p_i) = H_o(p_i) + H_1(q_i,p_i), \quad i = 1 \ldots N \tag{4.24}$$

where $H_1(q_i,p_i)$ is periodic in all q_i, and $H_o(p_i)$ depends only on the p_i. Once again, the KAM (Kolmogoroff, Arnold, Moser) Theorem for nonlinear systems states that the motion described by H_o will be appreciably affected by H_1 only if the following relationship holds for the variables describing the unperturbed motion:

$$\sum_{i=1}^{N} n_i \dot{q}_i = 0, \tag{4.25}$$

n_i being arbitrary integers. Making $\dot{q}_1 = \dot{\phi} = \Omega$, we will have:

$$\Omega = \sum_{i=2}^{N} n_i \Omega_i / n \tag{4.26}$$

That is, the bounce (trapping) frequency of the electron resonates with the Doppler shifted wave frequency differences. Since we have already fixed the origin at wave 1, there are no free parameters left and no additional constraint is imposed on n.

To see the effect of the resonances at a fixed point in space, and derive an expression for the radiation frequencies, we need to define an electron stream. For that, we take a set of electrons with trapping frequency Ω and an infinitesimally weak wave with a Doppler shifted frequency offset also equal to Ω. Such a wave is said to be resonant with the electrons because their relative phases are constant. Next we define the stream as a subset of those electrons having a chosen fixed phase relative to the electromagnetic wave at all points in space, and, consequently, at all instants of time. Since the wave at a fixed point in space turns with frequency $\Delta\omega = \Omega v_g/(v_\parallel + v_g)$, so will the phase ϕ of the electrons in the stream, which can now be written as:

$$\phi = \Omega(t - t_o) + \Delta\omega t_o + \phi_o \tag{4.27}$$

where t_o is the moment the electron at $z = -v_\parallel(t - t_o)$ enters the interaction region. The radiation coming from such a stream can be substituted for the radiation coming from the accelerated electrons. Since $\Delta\omega_i = \Omega_i v_g/(v_\parallel + v_g)$, the expression for the resonance frequencies can be rewritten as:

$$\Delta\omega = \sum_{i=2}^{N} n_i \Delta\omega_i / n \tag{4.28}$$

where $\Delta\omega$ is the oscillation frequency of a cross section of the stream we have just defined. The electron stream oscillations will FM modulate the reference wave monochromatic radiation, as mentioned in section 4.2, adding lines at $\omega = \omega_1 + m\Delta\omega$, m being an arbitrary integer. The radiation frequencies will then be:

$$\omega = \omega_1 + \frac{m}{n} \sum_{i=2}^{N} n_i \Delta\omega_i \tag{4.29}$$

Since $\Delta\omega_i = \omega_i - \omega_1$ and n_i can be substituted for mn_i because both are arbitrary integers, we can write:

$$\omega = \frac{\omega_1 \left(n - \sum_{i=2}^{N} n_i\right) + \sum_{i=2}^{N} n_i \omega_i}{n} \tag{4.30}$$

Defining $n_1 = (n - \sum_{i=2}^{N} n_i)$, we finally get:

$$\omega = \frac{\sum_{i=1}^{N} n_i \omega_i}{\sum_{i=1}^{N} n_i} \tag{4.31}$$

which is the same formula for the frequencies as obtained in chapter 3.

4.5. Electron Motion for Non-Resonant Values of $V_\parallel$

If we use the explicitly time-dependent form of the Hamiltonian, and put $\Omega_{ti}^2 = \epsilon A_i$, we have

$$h(\phi, j, t) = h_o(\phi, j, t) + \epsilon h_1(\phi, j, t) \tag{4.32}$$

with

$$h_o = h_o(j), \quad h_1 = -\sum_{i=2}^{N} \sum_{n=-\infty}^{\infty} A_i V_n(j) \cos(n\phi - \Omega_i t + \phi_i) \tag{4.33}$$

To study non-resonant terms, using the Lie perturbation method described in chapter 3, we ignore all resonances, and put in the K_n only constant terms. To get the simplest non-trivial result we have to go up to second order in the perturbation expansion. Doing this, we get $K_o = h_o$ and $K_1 = 0$ (because h_1 has no constant terms).

This implies

$$W_1 = -\int^t d\tau\ h_1[\Phi + \Omega_i(\tau - t), J, \tau] = \sum_{i=2}^{N} \sum_{n=-\infty}^{\infty} \frac{A_i V_n(J)}{n\Omega_i(J) - \Omega_i} \sin(n\Phi - \Omega_i t + \phi_i) \tag{4.34}$$

We then choose

$$2K_2 = \langle L_1 h_1 \rangle = \langle \{W_1, h_1\} \rangle \tag{4.35}$$

A straightforward calculation shows that

$$\begin{aligned} \{W_1, h_1\} &= \frac{\partial W_1}{\partial \Phi}\frac{\partial h_1}{\partial J} - \frac{\partial W_1}{\partial J}\frac{\partial h_1}{\partial \Phi} \\ &= 1/2 \sum_{i,j=2}^{N} \sum_{m,n=-\infty}^{\infty} A_j(ma'_{in}V_m - na_{in}V'_m)\cos[(n+m)\Phi - (\Omega_i + \Omega_j)t + \phi_i + \phi_j] \\ &- 1/2 \sum_{i,j=2}^{N} \sum_{m,n=-\infty}^{\infty} A_j(ma'_{in}V_m + na_{in}V'_m)\cos[(n-m)\Phi - (\Omega_i - \Omega_j)t + \phi_i - \phi_j] \end{aligned} \tag{4.36}$$

where

$$a_{in} = \frac{A_i V_n(J)}{n\Omega_i(J) - \Omega_i} \tag{4.37}$$

and the prime indicates differentiation with respect to J. If $\Omega_i \neq -\Omega_j$ (no symmetrically placed waves in the system),

$$K_2 = K_2^o = \frac{1}{2}\langle \{W_1, h_1\} \rangle = -\frac{1}{4}\sum_{i,n} A_i(na'_{in}V_n + na_{in}V'_n) = -\frac{1}{4}\sum_{i,n} A_i n(a_{in}V_n)' \tag{4.38}$$

and

$$K = h_o(J) - \frac{\epsilon^2}{4}\sum_{i,n} \frac{nA_i^2 V_n^2}{n\Omega_t - \Omega_i}\left[\frac{2V'_n}{V_n} - \frac{n\Omega'_t}{n\Omega_t - \Omega_i}\right] \tag{4.39}$$

Hamilton's equations of motion for K can be solved :

$$\dot{J} = -\frac{\partial K}{\partial \Phi} = 0 \tag{4.40}$$

$$\dot{\Phi} = \frac{\partial K}{\partial J} = \frac{\partial h_o(J)}{\partial J} + \epsilon^2 \frac{\partial K_2^o}{\partial J} = \Omega \tag{4.41}$$

The solution is

$$J = J_o \tag{4.42}$$

$$\Phi = \Omega t + \Phi_o = \Omega_t(J_o)t + \epsilon^2 \frac{\partial K_2^o}{\partial J} t + \Phi_o \tag{4.43}$$

The trasformation back to (ϕ, j), keeping only first order terms and constant second order terms, is given by

$$\phi = \Phi - \epsilon \frac{\partial W_1}{\partial J} - \frac{\epsilon^2}{2}\langle \{W_1, \frac{\partial W_1}{\partial J}\} \rangle \tag{4.44}$$

$$j = J + \epsilon \frac{\partial W_1}{\partial \Phi} + \frac{\epsilon^2}{2} \langle \{W_1, \frac{\partial W_1}{\partial \Phi}\} \rangle \tag{4.45}$$

Evaluation of the Poisson brackets gives

$$\langle \{W_1, \frac{\partial W_1}{\partial J}\} \rangle = 0 \tag{4.46}$$

and

$$\langle \{W_1, \frac{\partial W_1}{\partial \Phi}\} \rangle = \sum_{i,n} A_i n^2 a_{in} a'_{in} \tag{4.47}$$

which gives

$$\phi = \Phi - \epsilon \sum_{i,n} \frac{A_i V_n}{n\Omega_t - \Omega_i} \left[\frac{V'_n}{V_n} - \frac{n\Omega'_t}{n\Omega_t - \Omega_i} \right] \sin(n\Phi - \Omega_i t + \phi_i) \tag{4.48}$$

$$j = J + \frac{\epsilon^2}{2} \sum_{i,n} \frac{n^2 A_i^2 V_n^2}{(n\Omega_t - \Omega_i)^2} \left[\frac{V'_n}{V_n} - \frac{n\Omega'_t}{n\Omega_t - \Omega_i} \right] + \epsilon \sum_{i,n} \frac{n A_i V_n}{n\Omega_t - \Omega_i} \cos(n\Phi - \Omega_i t + \phi_i) \tag{4.49}$$

We see that up to zeroth order (j, ϕ) is equal to (J, Φ), and the motion is just the normal oscillation, with frequency $\Omega_t(J_o)$, of the electron inside the potential well.

The first order oscillatory terms in the above equations predict the existence of a conditionally periodic jittering motion superimposed on the main electron motion, maximized when $n\Omega_t \approx \Omega_i$ for some i and n. Under those conditions, the particle motion will add to the bunching associated with such a resonance.

The second order corrections describe an important effect, here due to the adiabatic invariance of J: If we average away the oscillatory terms, and assume that a certain particle has $j = J_o$ for $\epsilon = 0$, and that the wave fields are adiabatically turned on, then J will remain constant, and $\dot{\phi}$ will vary as:

$$\dot{\phi} = \Omega_t(J_o) + \epsilon^2 \frac{\partial K_2^o(J_o)}{\partial J_o} \tag{4.50}$$

If J_o is such that $n\Omega_t(J_o) \approx \Omega_i$, for a certain i,

$$j = J_o + \Delta j \approx J_o - \frac{\epsilon^2}{2} \frac{n^3 A_i^2 V_n^2 \Omega'_t}{(n\Omega_t - \Omega_i)^3} \tag{4.51}$$

and

$$\dot{\phi} \approx \Omega_t(J_o) + \Omega'_t \Delta j \approx \Omega_t(J_o) - \frac{\epsilon^2}{2} \frac{n^3 A_i^2 V_n^2 \Omega'^2_t}{(n\Omega_t - \Omega_i)^3} \tag{4.52}$$

The particle will be shifted due to the presence of the waves, the forces being such that each wave tends to pull the particle towards points where the wave Doppler shifted frequency offset is a multiple of the particle trapping frequency. This shift will create a gradient around those points, increasing the growth rate of sideband waves associated with resonances located at those frequencies. (Those will be the first order resonances described in the next section).

Since radiation is a collective phenomenon, it will be extremely convenient to observe the effects of the electron motion, using a stream defined according to the outlines established in section 4.4. The whole electron distribution can be broken down into such streams, their bunching and distortions determining the radiation characteristics of the system. Those streams will also be the loci of the equilibrium points for the resonances to be studied in the following sections. The stream will be

composed of electrons with trapping frequency Ω, and its cross section will oscillate at the frequency $\Delta\omega = \Omega v_g/(v_\parallel + v_g)$. The phase of the component electrons can be obtained by conveniently defining Φ_o in the general solution for Φ:

$$\Phi = \Omega t + \Phi_o = \Omega(t - t_o) + \Delta\omega t_o + \Delta\phi \tag{4.53}$$

The electrons in such a stream have equal radiation characteristics, because they all describe the same path in the wave potential (with the right phase delays to account for the finite radiation propagation velocity). The stream forms a rigid DC current line consisting of a spatially periodic distorted straight line wound around a spiral path, and its motion can be studied in a variety of ways. The most convenient is to observe the motion of its cross-section at a fixed point in space. From the above equation it can be seen that such a motion will be oscillatory with frequency $\Delta\omega$, producing radiation at multiples of the oscillation frequency. We see that individual electron motion after integration over the stream, becomes only indirectly relevant. The stream can be so short that no electron in it will have time to perform a full oscillation in the potential well. However, the stream can still continuously execute full oscillations, radiating at well defined frequencies, if the electron flow is never interrupted.

4.6. First Harmonic Resonance and Associated Subharmonics

To study first order resonances we put :

$$K_o = h_o \tag{4.54}$$

and choose

$$K_1 = -A_j V_m(J)\cos(m\Phi - \Omega_j t + \phi_j) \tag{4.55}$$

if $\Omega_i \neq -\Omega_j$, for all i. This implies

$$W_1 = \sum_{\substack{(i\neq j)\text{or} \\ (n\neq m)}} \frac{A_i V_n(J)}{n\Omega_i(J) - \Omega_i}\sin(n\Phi - \Omega_i t + \phi_i) \tag{4.56}$$

and

$$K = h_o(J) - \epsilon A_j V_m(J)\cos(m\Phi - \Omega_j t + \phi_j) \tag{4.57}$$

Hamilton's equations applied to K, will give:

$$\dot{J} = -\frac{\partial K}{\partial \Phi} = -\epsilon m A_j V_m(J)\sin(m\Phi - \Omega_j t + \phi_j) \tag{4.58}$$

$$\dot{\Phi} = \frac{\partial K}{\partial J} = \frac{\partial h_o(J)}{\partial J} - \epsilon A_j V_m'(J)\cos(m\Phi - \Omega_j t + \phi_j) \tag{4.59}$$

$$\ddot{\Phi} \approx \frac{\partial^2 h_o(J)}{\partial J^2}\dot{J} = -\epsilon\frac{\partial^2 h_o(J)}{\partial J^2} m A_j V_m(J)\sin(m\Phi - \Omega_j t + \phi_j) \tag{4.60}$$

Defining

$$\Delta\Phi = m\Phi - \Omega_j t + \phi_j \tag{4.61}$$

we can write the equation of motion as:

$$\Delta\ddot{\Phi} = -\epsilon m^2 A_j \frac{\partial^2 h_o(J)}{\partial J^2} V_m(J)\sin(\Delta\Phi) \tag{4.62}$$

This resonance has a full width, in the $\dot{\Phi}$ variable, equal to:

$$\Gamma_1 = 4\left[\epsilon A_j \left|\frac{\partial^2 h_o(J)}{\partial J^2} V_m(J)\right|\right]^{\frac{1}{2}} \tag{4.63}$$

The width in J is obtained by noticing that

$$\dot{\Phi} = \Omega_{t1} - J/8 + \ldots \tag{4.64}$$

which implies $\Gamma_1(J) = 8\Gamma_1(\dot{\Phi})$.

If $m < 0$ and odd, the equilibrium points will be $\Delta\Phi = 2k\pi$, otherwise they will be given by $\Delta\Phi = (2k+1)\pi$. The electrons at the equilibrium points will oscillate with frequency $\dot{\Phi}$ subject to the following constraints:

$$0 \leq \dot{\Phi} = \frac{\Omega_j}{m} \leq \Omega_{t1} \tag{4.65}$$

which gives a minimum value for $|m|$ for a given wave trapping frequency:

$$|m| \geq |\Omega_j|/\Omega_{t1} \tag{4.66}$$

Using the expression for ϕ_j from equation (4.3), we get for the motion of the equilibrium streams:

$$\Phi = \frac{\Delta\omega_j}{m} t_o + \frac{\Omega_j(t-t_o)}{m} + \frac{(2k+1)\pi - \Delta\phi}{m}, \quad k = 0 \ldots (|m|-1) \tag{4.67}$$

The equation describes a $|m|$-lobed resonance oscillating inside the potential well at a fixed point in space with frequency $\Delta\omega_j/m$. To look at the stream motion in the (j,ϕ) variables, we need the transformation equations:

$$\phi = \Phi - \epsilon \sum_{\substack{(i\neq j)\text{or} \\ (n\neq m)}} \frac{A_i V_n}{n\Omega_t - \Omega_i}\left[\frac{V_n'}{V_n} - \frac{n\Omega_t'}{n\Omega_t - \Omega_i}\right]\sin(n\Phi - \Omega_i t + \phi_i) \tag{4.68}$$

$$j = J + \frac{\epsilon^2}{2}\sum_{\substack{(i\neq j)\text{or} \\ (n\neq m)}} \frac{n^2 A_i^2 V_n^2}{(n\Omega_t - \Omega_i)^2}\left[\frac{V_n'}{V_n} - \frac{n\Omega_t'}{n\Omega_t - \Omega_i}\right] + \epsilon \sum_{\substack{(i\neq j)\text{or} \\ (n\neq m)}} \frac{nA_i V_n}{n\Omega_t - \Omega_i}\cos(n\Phi - \Omega_i t + \phi_i) \tag{4.69}$$

Since $m\Omega_t = \Omega_j$ and $m\Phi - \Omega_j t + \phi_j = (2k+1)\pi$, we can put

$$n\Phi - \Omega_i t + \phi_i = \frac{(n\Delta\omega_j - m\Delta\omega_i)}{m} t_o + \Phi_{ijnmk} \tag{4.70}$$

From the equations of motion we can also get:

$$\Omega_t = \Omega_j/m = \Omega_{t1} - J/8 + \epsilon A_j V_m' \tag{4.71}$$

Combining those equations, we have the expressions for the coordinate transformations:

$$\phi = \frac{\Delta\omega_j}{m} t_o + \Phi_{ok} - \epsilon \sum_{\substack{(i\neq j)\text{or} \\ (n\neq m)}} \frac{mA_i V_n}{n\Omega_j - m\Omega_i}\left[\frac{V_n'}{V_n} - \frac{mn\Omega_i'}{n\Omega_j - m\Omega_i}\right]\sin\left[\frac{(n\Delta\omega_j - m\Delta\omega_i)}{m} t_o + \Phi_{ijnmk}\right] \tag{4.72}$$

$$j = 8(\Omega_{t1} - \Omega_j/m) + 8\epsilon A_j V'_m + \epsilon \sum_{\substack{(i\neq j) \text{or} \\ (n\neq m)}} \frac{nmA_iV_n}{n\Omega_j - m\Omega_i} \cos\left[\frac{(n\Delta\omega_j - m\Delta\omega_i)}{m} t_o + \Phi_{ijnmk}\right] \quad (4.73)$$

The equations show that points in the resonance rotate with an average frequency $\Delta\omega_j/m$ and are slightly shifted in j towards regions of higher potential, V_m. This rotation in phase space is equivalent to oscillations around the mean rotation frequency of the electron stream in real space, creating an FM modulation of the radiation coming from the carrier. The resulting radiation spectrum has lines with frequencies $\omega_1 + \frac{n}{m}\Delta\omega_j$, $-\infty < n < \infty$, for a single lobe. The multiple lobed structure changes the spectrum appreciably. If all lobes have exactly the same electron distribution, the system will repeat itself at $m(\Delta\omega_j/m)$ and the spectrum will have frequencies $\omega_1 + n\Delta\omega_j$. Since different lobes will have somewhat different electron distributions, subharmonic radiation will show up at frequencies $\omega_1 + \frac{nk}{m}\Delta\omega_j$, $1 \leq k < m$. Since the differences in electron population will not be very large, those subharmonics will in general have smaller amplitudes than the integer harmonics of $\Delta\omega_j$.

Since the maximum frequency shift in the instantaneous radiation frequency, $\Delta\omega_{shft}$, is equal to $2\Delta\omega_{t1}$, the resonance half-width that the electron stream sees, and $\Delta\omega \leq \Delta\omega_{t1}$, where $\Delta\omega_{t1} = \Omega_{t1}v_g/(v_\parallel + v_g)$ is the carrier trapping frequency for the electron stream, the modulation index, $\Delta\omega_{shft}/\Delta\omega$, can easily be of the order of 1, generating quite a wideband spectrum.

If $n\Omega_j \neq m\Omega_i$ for all i and n, the time dependent distortions of order ϵ present in the transformation equations for (j,ϕ) will give contributions of order $\epsilon\cdot\epsilon^{\frac{1}{2}}$ to the radiation and will be negligible up to the second order effects we will be analyzing in this chapter. They might be important, however, when compared to higher order terms. If, on the other hand $n\Omega_j \approx m\Omega_i$ for some i and n, then resonance overlaps are present and the choice for K_1 has not been correctly made.

4.7. Second-Order Resonances

4.7.1. General Expressions

To look for second-order resonances, we choose K_o, K_1, and W_1 to be the same as in the non-resonant case. $2K_2$ will be obtained from terms in $\{W_1, h_1\}$:

$$\begin{aligned}\{W_1, h_1\} = 1/2 \sum_{i,j=2}^{N} \sum_{m,n=-\infty}^{\infty} A_j(ma'_{in}V_m - na_{in}V'_m)\cos[(n+m)\Phi - (\Omega_i + \Omega_j)t + \phi_i + \phi_j] \\ - 1/2 \sum_{i,j=2}^{N} \sum_{m,n=-\infty}^{\infty} A_j(ma'_{in}V_m + na_{in}V'_m)\cos[(n-m)\Phi - (\Omega_i - \Omega_j)t + \phi_i - \phi_j]\end{aligned} \quad (4.74)$$

K_2 will always consist of K_2^o, the constant term obtainable from $\{W_1, h_1\}$, plus a chosen resonant term. In all cases, K_2 can be written as:

$$K_2 = K_2^o + K_2^1 \cos(l\Phi - \Omega_{ij}t + \phi_{ij}) \quad (4.75)$$

and

$$K = h_o + \epsilon^2 K_2^o + \epsilon^2 K_2^1 \cos(l\Phi - \Omega_{ij}t + \phi_{ij}) \quad (4.76)$$

with $\phi_{ij} = (\Omega_{ij} - \Delta\omega_{ij})t_o + \Delta\phi_{ij}$.

Hamilton's equations will be:

$$\dot{J} = -\frac{\partial K}{\partial \Phi} = \epsilon^2 l K_2^1 \sin(l\Phi - \Omega_{ij}t + \phi_{ij}) \tag{4.77}$$

$$\dot{\Phi} = \frac{\partial K}{\partial J} = \frac{\partial h_o(J)}{\partial J} + \epsilon^2 K_2^{o\prime} + \epsilon^2 K_2^{1\prime} \cos(l\Phi - \Omega_{ij}t + \phi_{ij}) \tag{4.78}$$

$$\ddot{\Phi} \approx \frac{\partial^2 h_o(J)}{\partial J^2}\dot{J} = \epsilon^2 l \frac{\partial^2 h_o(J)}{\partial J^2} K_2^1 \sin(l\Phi - \Omega_{ij}t + \phi_{ij}) \tag{4.79}$$

Defining

$$\Delta\Phi = l\Phi - \Omega_{ij}t + \phi_{ij} \tag{4.80}$$

we can write the equation of motion as:

$$\Delta\ddot{\Phi} = \epsilon^2 l^2 \frac{\partial^2 h_o(J)}{\partial J^2} K_2^1 \sin(\Delta\Phi) \tag{4.81}$$

The resonances have full widths, in the $\dot{\Phi}$ variable, equal to:

$$\Gamma_- = 4\epsilon \left[\left| \frac{\partial^2 h_o(J)}{\partial J^2} K_2^1 \right| \right]^{\frac{1}{2}} \tag{4.82}$$

Since $\frac{\partial^2 h_o(J)}{\partial J^2} < 0$, the equilibrium values of $\Delta\Phi$ will be:

$$\Delta\Phi_o = (2k+1)\pi \quad \text{if} \quad K_2^1 < 0 \tag{4.83}$$

$$\Delta\Phi_o = 2k\pi \quad \text{if} \quad K_2^1 > 0 \tag{4.84}$$

with $k = 0 \ldots (|l| - 1)$. For those equilibrium points, which define $|l|$-lobed resonances, Φ will vary as:

$$\Phi = \frac{\Omega_{ij}t - \phi_{ij} + \Delta\Phi_o}{l} \tag{4.85}$$

which can be rewritten as:

$$\Phi = \frac{\Delta\omega_{ij}t_o}{l} + \frac{\Omega_{ij}(t - t_o)}{l} - \frac{\Delta\phi_{ij} - \Delta\Phi_o}{l} \tag{4.86}$$

The resonances will oscillate in the potential well with frequencies

$$\Delta\omega = \frac{\Delta\omega_{ij}}{l} \tag{4.87}$$

and will radiate at the frequencies

$$\omega = \omega_1 + \frac{n\Delta\omega_{ij}}{l} \tag{4.88}$$

with enhanced amplitudes at frequencies such that n/l is an integer.

4.7.2 Three-Wave Resonances: Intermodulation

Frequency Subtraction

If we take two distinct waves with frequencies Ω_i and Ω_j, the term in $\{W_1, h_1\}$ asymmetrical under permutation of the indices i and j gives:

$$4(K_2 - K_2^o) = -\sum_{n-m=l} (\beta_{ijmn} + \beta_{jinm}) \cos[l\Phi - (\Omega_i - \Omega_j)t + \phi_i - \phi_j] \tag{4.89}$$

with

$$\beta_{ijmn} = A_j(ma'_{in}V_m + na_{in}V'_m) \tag{4.90}$$

Calculation of the β's leads to the following expression for K_2:

$$\begin{aligned} K_2 - K_2^o = {} & \frac{A_i A_j}{2} \sum_{n=-\infty}^{\infty} \frac{lV_nV_{n-l}(n-l)n}{(l-n)\Omega_i + n\Omega_j} \\ & \left[\frac{V'_n}{nV_n} + \frac{V'_{n-l}}{(n-l)V_{n-l}} + \frac{l\Omega'_t}{(l-n)\Omega_i + n\Omega_j}\right] \cos[l\Phi - (\Omega_i - \Omega_j)t + \phi_i - \phi_j] \end{aligned} \tag{4.91}$$

or

$$K_2 - K_2^o = \sum_{n=-\infty}^{\infty} d(n) \cos[l\Phi - (\Omega_i - \Omega_j)t + \phi_i - \phi_j] \tag{4.92}$$

It is possible to rewrite the summation in such a way that one of its limits is finite and terms of same magnitude are added together. To do this we notice that if l is odd,

$$\sum_{n=-\infty}^{\infty} d(n) = \sum_{n=(l+1)/2}^{\infty} d(n) + d(l-n) \tag{4.93}$$

and if l is even,

$$\sum_{n=-\infty}^{\infty} d(n) = d(l/2) + \sum_{n=l/2+1}^{\infty} d(n) + d(l-n) = \sum_{n=l/2}^{\infty} (1 - \frac{\delta_{n\frac{l}{2}}}{2})[d(n) + d(l-n)] \tag{4.94}$$

where δ represents the Kronecker delta function.

Evaluation of $d(n) + d(l-n)$ for odd l leads to the expression:

$$\begin{aligned} K_2 = K_2^o + {} & \frac{A_i A_j}{2} \sum_{n=(l+1)/2}^{\infty} \frac{l^2 V_n V_{n-l}(n-l)n(\Omega_i + \Omega_j)}{l^2\Omega_i\Omega_j + n(l-n)(\Omega_i - \Omega_j)^2} \\ & \left\{\frac{V'_n}{nV_n} + \frac{V'_{n-l}}{(n-l)V_{n-l}} + \frac{(2n-l)(\Omega_i - \Omega_j)}{l^2\Omega_i\Omega_j + n(l-n)(\Omega_i - \Omega_j)^2} l\Omega'_t\right\} \\ & \cos[l\Phi - (\Omega_i - \Omega_j)t + \phi_i - \phi_j] \end{aligned} \tag{4.95}$$

and for even l:

$$\begin{aligned} K_2 = K_2^o + {} & \frac{A_i A_j}{2} \sum_{n=l/2}^{\infty} (1 - \frac{\delta_{n\frac{l}{2}}}{2}) \frac{lV_nV_{n-l}(n-l)n}{l^2\Omega_i\Omega_j + n(l-n)(\Omega_i - \Omega_j)^2} \\ & \left\{\left[\frac{V'_n}{nV_n} + \frac{V'_{n-l}}{(n-l)V_{n-l}}\right](2n-l)(\Omega_i - \Omega_j) + \frac{l^2(\Omega_i^2 + \Omega_j^2) - 2n(l-n)(\Omega_i - \Omega_j)^2}{l^2\Omega_i\Omega_j + n(l-n)(\Omega_i - \Omega_j)^2} l\Omega'_t\right\} \\ & \cos[l\Phi - (\Omega_i - \Omega_j)t + \phi_i - \phi_j] \end{aligned} \tag{4.96}$$

In both cases, K_2 can be written as:

$$K_2 = K_2^o + K_2^- \cos\left[l\Phi - (\Omega_i - \Omega_j)t + (\phi_i - \phi_j)\right] \tag{4.97}$$

The resonance described by K_2 has a full width, in the $\dot{\Phi}$ variable, equal to:

$$\Gamma_- = 4\epsilon \left[\left|\frac{\partial^2 h_o(J)}{\partial J^2} K_2^-\right|\right]^{\frac{1}{2}}, \tag{4.98}$$

it will oscillate in the potential well with frequency

$$\Delta\omega = \frac{\Delta\omega_i - \Delta\omega_j}{l} = \frac{\omega_i - \omega_j}{l}, \tag{4.99}$$

and will radiate at the frequencies

$$\omega = \omega_1 + \frac{n(\omega_i - \omega_j)}{l} \tag{4.100}$$

If for odd l we take the case of two waves extremely distant from the main carrier, but having a finite frequency separation, we can find an approximate expression for K_2, by taking the limit $\Omega_{i,j} \to \infty$ with $\Omega_i - \Omega_j$ finite:

$$K_2 = K_2^o + \frac{A_i A_j}{\Omega_i} S_l(J) \cos\left[l\Phi - (\Omega_i - \Omega_j)t + \phi_i - \phi_j\right] \tag{4.101}$$

with

$$S_l(J) = \sum_{n=(l+1)/2}^{\infty} (n-l) V_{n-l} V_n' + n V_n V_{n-l}' \tag{4.102}$$

This resonance will have a width

$$\Gamma_- = \frac{4\epsilon}{\sqrt{\Omega_i}} \left[A_i A_j \left|\frac{\partial^2 h_o(J)}{\partial J^2} S_l(J)\right|\right]^{\frac{1}{2}} \tag{4.103}$$

Since $\Gamma_- \propto 1/\sqrt{\Omega_i}$, the resonance width may be sizable even when large distances separate the main wave from the perturbation. In particular, if a large set of weak and equally spaced waves perturbs the main carrier, the total perturbation will be a function of a large number of those weak waves, and the overall effect, although in practice only a few times larger in magnitude than the one created by a single pair of lines, will be non-local, with properties not entirely atributable to any wave pair in particular.

The general expression for K_2 is a sum over n, of terms containing as a denominator the expression $l^2\Omega_i\Omega_j + n(l-n)(\Omega_i - \Omega_j)^2 = [(l-n)\Omega_i + n\Omega_j]\,[(l-n)\Omega_j + n\Omega_i]$. If for some n we have either

$$n = n_1 \approx \frac{l\Omega_i}{\Omega_i - \Omega_j}, \tag{4.104}$$

or

$$n = n_2 \approx -\frac{l\Omega_j}{\Omega_i - \Omega_j}, \tag{4.105}$$

the summation can be approximated by the term that has such a value of n alone. Since $n_1 + n_2 = l$, $n_1 \neq n_2$, and $n_{1,2} \geq l/2$, at most one value of n will satisfy any of the two equations. Such value

if it exists will be $n = \text{Max}(n_1, n_2)$, which we will assume for simplicity to be n_1. Because the perturbation expansion converges only if there is no resonance overlap inside the carrier potential well, which causes chaos, and the enhancement of the term we are looking at is caused by the existence of a $|n_1|$-lobed first order resonance caused by wave i alone, we must have as the closest possible spacing for the two resonances:

$$\frac{\Omega_i - \Omega_j}{l} - \frac{\Omega_i}{n} = 2\sqrt{\epsilon A_i |V_n|/8} \tag{4.106}$$

Under those conditions K_2^o and K_2^- can be rewritten as:

$$K_2^o \approx \frac{f_2^o}{\sqrt{\epsilon}} \tag{4.107}$$

$$K_2^- \approx \frac{f_2^-}{\sqrt{\epsilon}} \cos\left[l\Phi - (\Omega_i - \Omega_j)t + \phi_i - \phi_j\right] \tag{4.108}$$

or

$$K = h_o + \epsilon^{\frac{3}{2}} f_2^o + \epsilon^{\frac{3}{2}} f_2^- \cos\left[l\Phi - (\Omega_i - \Omega_j)t + \phi_i - \phi_j\right] \tag{4.109}$$

This will lead to an enhanced resonance width:

$$\Gamma_- = \epsilon^{\frac{3}{4}} \left[\left|\frac{\partial^2 h_o(J)}{\partial J^2} f_2^-\right|\right]^{\frac{1}{2}} \tag{4.110}$$

putting the resonance halfway between a first and a second order effect in terms of its magnitude.

We note that the width of this type of resonance when created by the processes described in chapter 3, is a totally symmetric function of the wave amplitudes, i.e, the width remains invariant if any permutation is made among the interacting carriers. This is not the case when the same effect is described by a trapped resonance, since it is highly convenient that the wave that contains the resonance be the strongest of them all, so that the required value of $|l|$ is minimized and the radiation is as strong as possible.

Frequency Addition

If we take two distinct waves with frequencies Ω_i and Ω_j, the term symmetrical under permutation of the indices i and j gives:

$$4(K_2 - K_2^o) = \sum_{m+n=l} (\alpha_{ijmn} + \alpha_{jimn}) \cos\left[l\Phi - (\Omega_i + \Omega_j)t + \phi_i + \phi_j\right] \tag{4.111}$$

with

$$\alpha_{ijmn} = A_j(ma'_{in}V_m - na_{in}V'_m) \tag{4.112}$$

Calculation of the α's leads to the following expression for K_2:

$$K_2 - K_2^o = \frac{A_i A_j}{4} \sum_{n=-\infty}^{\infty} \frac{lV_n V_{l-n}(l-n)n}{l^2\Omega_i\Omega_j - n(l-n)(\Omega_i + \Omega_j)^2} \left\{(2n-l)(\Omega_i + \Omega_j)\left[\frac{V'_n}{nV_n} - \frac{V'_{l-n}}{(l-n)V_{l-n}}\right] - \frac{l^2(\Omega_i^2 + \Omega_j^2) - 2n(l-n)(\Omega_i + \Omega_j)^2}{l^2\Omega_i\Omega_j - n(l-n)(\Omega_i + \Omega_j)^2} l\Omega'_i\right\} \cos\left[l\Phi - (\Omega_i + \Omega_j)t + \phi_i + \phi_j\right] \tag{4.113}$$

or

$$K_2 - K_2^o = \sum_{n=-\infty}^{\infty} c(n) \cos\left[l\Phi - (\Omega_i + \Omega_j)t + \phi_i + \phi_j\right] \tag{4.114}$$

Since $c(n) = c(l-n)$, we are led to the following simplifications:

For odd l,

$$K_2 = K_2^o + \frac{1}{2} \sum_{n=(l+1)/2}^{\infty} c(n) \cos\left[l\Phi - (\Omega_i + \Omega_j)t + \phi_i + \phi_j\right] \tag{4.115}$$

For even l,

$$K_2 = K_2^o + \frac{1}{4} \sum_{n=l/2}^{\infty} (2 - \delta_{n\frac{l}{2}}) c(n) \cos\left[l\Phi - (\Omega_i + \Omega_j)t + \phi_i + \phi_j\right] \tag{4.116}$$

In both cases, K_2 can be written as:

$$K_2 = K_2^o + K_2^+ \cos\left[l\Phi - (\Omega_i + \Omega_j)t + (\phi_i + \phi_j)\right] \tag{4.117}$$

The resonance described by K_2 has a full width, in the $\dot{\Phi}$ variable, equal to:

$$\Gamma_+ = 4\epsilon \left[\left|\frac{\partial^2 h_o(J)}{\partial J^2} K_2^+\right|\right]^{\frac{1}{2}}, \tag{4.118}$$

it will oscillate in the potential well with frequency

$$\Delta\omega = \frac{\Delta\omega_i + \Delta\omega_j}{l}, \tag{4.119}$$

and will radiate at the frequencies

$$\omega = \omega_1 + \frac{n(\Delta\omega_i + \Delta\omega_j)}{l} \tag{4.120}$$

An example of this type of resonance is shown in Figure 4.5 for $l = -2$, $\Omega_i = 7\Omega_o$ and $\Omega_j = -9\Omega_o$, with $\Omega_o \approx \Omega_{t1}$. In this example it can be seen that the main wave trapping frequency imposes no constraints on the required perturbing carrier frequency separations or on the bandwith and line separations of the radiated spectrum. The perturbing carriers are positioned several times Ω_{t1} away from the main wave potential, and the resonance produces a spectrum with main lines separated by $2\Omega_o > \Omega_{t1}$.

Similarly to the previous subsection, due to the poles in its denominators, K_2 will be enhanced if

$$n = n_{1,2} \approx \frac{l\Omega_{i,j}}{\Omega_i + \Omega_j}, \tag{4.121}$$

Under those conditions K_2^o and K_2^+ can be written as:

$$K_2^o \approx \frac{f_2^o}{\sqrt{\epsilon}} \tag{4.122}$$

$$K_2^+ \approx \frac{f_2^+}{\sqrt{\epsilon}} \cos\left[l\Phi - (\Omega_i + \Omega_j)t + \phi_i + \phi_j\right] \tag{4.123}$$

or

$$K = h_o + \epsilon^{\frac{3}{2}} f_2^o + \epsilon^{\frac{3}{2}} f_2^+ \cos\left[l\Phi - (\Omega_i + \Omega_j)t + \phi_i + \phi_j\right] \tag{4.124}$$

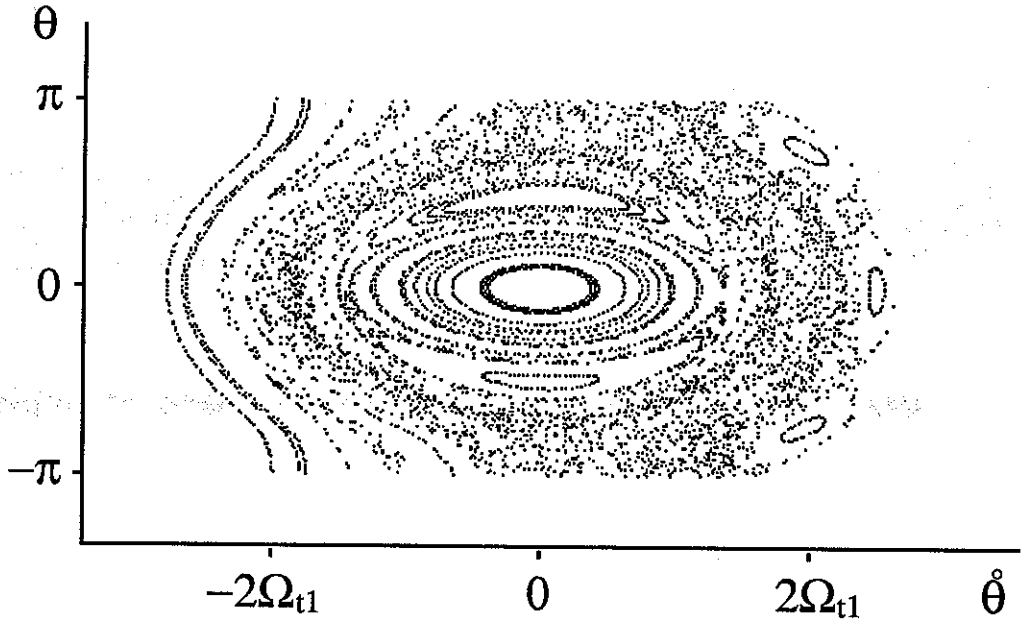

Fig. 4.5. Frequency addition intermodulation resonance for $l = -2$, $\Omega_i = 7\Omega_o$ and $\Omega_j = -9\Omega_o$, with $\Omega_o = 6/7\Omega_{t1}$. The resonance consists of the two crescent shapes symmetrically placed relative to the $\theta = 0$ axis, and centered at $\dot{\theta} = 0$. As time flows, they will turn with frequency $\Delta\omega = (\Omega_i + \Omega_j)/l\,[v_g/(v_\parallel + v_g)]$. The three lobes at the right, located at $\dot{\theta} = 2\Omega_{t1}$ and $\theta = 0, \pm 2\pi/3$, represent an external 1/3-harmonic resonance created by wave i and the main wave. At the left the external resonance for the interaction $\omega = \omega_i + \omega_j - \omega_1$ ($\dot{\theta} = -2\Omega_o$ and $\theta = \pi$) can also be seen. A sizable chaotic band is seen circling the main resonance. Its presence will decrease main wave growth.

Which also leads to a larger resonance width:

$$\Gamma_- = \epsilon^{\frac{3}{4}} \left[\left| \frac{\partial^2 h_o(J)}{\partial J^2} f_2^+ \right| \right]^{\frac{1}{2}} \tag{4.125}$$

4.7.3. Two-Wave Effects: Second Harmonic

If in the expression for $\{W_1, h_1\}$, we select the terms symmetrical under permutation of i and j, but assume $i = j$, we get a new type of resonance. Since we do not want this resonance to fall on top of any already present first order resonances, we choose $m + n = l$ to be an odd number. The expression for K_2 can then be either directly calculated or obtained from the frequency addition resonance by putting $i = j$ and dividing all terms by two. We then get:

$$K_2 = K_2^o + \frac{A_i^2}{2} \sum_{n=(l+1)/2}^{\infty} \frac{l V_n V_{l-n} (l-n) n}{(2n-l)\Omega_i} \left[\frac{V_n'}{n V_n} - \frac{V_{l-n}'}{(l-n) V_{l-n}} - \frac{l\Omega_i'}{(2n-l)\Omega_i} \right] \cos(l\Phi - 2\Omega_i t + 2\phi_i) \tag{4.126}$$

Which can be written as:

$$K_2 = K_2^o + K_2^2 \cos(l\Phi - 2\Omega_i t + 2\phi_i) \tag{4.127}$$

The resonance described by K_2 has a full width, in the $\dot{\Phi}$ variable, equal to:

$$\Gamma_2 = 4\epsilon \left[\left| \frac{\partial^2 h_o(J)}{\partial J^2} K_2^2 \right| \right]^{\frac{1}{2}}, \tag{4.128}$$

it will oscillate in the potential well with frequency

$$\Delta\omega = \frac{2\Delta\omega_i}{l}, \quad (\text{odd } l) \tag{4.129}$$

and will radiate at the frequencies

$$\omega = \omega_1 + \frac{2n\Delta\omega_i}{l}, \quad (\text{odd } l) \tag{4.130}$$

This is a second harmonic resonance, that will produce most of its radiation at even multiples of the frequency separation, $\Delta\omega_i$. There will also be some radiation at subharmonic frequencies, adding to the spectrum weaker lines separated by multiples of $2\Delta\omega_i/l$.

4.8. Interference Effects

In the case of first order resonances, if we happen to have two waves, l and j, such that $\Omega_l = -\Omega_j$, the same value of $\dot{\Phi}$ will be simultaneously resonant with both. We are faced with the case of resonance interference. For a first order Hamiltonian we must then choose,

$$K_1 = -A_l V_{-m}(J)\cos(-m\Phi - \Omega_l t + \phi_l) - A_j V_m(J)\cos(m\Phi - \Omega_j t + \phi_j) \tag{4.131}$$

which is equal to:

$$K_1 = -A_l(-1)^m V_m(J)\cos(m\Phi - \Omega_j t - \phi_l) - A_j V_m(J)\cos(m\Phi - \Omega_j t + \phi_j) \tag{4.132}$$

and can be rewritten as

$$K_1 = r\cos(m\Phi - \Omega_j t - \Phi_o) \tag{4.133}$$

with

$$\tan\Phi_o = \frac{A_l(-1)^m \sin\phi_l - A_j \sin\phi_j}{A_l(-1)^m \cos\phi_l + A_j \cos\phi_j} \tag{4.134}$$

and

$$r^2 = A_l^2 + A_j^2 + 2(-1)^m A_j A_l \cos(\phi_j + \phi_l) \tag{4.135}$$

If $\phi_j + \phi_l = \pi$,

$$r = |V_m||A_j(-1)^m - A_l| \tag{4.136}$$

which is minimized if m is even, and zero if additionally $A_j = A_l$. In this case, all even m, first order radiated subharmonics will have zero amplitude, and odd ones will be reinforced.

If $\phi_j + \phi_l = 0$,

$$r = |V_m||A_j(-1)^m + A_l| \tag{4.137}$$

which is minimized for m odd, and zero if $A_j = A_l$. If this happens, all even m first order radiated subharmonics will be reinforced, and the odd ones will be weakened. The odd ones will not be

completely cancelled because it is always possible to get radiation at their frequencies from an even resonance with an appropriate m.

Those interference effects, are a simple consequence of the well defined parity properties of the Hamiltonians generated in the wave-wave interaction process. Such reflection properties will also be present in higher order terms. For instance, it is possible to show that for all of the already calculated second order terms, the parity of the Hamiltonian is equal to $(-1)^l$. As a consequence, interference effects, similar in nature to the ones above described, should also occur among them.

4.9. Higher Order Effects

From the examples seen in the previous sections and from the way each term is obtained, it is possible to extrapolate the possible frequencies for effects of order n:

$$\Delta\omega = \sum_{i=2}^{N} n_i \Delta\omega_i / l \tag{4.138}$$

with $\sum_{i=2}^{N} |n_i| = n$. It is clear that terms of order n contain at most $n+1$ interacting waves.

Two given waves can generate a n order harmonic by two different processes:

1. First harmonic radiation by a n order harmonic resonance.
2. High order harmonic radiation from a low order resonance.

The n order resonance widths are of the order $\epsilon^{\frac{n}{2}}$. The amplitude of their first harmonics should therefore go down exponentially with n. High order harmonics coming from a low order resonance have amplitudes proportional to the Bessel functions J_n which decrease in value, as a function of n, faster than an exponential, and can therefore be neglected. We are led then to the conclusion that harmonic sidebands created by two waves through trapping effects should have an exponential amplitude slope as a first approximation, as is indeed borne out by the data.

4.10. Conclusions

As main results from trapping effects we can quote:

1. Because their frequencies are independent of $v_\perp$, and because if $|n|$ is large enough a resonance will fit in any wave potential, sidebands have narrow linewidths and well defined frequencies, and can be produced independently of carrier amplitude values or variations. However, weaker waves will have a spectrum more finely divided by subharmonics because higher values of $|n|$ will be involved. Integration over different pitch angles will not smear out the resonances.
2. Electrons interact with Doppler shifted wave separations which may be larger than the nominal frequency separations by a factor of three or more. The resulting effect can be understood as either a decrease in the time constants of the system or a decrease in the interacting wave amplitudes.
3. Since around the equator electrons can always be temporarily trapped, i.e. they will describe part of a closed orbit if put inside the main wave potential well, electron streams can always exist giving rise to trapping effects with arbitrarily weak fields, independently of inhomogeneity effects.

4. Due to the FM modulation process, sidebands are created in symmetric pairs. Line growth can change their amplitudes and symmetry appreciably.
5. Trapping predicts an approximately exponential fall-off for the harmonic spectrum, line-line interference effects, and a slow fall-off with distance (in frequency space) of the interaction strength for some resonance types. This last point indicates that a comb of weak, equally separated lines can appreciably affect sideband formation if the number of lines is large enough (the effect is divergent for an infinite set of lines).
6. Although line amplitudes are different, sidebands due to trapping effects are created at the same frequencies as the ones due to external resonances:

$$\omega = \frac{\sum_{i=1}^{N} n_i \omega_i}{\sum_{i=1}^{N} n_i} \tag{4.31}$$

7. Sidebands due to trapping also need a non-zero gradient in $v_{\|}$ to be created.
8. Individual electron oscillations and the continuous spectrum of their frequencies ("trapping" oscillation frequencies) do not directly affect the observed sideband spectra. Those oscillations are convective, occurring as the electron, as part of a stream, moves along the interaction region, and may not even exist for a full cycle. Radiated frequencies are associated with oscillation frequencies of the streams to which the electrons belong. Those oscillation frequencies are only indirectly related to the trapping frequencies, and the frequencies they radiate may be almost an order of magnitude away from available trapping frequencies. The total emitted radiation will be a combined result from all such stream oscillations, and its spectrum will reflect the frequency structure of the externally accelerating forces, and not of the overall electron population.
9. Chaos, always present when internal resonances are formed, is an important factor in the formation of the final radiation spectra, contributing to saturation effects.
10. Trapped resonances are more protected from inhomogeneity effects than external resonances and should produce radiation over a longer length of the interaction region around the equator.

5. Effect of The Inhomogeneity on Sideband Resonances

5.1. Introduction

This chapter will analyze the effect of the inhomogeneity of the magnetic field of the earth on the resonances studied in chapters 3 and 4. The analytical and numerical methods used are the same as in chapter 3, and so is the notation. A familiarity with chapters 3 and 4 is required.

In section 5.2 of this chapter, phase plots are used to show graphically the effects of the inhomogeneity on the resonances we had previously studied in a homogeneous medium. It is seen that those effects consist mainly of phase shifts superposed on the resonance positions, coupled with complete resonance destruction if the value of the inhomogeneity is large enough. In section 5.3 the electron equations of motion are rewritten to include the inhomogeneity, and in section 5.4 the Lie perturbation method is applied to them to study analytically the effect of the inhomogeneity on the "trapped" resonances. In section 5.5 we explain how the phase shifts created by the inhomogeneity can, even when locally constant in time, produce frequency shifts and line broadening in the sideband radiation received at the end of the interaction region. In section 5.6 we apply the Lie perturbation method to external resonances obtaining results similar to the ones found in sections 5.4 and 5.5 for internal resonances. Section 5.7 takes a look at some general properties of higher order resonances, and section 5.8 contains the conclusions, a chief one among them being that the inhomogeneity is a principal cause for the peculiar but experimentally observed fact that vanishingly small carriers can create sizable sidebands if the sideband producing interaction includes at least one strong carrier.

5.2. Phase Plots and Relation Between Frequency and Phase Shifts

Figure 5.1 shows phase plots for an $l = 2$ first order "trapped" resonance created by perturbing the main wave with a weaker carrier located at $\dot{\theta} = \Omega$. This resonance will radiate mainly at the frequencies $\pm\Omega$ and $\pm\Omega/2$. Figure 5.1.a shows the phase plot for the zero inhomogeneity case, where we can see the two lobed structure of the resonance inside the main wave potential well, and the perturbing carrier to the right, shifted 180° in phase relative to the main wave.

Figure 5.1.b shows the effect of a positive inhomogeneity (a positive gradient of the intensity of the magnetic field of the earth) on the resonances. The resonance associated with the perturbing carrier has been completely wiped out, and therefore such a carrier will experience no growth. However, the "trapped" resonance that it creates is still present and can give rise to growing lines. Since the original amplitude of the perturbing carrier is only 2% (-33dB) of the main carrier, the weak carrier will not be easily seen in the sideband spectrum, but the sidebands it creates will. In the same picture it can be seen that the outermost phase trajectories have been stripped away from the main carrier resonance and that the two lobes in the "trapped" resonance have acquired different negative phase shifts. The first effect is widely known, the second one will be described in detail in section 5.4. There is also a small inward shift of the trapped resonance and a positive phase shift (upward displacement) of the main carrier resonance. This phase shift can easily be shown to be equal to $\sin^{-1}(\tau/\Omega_{t1}^2)$ where τ is the torque associated with the inhomogeneity (see section 5.4), and

Ω_{t1} is the main wave trapping frequency. The internal resonance phase shift will affect the frequency separation between radiated harmonics and sub harmonics. The phase shift in the main resonance will affect the main carrier frequency. (The mechanism for translation of phase shifts into frequency shifts is discussed in section 5.5.)

Figure 5.1.c shows the consequence of moving the perturbing carrier from Ω to $-\Omega$. The equilibrium points in the resonance are reflected around a vertical axis going through $\dot{\theta} = 0$. As a consequence, both their phase shifts become positive.

Figure 5.1.d shows the effect on the phase plot of changing the sign of the inhomogeneity, but keeping the perturbing wave at the frequency Ω. The resonance equilibrium points are reflected around a horizontal axis going through $\theta = 0$. That implies a change in sign of each phase shift in the "trapped" resonance and a change in sign of the main wave upward shift. The total phase shift associated with each radiated sideband is consequently multiplied by minus one.

Figure 5.2 compares the effects of the inhomogeneity on "trapped" and external resonances having the same approximate initial widths.

Figure 5.2.a shows a three wave resonance, already described in chapter 4, for the case of zero inhomogeneity. Figure 5.2.b shows the effect on it of a fairly large inhomogeneity. As in Figure 5.1, it can be seen that the external resonances are completely wiped out, that there is a phase shift, now positive, added to each resonance lobe, that external phase trajectories are stripped away, and that, now in a more pronounced way, there is an upward shift of the main wave resonance together with an appreciable inward motion of the internal resonance. This inward displacement protects and extends the lifetime of the resonance by moving it away from the outward trajectories that are soon destroyed by the inhomogeneity. The inhomogeneity in this case is 0.18 Ω_{t1}^2.

Figure 5.2.c shows several external resonances between two equal intensity carriers for the case of zero inhomogeneity. Figure 5.2.d shows the effect of an inhomogeneity just strong enough to destroy all external resonances including the half harmonic. The value of the inhomogeneity in this case is only .03 Ω_{t1}^2. Since the resonance shown in Figure 5.2.a is in reality still present for inhomogeneities of the order of .25 Ω_{t1}^2, and since the size of the interaction region is proportional to the maximum inhomogeneity that a resonance can withstand, we arrive at the important conclusion that "trapped" resonances can exist over an interaction region almost 10 times as large as external resonances.

5.3. Modification of the Electron Equation of Motion by a Non-Zero Inhomogeneity

The effect of the inhomogeneity on the electron motion can be locally described by a time dependent torque [*Dysthe*, 1971; *Inan et al.*, 1978; *Bell and Inan*, 1981; *Serra*, 1984] applied to the perturbed pendulum equations developed in the preceding chapters. The equation describing the electron motion under the influence of N waves will be then

$$\ddot{\theta} = \tau(t) - \sum_{i=1}^{N} \Omega_{ti}^2 \sin(\theta - \Omega_i t + \phi_i) \tag{5.1}$$

where τ is the inhomogeneity.

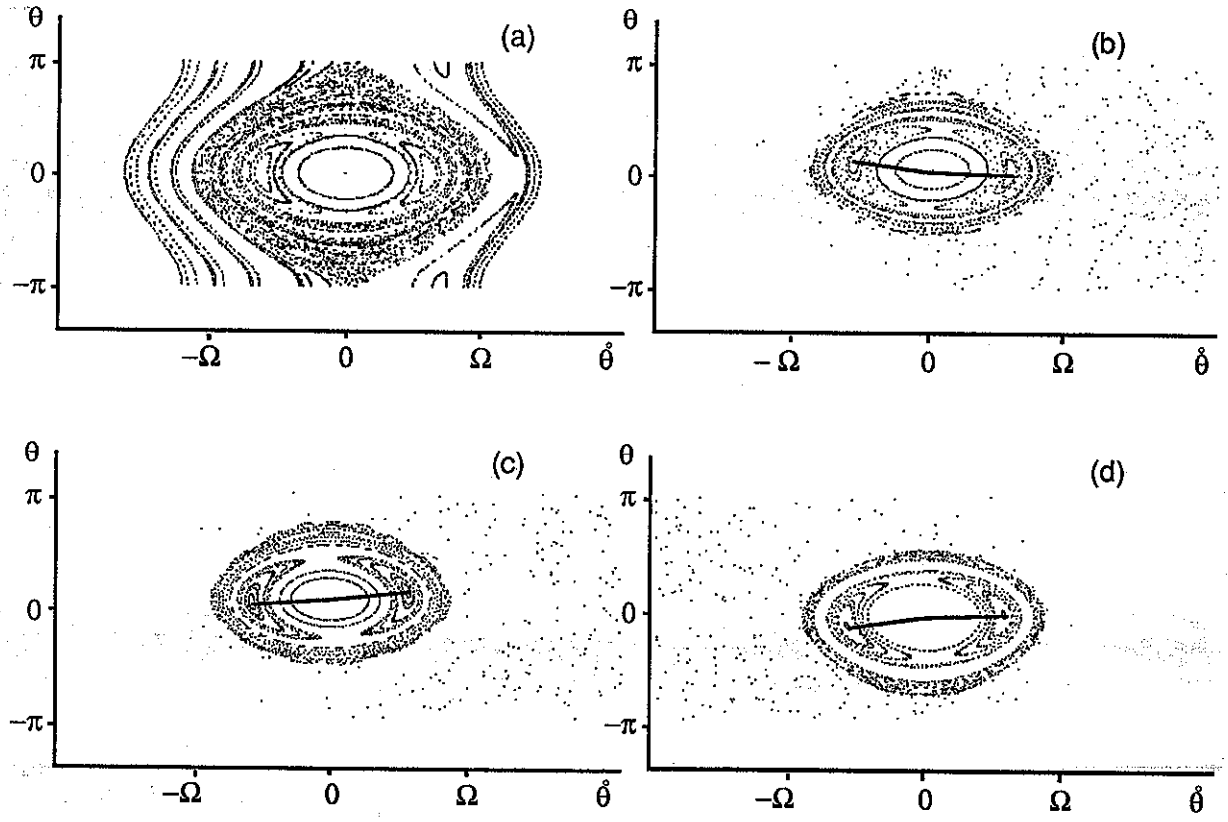

Fig. 5.1. Effect of the inhomogeneity on a half harmonic "trapped" resonance . The main carrier is located at $\dot{\theta} = 0$. The main carrier trapping frequency is slightly above $\Omega/2$, and the weak to main carrier amplitude ratio is 0.02 (-34dB). The weak carrier is shifted in phase by 180° relative to the main carrier: (a) $\tau/\Omega_i^2 = 0$. The weaker carrier is located at $\dot{\theta} = \Omega$. Chaos, the perturbing wave resonance, and the two-lobed half harmonic can be readily seen. (b) $\tau/\Omega_i^2 = 0.08$. The weaker carrier is still located at $\dot{\theta} = \Omega$. Chaos and the perturbing wave resonance have been swept away, but the resonance that the latter creates is still present. Both resonance lobes have acquired a negative phase shift. The main wave resonance has a slight shift upwards. (c) $\tau/\Omega_i^2 = 0.08$. The weaker carrier is now located at $\dot{\theta} = -\Omega$. The resulting plot can be obtained from (b) by a reflection around a vertical axis going through $\dot{\theta} = 0$. As a consequence, the two lobes have their shifts swapped and changed in sign. (d) $\tau/\Omega_i^2 = -0.08$. The weaker carrier is at $\dot{\theta} = \Omega$. The plot can be obtained by reflecting (b) around a horizontal axis going through $\theta = 0$. Both lobes and the main wave resonance have their phase shifts changed in sign.

For the study of external resonances, the $(\theta, \dot{\theta}) = (q, p)$ pair of coordinates is maintained and an equivalent Hamiltonian can be written:

$$h(q,p,t) = p^2/2 - \tau q - \sum_{i=1}^{N} \Omega_{ti}^2 \cos(q - \Omega_i t + \phi_i) \tag{5.2}$$

For the study of internal resonances created by the wave-wave interaction process, we will use

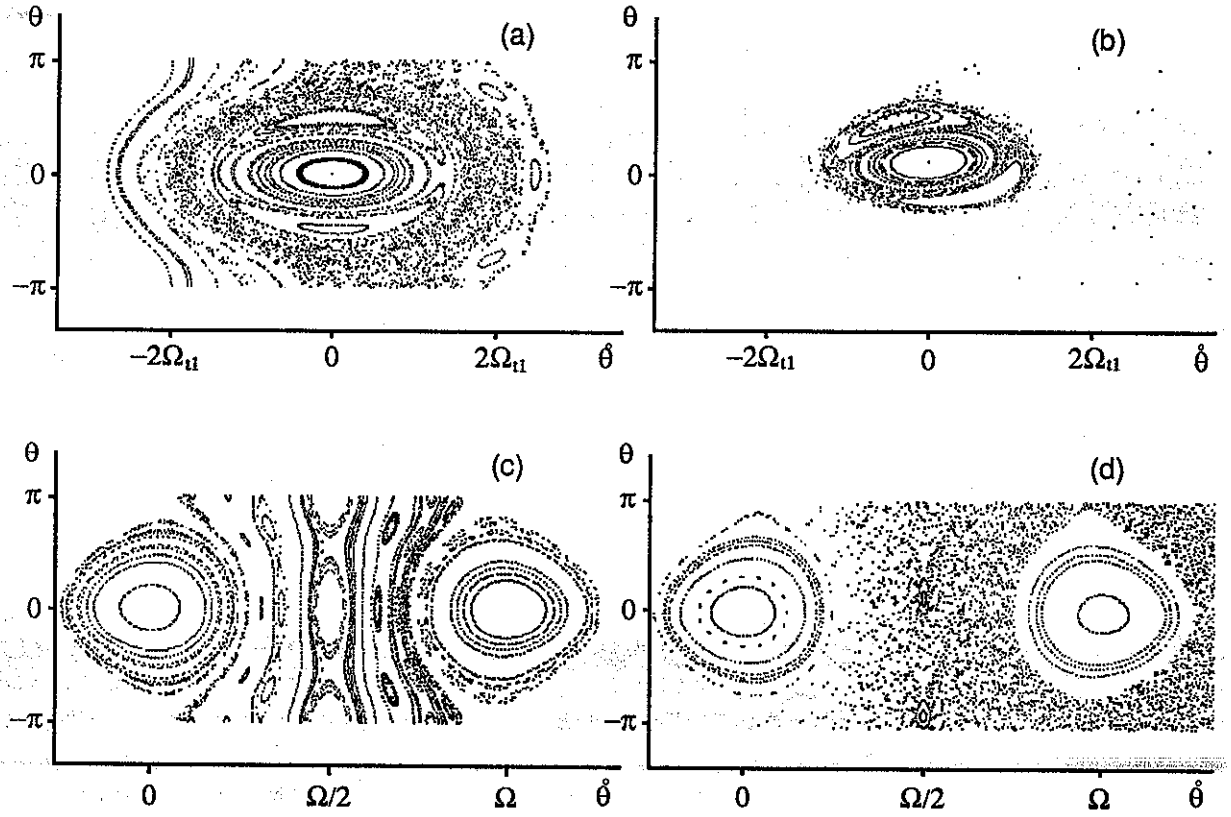

Fig. 5.2. Relative effects of the inhomogeneity on "trapped" and external resonances: (a) $\tau/\Omega_i^2 = 0.0$. Second order two-lobed resonance created by the interaction of three different carriers. (b) $\tau/\Omega_i^2 = 0.18$. Despite the existence of a fairly large inhomogeneity, the resonance is still intact. The most apparent effects on it are the creation of a positive phase shift, and a displacement of its orbit towards the center of the main wave. An upward shift of the main wave resonance can also be seen. (c) $\tau/\Omega_i^2 = 0.0$. Half and one-third harmonic resonances created outside the potential wells of two equal amplitude waves. (d) $\tau/\Omega_i^2 = 0.03$. An extremely small inhomogeneity completely wipes out the one-third and almost completely destroys the half harmonic resonance.

the (ϕ, j) pair of canonical coordinates that gives rise to the following Hamiltonian:

$$h(\phi, j, t) = h_o(j) - \tau\theta(\phi, j) - \sum_{i=2}^{N} \sum_{n=-\infty}^{\infty} \Omega_{ii}^2 V_n(j) \cos(n\phi - \Omega_i t + \phi_i) \tag{5.3}$$

where

$$\theta = 2\sin^{-1}\left[\kappa \, \mathrm{sn}\left(\frac{2K(\kappa)\phi}{\pi}\right)\right] \tag{5.4}$$

can be rewritten as [*Chirikov*, 1979]:

$$\theta = \sum_{n=1}^{\infty} b_n(j) \sin\left[(2n-1)\phi\right] \tag{5.5}$$

with

$$b_n(j) = 2\left(\frac{\Omega_{t1}}{\Omega_t}\right)^2 \frac{V_{2n-1}(j)}{(2n-1)^2} \tag{5.6}$$

Those equations will be used to study analytically the inhomogeneity effects observed in the phase plots described in the preceding sections.

5.4. First Order Internal Resonances

If we put $\Omega_{ti}^2 = \epsilon A_i$, we can write the Hamiltonian as

$$h(\phi, j, t) = h_o(j) + \epsilon h_1(\phi, j, t) \tag{5.7}$$

with

$$h_1 = -\tau\theta(\phi, j) - \sum_{i=2}^{N} \sum_{n=-\infty}^{\infty} A_i V_n(j) \cos(n\phi - \Omega_i t + \phi_i) \tag{5.8}$$

(We have substituted $\epsilon\tau$ for τ in $h(\phi, j, t)$ to explicitly show that perturbations from the inhomogeneity and from the additional carriers on the main wave have the same order of magnitude.)

To study first order resonances we put :

$$K_o = h_o \tag{5.9}$$

and choose

$$K_1 = -A_j V_l(J) \cos(l\Phi - \Omega_j t + \phi_j) \tag{5.10}$$

This implies

$$W_1 = -\int^t d\tau \ \{h_1[\Phi + \Omega_t(\tau - t), J, \tau] - K_1[\Phi + \Omega_t(\tau - t), J, \tau]\}$$

or

$$W_1 = -\frac{\tau}{\Omega_t(J)} \sum_{n=1}^{\infty} \frac{b_n(J)}{(2n-1)} \cos[(2n-1)\Phi] + \sum_{\substack{(i\neq j) \text{or} \\ (n\neq l)}} a_{in} \sin(n\Phi - \Omega_i t + \phi_i) \tag{5.11}$$

with

$$a_{in} = \frac{A_i V_n(J)}{n\Omega_t(J) - \Omega_i} \tag{5.12}$$

The corrections to the resonance due to the inhomogeneity, are second order terms that must be transferred to K_2 from

$$\{W_1, h_1 + K_1\} = \frac{\partial W_1}{\partial \Phi}\frac{\partial(h_1 + K_1)}{\partial J} - \frac{\partial W_1}{\partial J}\frac{\partial(h_1 + K_1)}{\partial \Phi} \tag{5.13}$$

where $h_1 + K_1$ can be written as:

$$h_1 + K_1 = -\tau\theta(\Phi, J) - \sum_{i,n}(1 + \delta_{ij}\delta_{nl}) A_i V_n \cos(n\Phi - \Omega_i t + \phi_i) \tag{5.14}$$

Differentiating the above expression with respect to Φ and J, inserting the results in equation (5.13), transforming products of trigonometric functions into sums and differences, and putting into K_2 all resulting time independent and resonant terms, we get:

$$\begin{aligned} 2K_2 =& 2K_2^o - \frac{\tau^2}{2\Omega_t}\frac{d}{dJ}\sum_{n=1}^{\infty} b_n^2 + \\ & \frac{\tau A_j}{2\Omega_t} \sum_{m=1}^{\infty} \left[\frac{(b_m' - b_m \frac{\Omega_t'}{\Omega_t})}{(2m-1)}(n_+ V_{n_+} + n_- V_{n_-}) + b_m(V_{n_+}' - V_{n_-}') \right] \sin(l\Phi - \Omega_j t + \phi_j) \end{aligned} \tag{5.15}$$

where $n_\pm = l \pm (2m-1)$. Computer analysis shows that keeping only the first term in both summations leads to a very good approximation to the equation above. If we take into consideration that

$$b_1' = b_1\left(\frac{V_1'}{V_1} - 2\frac{\Omega_t'}{\Omega_t}\right) \tag{5.16}$$

we get for K_2:

$$K_2 = K_2^o - \frac{\tau^2}{4\Omega_t}\frac{db_1^2}{dJ} + \frac{\tau}{2}\frac{b_1 A_j}{\Omega_t}\left\{\left(\frac{V_1'}{V_1} - \frac{5}{2}\frac{\Omega_t'}{\Omega_t}\right)[(l+1)V_{l+1} + (l-1)V_{l-1}] + (V_{l+1}' - V_{l-1}')\right\}\sin(l\Phi - \Omega_j t + \phi_j) \tag{5.17}$$

It will be convenient to transform the derivatives in the above expression into derivatives with respect to the adimensional variable κ^2, using the operator identity

$$\frac{\partial}{\partial J} = \frac{\Omega_t}{2\Omega_{t1}^2}\frac{\partial}{\partial \kappa^2} \tag{5.18}$$

We can then write:

$$K_2 = K_2^o - \frac{1}{8}\left(\frac{\tau}{\Omega_{t1}}\right)^2\frac{db_1^2}{d\kappa^2} + \tau\frac{A_j}{\Omega_{t1}^2}f_l(\kappa^2)\sin(l\Phi - \Omega_j t + \phi_j) \tag{5.19}$$

with

$$f_l(\kappa^2) = \frac{b_1}{4}\left\{\left(\frac{V_1'}{V_1} - \frac{5}{2}\frac{\Omega_t'}{\Omega_t}\right)[(l+1)V_{l+1} + (l-1)V_{l-1}] + (V_{l+1}' - V_{l-1}')\right\} \tag{5.20}$$

where a primed variable, in the above equation only, means it is differentiated with respect to κ^2. The total Hamiltonian will be

$$K = h_o - \epsilon A_j V_l\cos(l\Phi - \Omega_j t + \phi_j) + \epsilon^2 K_2^o - \frac{\epsilon^2}{8}\left(\frac{\tau}{\Omega_{t1}}\right)^2\frac{db_1^2}{d\kappa^2} + \epsilon^2\tau\frac{A_j}{\Omega_{t1}^2}f_l(\kappa^2)\sin(l\Phi - \Omega_j t + \phi_j) \tag{5.21}$$

If we define

$$\Phi_o(l,\kappa^2) = \frac{\epsilon\tau}{\Omega_{t1}^2}\frac{f_l(\kappa^2)}{lV_l(\kappa^2)} = \frac{\epsilon\tau}{\Omega_{t1}^2}\Phi_{norm} \tag{5.22}$$

and assume $\sin(l\Phi_o) \approx l\Phi_o$, we can finally write

$$K = h_o + \epsilon^2 K_2^o - \frac{\epsilon^2}{8}\left(\frac{\tau}{\Omega_{t1}}\right)^2\frac{db_1^2}{d\kappa^2} - \epsilon A_j V_l\cos[l(\Phi + \Phi_o) - \Omega_j t + \phi_j] \tag{5.23}$$

Figure 5.3 shows plots of Φ_{norm} as a function of κ^2 for a few low values of l and also the asymptotic value when $l \to \infty$.

From the way Φ_o was calculated, it is possible to have an understanding of the meaning of such a phase shift. Because the inhomogeneity is only a perturbation, the electron stream motion is mainly controlled by the main wave. The oscillatory motion imparted on the stream inside the main wave potential well makes the potential from the inhomogeneity, which is linear in θ, seem oscillatory with a frequency $\dot{\Phi}$. The first term in the series for this effective oscillatory potential is equivalent to a first order resonance with $l = 1$ and $\Omega_i = 0$. The phase shift we are looking for is a second order effect that comes from the interaction of this effective resonance with two first order

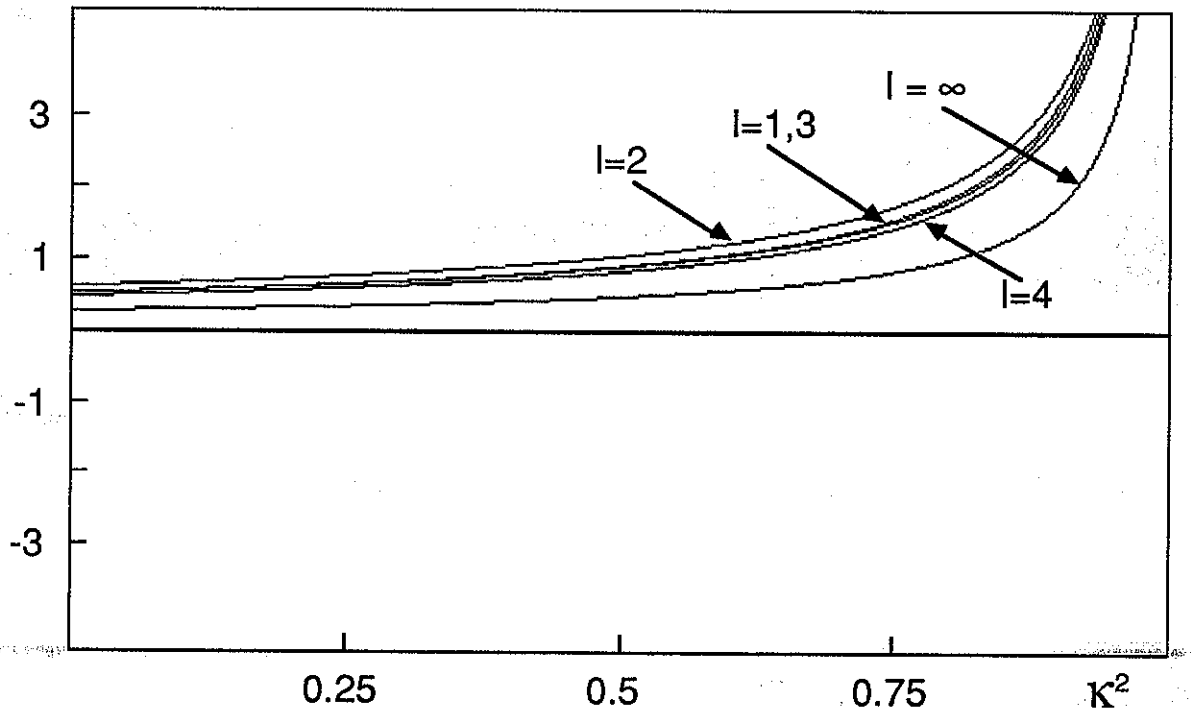

Fig. 5.3. Plot of $\Phi_{norm} = (\Omega_{t1}^2/\tau)\Phi_o$, the normalized constant part of the phase shift caused by the action of the inhomogeneity on first order resonances. The picture shows plots for $l = 1 \ldots 4$ and the asymptotic value $l = \infty$. The divergences at $\kappa^2 = 1$ indicate the breakdown of the expressions near the separatrix due to the existence of chaos and the stripping away of closed phase orbits by the inhomogeneity.

resonances having parameters $(l+1, \Omega_j)$ and $(l-1, \Omega_j)$. Their interaction gives rise to a second order resonance with parameters (l, Ω_j), shifted by $-90°$ in phase relative to the initial trapped resonance. The coherent superposition of these two resonances gives rise to the phase shifted resonance.

Hamilton's equations applied to K, will give:

$$\dot{J} = -\frac{\partial K}{\partial \Phi} = -\epsilon l A_j V_l(J) \sin\left[l(\Phi + \Phi_o) - \Omega_j t + \phi_j\right] \tag{5.24}$$

$$\begin{aligned}\dot{\Phi} = \frac{\partial K}{\partial J} =& \frac{dh_o(J)}{dJ} + \epsilon^2 \frac{dK_2^o}{dJ} - \frac{\epsilon^2}{16}\left(\frac{\tau}{\Omega_{t1}^2}\right)^2 \Omega_t \frac{d^2 b_1^2}{d(\kappa^2)^2} - \\ & \epsilon A_j \frac{dV_l(J)}{dJ} \cos\left[l(\Phi + \Phi_o) - \Omega_j t + \phi_j\right] + \\ & \epsilon l A_j V_l(J) \frac{d\Phi_o}{dJ} \sin\left[l(\Phi + \Phi_o) - \Omega_j t + \phi_j\right]\end{aligned} \tag{5.25}$$

Since

$$\ddot{\Phi} = \frac{\partial \dot{\Phi}}{\partial J}\dot{J} + \frac{\partial \dot{\Phi}}{\partial \Phi}\dot{\Phi} + \frac{\partial \dot{\Phi}}{\partial t} \tag{5.26}$$

we can put

$$\ddot{\Phi} \approx \frac{d^2 h_o(J)}{dJ^2}\dot{J} = -\epsilon \frac{d^2 h_o(J)}{dJ^2} l A_j V_l(J) \sin\left[l(\Phi + \Phi_o) - \Omega_j t + \phi_j\right] \tag{5.27}$$

The equation describes an $|l|$-lobed resonance oscillating inside the main wave potential well with frequency $\Delta\omega_j/l$ and shifted in phase by $-\Phi_o$. ($\Delta\omega_j$ is the frequency separation between the perturbing wave j and the main wave.)

From the $\dot{\Phi}$ equation we also get at resonance:

$$\Omega_j/l = \Omega_t + \epsilon A_j \frac{dV_l}{dJ} + \epsilon^2 \frac{dK_2^o}{dJ} - \frac{\epsilon^2}{16}\left(\frac{\tau}{\Omega_{t1}^2}\right)^2 \Omega_t \frac{d^2 b_1^2}{d(\kappa^2)^2} \tag{5.28}$$

Defining J_o as the value of J associated with the resonance as $\epsilon \longrightarrow 0$, and expanding Ω_t around this value, we get:

$$\Omega_t(J) = \Omega_t(J_o) - \left|\frac{d\Omega_t}{dJ}\right| \Delta J = \Omega_j/l - \left|\frac{d\Omega_t}{dJ}\right| \Delta J \tag{5.29}$$

Substituting the last expression into equation (5.28), we can calculate J and ΔJ :

$$J = J_o + \Delta J = J_o + \Delta J_{hom} + \Delta J_{inhom} \tag{5.30}$$

where

$$\Delta J_{hom} = \left(\epsilon A_j \frac{dV_l}{dJ} + \epsilon^2 \frac{dK_2^o}{dJ}\right) \left|\frac{d\Omega_t}{dJ}\right|^{-1} \tag{5.31}$$

and

$$\Delta J_{inhom} = -\frac{\epsilon^2}{16}\Omega_t \left|\frac{d\Omega_t}{dJ}\right|^{-1} \left(\frac{\tau}{\Omega_{t1}^2}\right)^2 \frac{d^2 b_1^2}{d(\kappa^2)^2} \tag{5.32}$$

Since the second derivative of b_1^2 is positive, in the (Φ, J) coordinate system the inhomogeneity has the effect of decreasing the value of J, i.e, of pulling the resonance towards the center of oscillation.

To look at the stream motion in the (ϕ, j) variables, we need the transformation equations correct to second order:

$$\phi = \Phi - \epsilon \frac{\partial W_1}{\partial J} - \frac{\epsilon^2}{2}\langle\{W_1, \frac{\partial W_1}{\partial J}\}\rangle \tag{5.33}$$

$$j = J + \epsilon \frac{\partial W_1}{\partial \Phi} + \frac{\epsilon^2}{2}\langle\{W_1, \frac{\partial W_1}{\partial \Phi}\}\rangle \tag{5.34}$$

where the pointed brackets mean as always that the time independent part of the expression should be taken.

Evaluating specific terms we obtain:

$$\frac{\partial W_1}{\partial \Phi} = \frac{\tau}{\Omega_t}\sum_{n=1}^{\infty} b_n \sin\left[(2n-1)\Phi\right] + \sum_{\substack{(i\neq j)\text{or} \\ (n\neq l)}} n a_{in} \cos(n\Phi - \Omega_i t + \phi_i) \tag{5.35}$$

$$\frac{\partial W_1}{\partial J} = -\tau \sum_{n=1}^{\infty} \left(\frac{b_n}{\Omega_t}\right)' \frac{1}{(2n-1)} \cos\left[(2n-1)\Phi\right] + \sum_{\substack{(i\neq j)\text{or} \\ (n\neq l)}} a'_{in} \sin(n\Phi - \Omega_i t + \phi_i) \tag{5.36}$$

$$\langle\{W_1, \frac{\partial W_1}{\partial \Phi}\}\rangle = \frac{\tau^2}{\Omega_t}\sum_{n=1}^{\infty} b_n \left(\frac{b_n}{\Omega_t}\right)' + \sum_{\substack{(i\neq j)\text{or} \\ (n\neq l)}} n^2 a_{in} a'_{in} \tag{5.37}$$

$$\langle\{W_1, \frac{\partial W_1}{\partial J}\}\rangle = 0 \tag{5.38}$$

For the $J \rightarrow j$ transformation, we drop the first order time dependent terms, we keep only the first term of the time independent series in the expression for $\partial W_1/\partial\Phi$, and transform all derivatives into derivatives with respect to κ^2. We then get:

$$j = j_{hom} + \epsilon\frac{\tau}{\Omega_t}b_1\sin\Phi - \frac{\epsilon^2}{2}\Omega_t\left(\frac{\tau}{\Omega_{t1}^2}\right)^2\frac{d^2b_1^2}{d(\kappa^2)^2} + \frac{\epsilon^2}{4}\Omega_{t1}\left(\frac{\tau}{\Omega_{t1}^2}\right)^2 b_1\frac{d}{d\kappa^2}\left(\frac{\Omega_{t1}b_1}{\Omega_t}\right) \tag{5.39}$$

where

$$j_{hom} = J_o + \Delta J_{hom} + \sum_{\substack{(i\neq j)\text{or}\\(n\neq 1)}} n^2 a_{in}\frac{da_{in}}{dJ} \tag{5.40}$$

Which can be rewritten as:

$$j = j_{hom} + \epsilon\frac{\tau}{\Omega_t}b_1\sin\Phi + \epsilon^2\Omega_{t1}\left(\frac{\tau}{\Omega_{t1}^2}\right)^2\Delta j_{norm} \tag{5.41}$$

If τ is positive, the oscillatory term linear in ϵ is positive when θ is positive and negative otherwise. Its effect is to push all points in the phase trajectories upwards, and essentially describes the phase shift of the main wave resonance observed in the phase plots of Figures 5.1 and 5.2. The constant second order term describes a systematic shift of the "trapped" resonance towards a different orbit. Figure 5.4 has a plot of Δj_{norm}, which is adimensional and depends on κ^2 only. The plot shows it to be negative and therefore describing a displacement of the resonance towards the center of oscillation.

For the $\Phi \rightarrow \phi$ transformation we can write $\Phi = \Phi_{hom} - \Phi_o$, where Φ_{hom} is the value of Φ obtained from Hamilton's equations when $\tau = 0$. We then throw away all explicitly time dependent terms, and keep only the first term in the remaining series expansion for $\partial W_1/\partial J$, to get:

$$\phi = \Phi_{hom} - \Phi_o + \epsilon\tau\left(\frac{b_1}{\Omega_t}\right)'\cos\Phi \tag{5.42}$$

We see that added to the constant phase shift $-\Phi_o$, there is a periodic term that for positive τ is positive when $\dot{\theta}$ is positive and negative otherwise. For the two-lobed resonances shown in Figures 5.1 and 5.2, this term advances the motion of an equilibrium point at the right of the axis $\dot{\theta} = 0$ and retards its motion at the left. This term is the cause of the different phase shifts observed for the two lobes of the resonance in Figure 5.1. Such a term can be understood as a consequence of the upward shift of the main wave resonance that decreases the j values of the lower part of the phase trajectory, increasing the values of the trapping frequency, and does the opposite on top.

The expression above explains the values and reflection properties of the phase shifts observed in the phase plots of Figure 5.1:

We can rewrite it as

$$\phi = \Phi_{hom} - \Phi_o + \tau a\cos\Phi = \Phi_{hom} + \Delta\phi \tag{5.43}$$

Φ_{hom} is the equilibrium point of the resonances for $\tau = 0$. For the resonance located at $\Phi_{hom} = 0$, the phase shift will be:

$$\Delta\phi_1 = -\Phi_o + \tau a\cos\Phi_o \tag{5.44}$$

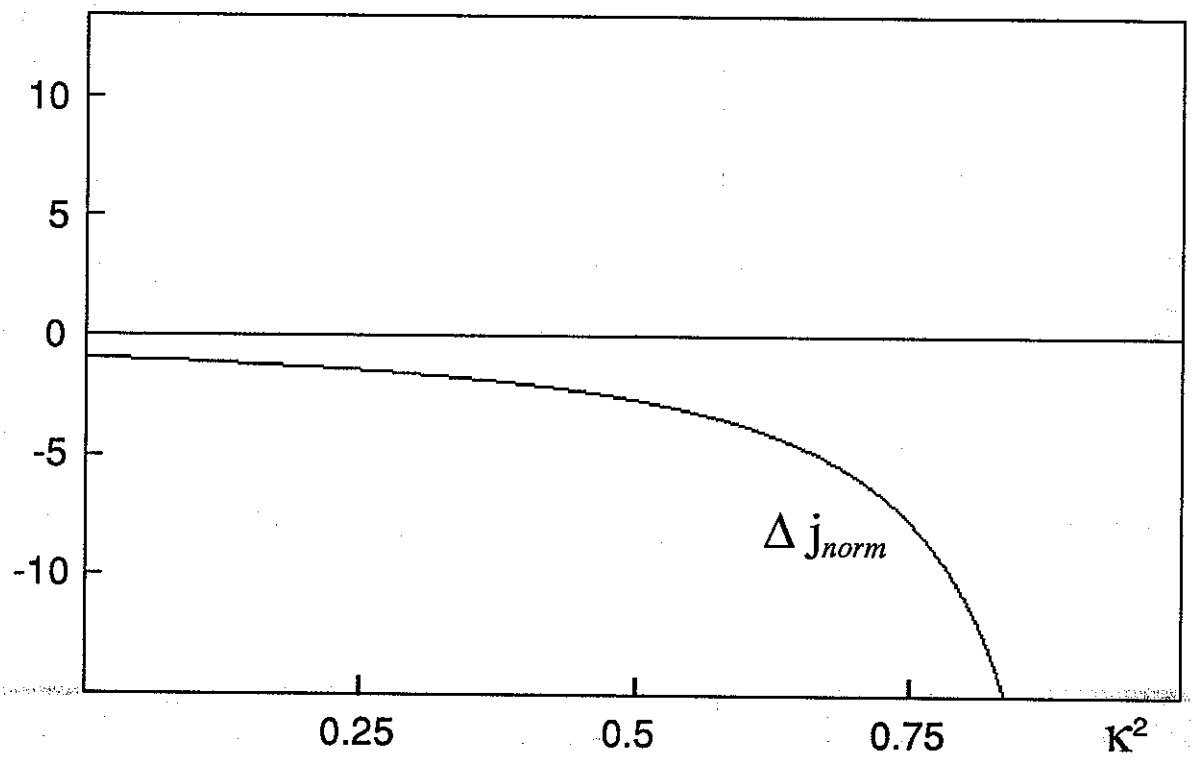

Fig. 5.4. Plot of Δj_{norm}, the normalized constant shift in j due to the action of the inhomogeneity on the main wave potential. The shift is negative and independent of the specific resonance under consideration. The divergence at $\kappa^2 = 1$ is due to chaos and the presence of the inhomogeneity that combined destroy the outer electron orbits of the main resonance rendering the analytical expressions inadequate.

and for the resonance at $\Phi_{hom} = \pi$,

$$\Delta\phi_2 = -\Phi_o - \tau a \cos\Phi_o \tag{5.45}$$

We see that in $\Delta\phi_1$ the two contributing terms have opposite signs and tend to cancel. For $\Delta\phi_2$ they add. This makes $|\Delta\phi_2| > |\Delta\phi_1|$ as seen in Figure 5.1.b.

When the perturbing wave is shifted from Ω to $-\Omega$, l changes to $-l$. It is fairly easy to show that Φ_o is odd under such a transformation, i.e, $\Phi_o(-l,\kappa^2) = -\Phi_o(l,\kappa^2)$. The effects on the phase shifts are:

$$\Delta\phi_1 \rightarrow \Phi_o + \tau a \cos\Phi_o = -\Delta\phi_2 \tag{5.46}$$

and

$$\Delta\phi_2 \rightarrow \Phi_o - \tau a \cos\Phi_o = -\Delta\phi_1 \tag{5.47}$$

Those two equations define the reflection transformation seen in Figure 5.1.c.

When the inhomogeneity is multiplied by -1, both terms change sign because they are proportional to τ. This implies

$$\Delta\phi_{1,2} \rightarrow -\Delta\phi_{1,2} \tag{5.48}$$

that are the reflection properties seen in Figure 5.1.d.

As will be shown in the next section, the relevant part of the phase shifts is the constant part, Φ_o, and the important result to be recalled is that Φ_o changes sign under either of the transformations considered above and represented in the phase plots of Figure 5.1.

5.5. Internal Resonance Radiation Frequency Shifts

The internal resonance phase shifts are a sum of two terms: a constant part, Φ_o, common to all points in the resonance, and an oscillatory part that depends on the angular location of each lobe. The oscillatory part is the cause of the unequal phase shifts in the phase plots described in section 5.2. Its presence will modulate the resonance motion producing additional radiation falling on already established sideband positions. This radiation will not affect the profile of the radiated spectrum to a great extent and its presence will be neglected. We will concentrate instead on the effect that Φ_o has on the resonance radiation.

If Ω_{t1} is time dependent, Φ_o will also be time dependent giving origin to frequency shifts. Reminding ourselves that Ω_t remains equal to Ω_j/l, independently of the variations in the wave trapping frequency, we can write :

$$\Omega_{t1} = \frac{2\Omega_j K(\kappa)}{\pi l} \tag{5.49}$$

and

$$\dot{\Omega}_{t1} = \frac{\Omega_{t1}}{K(\kappa)} \frac{dK(\kappa)}{d\kappa^2} \frac{d\kappa^2}{dt} \tag{5.50}$$

Differentiating Φ_o we will get the frequency drift $\Delta\omega_{local}$:

$$\Delta\omega_{local} = \Phi_o \frac{\dot{\Phi}_{norm}}{\Phi_{norm}} - 2\frac{\dot{\Omega}_{t1}}{\Omega_{t1}}\Phi_o \tag{5.51}$$

Since

$$\dot{\Phi}_{norm} = \frac{d\Phi_{norm}}{d\kappa^2} \frac{d\kappa^2}{dt} \tag{5.52}$$

we can write

$$\Delta\omega_{local} = \Phi_o \frac{\dot{\Omega}_{t1}}{\Omega_{t1}} \left[\frac{\Phi'_{norm}}{\Phi_{norm}} \frac{K(\kappa)}{K'(\kappa)} - 2 \right] \tag{5.53}$$

where the prime means differentiation with respect to κ^2, and the time derivatives should be taken at a fixed point in space.

It is possible to show that the first term within brackets is always larger than 2. Therefore, if the main wave amplitude is increasing, the frequency shift has always the same sign as the phase shift Φ_o.

Figure 5.5 shows how frequency shifts can be created at a receiver at the end of the interaction region even when Φ_o is locally constant in time. We assume that electrons propagate in the negative z-direction, and for simplicity we reduce the continuous interaction region to three localized points in space where radiation is created. The vertical axes represent the phase of the radiation produced by the resonances if the inhomogeneity were zero. We assume that the wave configuration is such as to produce a positive phase shift on the radiation at the beginning of the interaction region (B_2) and therefore a negative shift at its end (B_0). In the middle point there is no inhomogeneity and the shift

is zero. We assume that, at a certain moment, B_0 and B_2 have the same amplitude. The phase of the received radiation, B_t, will then be equal to zero. If over a time interval Δt, B_0 decreases and B_2 increases in amplitude, the resulting field, B_t, will undergo a positive phase shift, $\Delta\Phi$. This will be detected by the receiver as an increase in frequency, $\Delta\omega_{spatial} = \Delta\Phi/\Delta t$. We see that variations in amplitude of component fields having an inhomogeneity dependent phase shift are enough to create an overall variable frequency field, even when the phase shifts are locally constant in time.

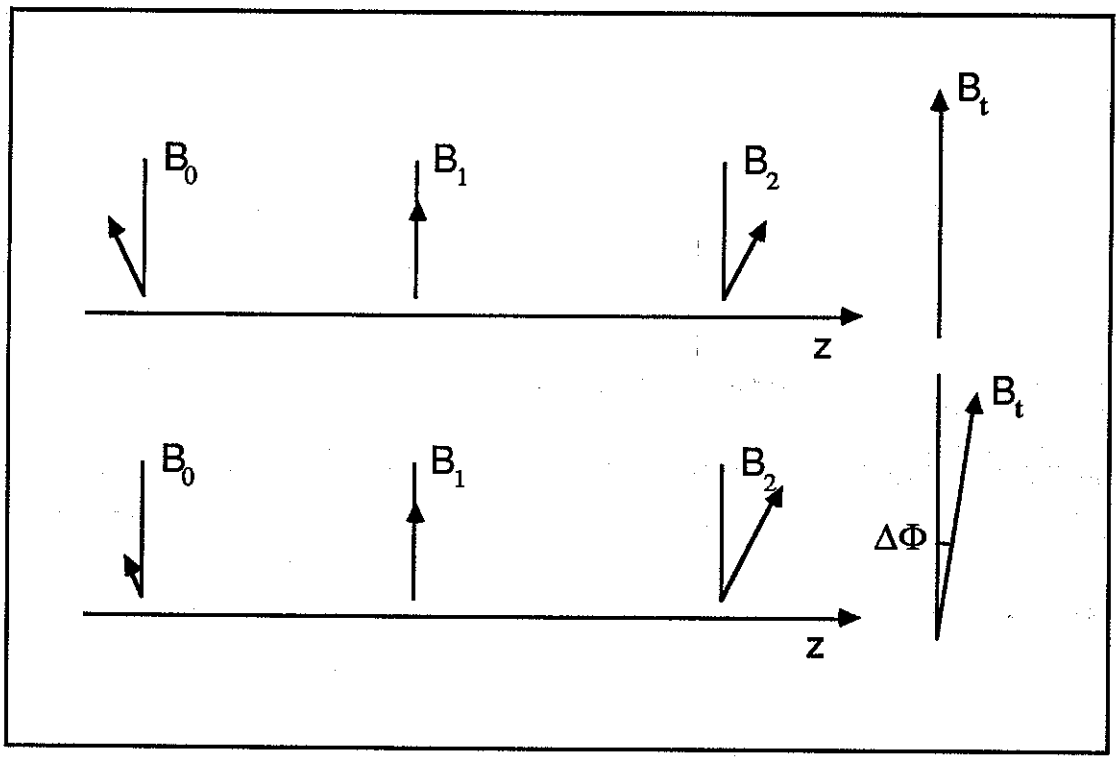

Fig. 5.5. Schematic representation of the transformation of resonance phase shifts into radiation frequency shifts. B_t is the vector sum of B_0, B_1, and B_2. The vertical axes represent the vector phases if the inhomogeneity were equal to zero. The upper part of the picture shows a situation in which the amplitudes of the component fields add up to a zero phase shifted B_t. The lower part shows what happens when component fields vary in magnitude keeping a constant phase. The result is a phase shift on B_t. If the shift $\Delta\Phi$ happens on a time interval Δt, the frequency shift will be $\Delta\omega_{spatial} \approx \Delta\Phi/\Delta t$.

Since the phase shifts are dependent on Ω_{t1}, and therefore on $v_\perp$, we conclude that associated with the shifts in frequency there will be an increase in the linewidths of the sideband waves as they move away from their original positions in the frequency axis.

5.6. External Resonances - Half Harmonic

To study external resonances, we start with the Hamiltonian written as a function of $(\theta, \dot{\theta}) = (q, p)$:

$$h(q,p,t) = h_o(q,p,t) + \epsilon h_1(q,p,t) \tag{5.54}$$

with

$$h_o = p^2/2, \quad h_1 = -\tau q - \sum_{i=1}^{N} A_i \cos(q - \Omega_i t + \phi_i) \tag{5.55}$$

where again a factor of ϵ was factored out of τ.

To arrive at the corrections created by the inhomogeneity on the half harmonic resonance, we choose $K_o = h_o$ and $K_1 = -\tau Q$. This implies

$$W_1 = \sum_{i=1}^{N} \frac{A_i}{(P - \Omega_i)} \sin(Q - \Omega_i t + \phi_i) \tag{5.56}$$

The second order Hamiltonian containing the half harmonic is chosen to be

$$K_2 = \frac{1}{4} \sum_{i=1}^{N} \frac{A_i^2}{(P-\Omega_i)^2} - \frac{A_i A_j}{4} \left[\frac{1}{(P-\Omega_i)^2} + \frac{1}{(P-\Omega_j)^2} \right] \cos(2Q - 2\Omega_{\frac{1}{2}} t + \phi_i + \phi_j) \tag{5.57}$$

The corrections to the resonance will show up in the K_3 terms depending both on τ and on the argument $(2Q - 2\Omega_{\frac{1}{2}} t + \phi_i + \phi_j)$. To calculate K_3 we need W_2 that can be found similarly to the homogeneous case to be:

$$\begin{aligned} W_2 = & \sum_{i,j=1}^{N} \frac{A_i A_j}{2(P-\Omega_i)^2 \left[2P - (\Omega_i + \Omega_j)\right]} \sin\left[2Q - (\Omega_i + \Omega_j)t + \phi_i + \phi_j\right] - \\ & \sum_{\substack{i,j=1 \\ i \neq j}}^{N} \frac{A_i A_j}{2(P-\Omega_i)^2(\Omega_i - \Omega_j)} \sin\left[(\Omega_i - \Omega_j)t - (\phi_i - \phi_j)\right] - \\ & 2\tau \sum_{i=1}^{N} \frac{A_i}{(P-\Omega_i)^3} \cos(Q - \Omega_i t + \phi_i) \end{aligned} \tag{5.58}$$

Relevant terms for K_3 will come only from $\frac{1}{2} L_2 h_1$ and from $\frac{1}{2} L_1^2 h_1$. They give:

$$\frac{1}{2} L_2 h_1 \to -\frac{3\tau A_i A_j}{2} \left[\frac{1}{(P-\Omega_i)^4} + \frac{1}{(P-\Omega_j)^4} \right] \sin(2Q - 2\Omega_{\frac{1}{2}} t + \phi_i + \phi_j) \tag{5.59}$$

and

$$\frac{1}{2} L_1^2 h_1 \to \frac{\tau A_i A_j}{2} \left[\frac{(P-\Omega_i)(P-\Omega_j) + (\Omega_i - \Omega_j)^2}{(P-\Omega_i)^3 (P-\Omega_j)^3} \right] \sin(2Q - 2\Omega_{\frac{1}{2}} t + \phi_i + \phi_j) \tag{5.60}$$

K_3 can, therefore, be written as

$$K_3 = -\tau A_i A_j f(P) \sin(2Q - 2\Omega_{\frac{1}{2}} t + \phi_i + \phi_j) \tag{5.61}$$

with

$$f(P) = \frac{1}{2} \left[\frac{1}{(P-\Omega_i)^4} + \frac{1}{(P-\Omega_j)^4} - \frac{1}{3} \frac{(P-\Omega_i)(P-\Omega_j) + (\Omega_i - \Omega_j)^2}{(P-\Omega_i)^3 (P-\Omega_j)^3} \right] \tag{5.62}$$

that has the following properties:

$$f(\Omega_{\frac{1}{2}}) = \frac{24}{(\Omega_i - \Omega_j)^4}, \quad f'(\Omega_{\frac{1}{2}}) = 0 \tag{5.63}$$

The full Hamiltonian is now

$$\begin{aligned} K =& \frac{P^2}{2} - \epsilon\tau Q + \frac{\epsilon^2}{4}\sum_{i=1}^{N}\frac{A_i^2}{(P-\Omega_i)^2} - \\ & \frac{\epsilon^2 A_i A_j}{4}\left[\frac{1}{(P-\Omega_i)^2} + \frac{1}{(P-\Omega_j)^2}\right]\cos(2Q - 2\Omega_{\frac{1}{2}}t + \phi_i + \phi_j) - \\ & \epsilon^3\tau A_i A_j f(P)\sin(2Q - 2\Omega_{\frac{1}{2}}t + \phi_i + \phi_j) \end{aligned} \tag{5.64}$$

Defining

$$2\theta_o = \frac{4\epsilon\tau f(P)(P-\Omega_i)^2(P-\Omega_j)^2}{(P-\Omega_i)^2 + (P-\Omega_j)^2} \approx \frac{12\epsilon\tau}{(\Omega_i - \Omega_j)^2} \tag{5.65}$$

where the approximate equality is valid near the resonance, the Hamiltonian can be rewritten as

$$\begin{aligned} K =& \frac{P^2}{2} - \epsilon\tau Q + \frac{\epsilon^2}{4}\sum_{i=1}^{N}\frac{A_i^2}{(P-\Omega_i)^2} - \\ & \frac{\epsilon^2 A_i A_j}{4}\left[\frac{1}{(P-\Omega_i)^2} + \frac{1}{(P-\Omega_j)^2}\right]\cos\left[2(Q-\theta_o) - 2\Omega_{\frac{1}{2}}t + \phi_i + \phi_j\right] \end{aligned} \tag{5.66}$$

We see that apart from creating a small initial phase shift on the equilibrium positions, the inhomogeneity acts on the half harmonic as it does on a regular resonance created directly by a single weak carrier propagating in the magnetosphere. If we calculate the equation of motion, we obtain:

$$\ddot{Q} = \epsilon\tau - \frac{4\epsilon^2 A_i A_j}{(\Omega_i - \Omega_j)^2}\sin\left[2(Q-\theta_o) - 2\Omega_{\frac{1}{2}}t + \phi_i + \phi_j\right] \tag{5.67}$$

The equilibrium points are shifted by

$$\Delta Q_{shft} = \theta_o + \frac{1}{2}\sin^{-1}\left[\frac{\tau(\Omega_i - \Omega_j)^2}{4\epsilon A_i A_j}\right] \tag{5.68}$$

from their original values. There will be no oscillatory motion if

$$|\tau| > \frac{4\epsilon A_i A_j}{(\Omega_i - \Omega_j)^2} \tag{5.69}$$

This is a very small value for the inhomogeneity meaning that the closed orbits associated with such resonances will be easily stripped away and the resonance destroyed as shown in Figure 5.2.d.

Frequency shifts and line broadening will also be observed in the radiation coming from external resonances. They are originated in a manner similar to the shifts and broadening associated with internal resonances described in section 5.5, a main difference being that for external resonances any interacting carrier amplitude variation will contribute to the local time dependence of the phase shifts.

5.7. Higher Order Resonances

Higher order "trapped" and external resonances can also be studied but the expressions describing the effects of the inhomogeneity are extremely complex and can only be arrived at with the help of an algebraic manipulation computer program. Those expressions will not be reproduced here, but a summary of the principal results is possible to make:

5.7.1. Internal Resonances

Some inhomogeneity effects come directly from the interaction between the main wave and the inhomogeneity and should not depend on the type of resonance under study. Therefore, we should expect to have the same expression for Δj describing the motion of the resonance towards the center of oscillation. The stripping away of the outward orbits of the main wave should remain unaltered, and so should the upward shift of the main resonance when τ is positive. An oscillatory component in the phase shift of the equilibrium points in higher order resonances should also be present and its mathematical expression should be exactly the same as for first order resonances, since such a shift is a consequence of the upward displacement of the main wave resonance, and is independent of the particular "trapped" resonance under consideration. The only effect that can and will depend on the type of resonance under study is the value of the constant part of the phase shift, Φ_o. Phase plots such as the one in Figure 5.2.b show that Φ_o values have all the same order of magnitude, but they do not always have the same sign. A phase plot analysis also shows that the reflection properties of those higher order phase shifts are the same as for the first order ones, i.e, they change sign when the frequency offset of all interacting carriers, or the inhomogeneity, is multiplied by minus one.

5.7.2. External Resonances

Higher order external resonances also have phase shifts proportional to ϵ in the position of their equilibrium points. Those shifts, although all of the same order of magnitude, vary appreciably from one resonance to another and can even be zero as, for example, in the case of the 1/3 subharmonic. Such shifts are, nevertheless, irrelevant because they are readily swamped by the direct effect of the inhomogeneity on each resonance. An nth order resonance will have a phase shift of the order of unity, and will be subsequently wiped out, when under the influence of an inhomogeneity with a torque $\tau \approx \epsilon^{n-1}$. This is a very small value indeed, and if no appreciable growth is present, those resonances will exist only over a very short interaction region around the equator.

5.8. Conclusions

The inhomogeneity of the magnetic field of the earth has the following main effects on resonances:

1. For an external resonance, it opens up its outer closed phase orbits, destroying it completely if the associated torque is strong enough, and introduces shifts in the positions of its stable equilibrium points. The resultant shifts have the same sign as the applied torque and, even when locally constant in time, are translated at the end of the interaction region into radiation frequency shifts. Since the phase shifts are dependent on $v_\perp$, the frequency drifts will be accompanied by an increase in the radiated sideband linewidth. Because the external resonances

that give rise to sidebands are naturally narrower than the ones associated with main carriers, they will be able to exist only over a short length of the interaction region located around the equator without being completely destroyed.

2. For a "trapped" resonance it creates a shift in its angular position inside the main wave and moves its orbit towards the center of the main wave resonance. The shift towards the center is independent of the resonance under consideration, and contributes to extend the lifetime of the resonance by moving it away from orbits easily opened by the inhomogeneity. The phase shifts take values partly dependent on the resonance under consideration, show well defined parity properties under reflection of the perturbing carriers around the main carrier position, and change sign when the inhomogeneity does. Those shifts, as in the case of external resonances, will be translated into frequency shifts and line broadenings at the receiving end of the interaction region.

The difference in resistance to the inhomogeneity between internal and external resonances is one of the reasons why it is possible to have carriers too weak to be seen in a spectral display creating easily visible sidebands. Since their own resonances are external and narrow, the orbits are opened up, the resonance destroyed, and growth eliminated. The weak carrier is not seen. However, since they can create resonances inside the strong main carrier, and since those resonances are not easily affected by the inhomogeneity, bunching can occur, radiation will be produced, and the sidebands seen.

6. Summary and Recommendations

6.1. Summary of the Present Work

The work presents a theory for whistler sideband formation based on the solution of the equation of motion for an electron under the influence of a set of discrete whistler-mode waves. The results are obtained both analitically, and through computer analysis with the help of phase plots. No integration is necessary to obtain any of the major results. The analytical work consists of a series of coordinate transformations to explicitly exhibit the resonances which lead to the radiation of the sidebands, and the numerical analysis consists of the generation of phase plots. Phase plots in the $(\theta, \dot{\theta})$ plane can be thought of as the set of vectors tangent to the phase curves $\dot{\theta} = \dot{\theta}(\theta)$ [*Littlejohn*, 1978], and can be obtained directly from the equations of motion without integration. This does not mean, however, that the electron distributions are also obtained without integration: the results of this work do not include an exact prediction of the long time evolution of systems containing resonances. When that is attempted, qualitative arguments are used, and only partial results are obtained. The long time evolution of resonance systems is still an open problem and its solution, very likely, will require massive amounts of numerical computer processing.

The main conclusions of this work are the following:

1. Magnetospheric sidebands are due to the interaction of two or more waves propagating in the plasma. Radiation comes from cyclotron resonances in the electron motion produced by such an interaction.
2. "Single-frequency" sidebands come from the interaction of a single carrier, with PLR harmonics present in the duct.
3. Sideband wave frequencies are given by a simple formula:

$$\omega = \frac{\sum_{i=1}^{N} n_i \omega_i}{\sum_{i=1}^{N} n_i} \tag{3.34}$$

   Although the formula is simple, it is recurrent, allowing for the generation of extremely complex spectral structures.
4. Radiated sideband frequencies and linewidths, to a good approximation, do not depend on the $v_\perp$ distribution, only the amplitudes do. Integration over different pitch angles will not smear out the resonances and increase the radiation linewidth.
5. Sideband waves do not have constant frequencies, but shift and increase their linewidths when the interacting waves have time dependent amplitudes. Such shifts are a perturbative correction to the sideband frequencies, proportional to the degree of inhomogeneity of the magnetic field of the earth, and should not be confused with the larger shifts mentioned in 1.3.b.
6. Carrier amplitudes involved in sideband formation are not critical. In particular, it is not necessary that any of the carriers be strong enough to "trap" the electrons in the plasma. If, in a set of interacting carriers, some have large enough amplitudes (say, 30dB above noise level), the others can be vanishingly small (at least 40dB lower in amplitude) and still participate in the generation of sizable sidebands (comparable in size to the large carriers).

7. The electron interaction time with the electromagnetic waves is not associated with the sideband spectral frequencies. Such a parameter is ill defined and cannot be the source of sharp frequencies or time constants in a theory of wave-wave interactions.
8. A wave in the plasma creates forces that pull the electrons in towards the resonance velocity. The resultant distortion in the electron density, combined with a natural fall-off of the original distribution as a function of $v_{\parallel}$, can explain why sideband growth is frequently more pronounced on the upper frequency side of a carrier.
9. Suppression of a weak wave by a strong wave can be explained either by massive production of chaotic motion inside the weak carrier resonance, or by a complete elimination of the weak carrier resonance when it falls inside the strong carrier resonance.
10. A mechanism for amplitude saturation emerges naturally from the present work: a wave saturates when its resonance is made up of "trapped" resonances, radiating at frequencies different from the wave frequency, interspersed with electrons undergoing chaotic motion.
11. Despite its low amplitude, PLR can produce noticeable effects, either by creating "trapped" resonances that will not be destroyed by the inhomogeneity, or by acting as a "comb" to efficiently produce certain types of resonances, such as the frequency difference intermodulation resonance described in chapter 3.
12. Sophisticated mathematical techniques are indispensable to analyze the interactions in this work. Lie Transform Perturbation Theory is chosen because it is applicable to any Hamiltonian system, and has the additional following advantages: it does not use mixed variables, allowing the perturbation expansion to be extended to arbitrarily high orders; it does not generate secular terms or small denominators if a judicious choice of the associated generating function is made; it is based on a Poisson brackets series, and is canonical and invariant in form under any canonical change of coordinates. The study of radiation frequency shifts, where the inhomogeneity of the magnetic field of the earth plays a very important role, and the calculation of high order sidebands, could not possibly have been made without its help.

6.2. Recommendations for Future Work

This work was made to be extended. It establishes a groundwork founded on the equations of motion, and containing only the basic general ideas necessary for the description of sideband formation and wave-wave interactions in the magnetosphere. Based on this work, models should be built to describe specific aspects of phenomena to be analyzed. In building a model, care should be taken that it contains a faithful description of the physical system under study in all its essential points. Deviations from reality, due to required approximations, should occur only in its secondary aspects. No fundamental property of a system should ever be dependent on model approximations.

Although analytical extensions, such as a generalization to include non-ducted waves, can be made to the formalism presented in this dissertation, most of the future work will, very likely, consist of computer simulations in which the long-time self-consistent evolution of a system will be studied. They will almost certainly require a lot of computer time, since large bandwidth electromagnetic waves, interacting for long times with the magnetospheric plasma, will be present. The most obvious

choices for such studies would be:

1. External and "trapped" resonances should be tested for their ability to generate sidebands. Since $v_\perp$ does not affect the sideband frequencies in a first approximation, the electron population could have only one value of $v_\perp$, but should have a continuous distribution in $v_\parallel$ with an adequate width and gradient. A continuous electron flux should cross the interaction region for at least the time necessary for the resonances to undergo several oscillation periods. Electron trapping by the waves would not be required.
2. The saturation mechanism suggested by the present work should be tested by creating a wave configuration that will produce the required "trapped" resonances, together with chaotic electron motion. The mechanism will work if the electron distribution has only one value of $v_\perp$. It is important to test its validity for an electron distribution having a continuous and realistic distribution in $v_\perp$.
3. Sidebands produced by PLR should be computer simulated. It would be important to verify the formation of growing sidebands by PLR harmonics too low in amplitude to be directly observable. The importance of PLR harmonic coherence in the formation of certain types of resonances, such as the frequency difference intermodulation resonance, should be tested.
4. Suppression should also be tested. The easiest way to do it would be to put a weak carrier inside a strong carrier resonance and see that, since it cannot create a resonance of its own, its growth will not be appreciable.

PLR contamination is an unwanted phenomenon (as the word "contamination" indicates) that shows up frequently in wave-wave interactions, but always indirectly and in a subtle way. It generally manifests itself as an apparent natural time or frequency constant of the system. Since it is unwanted, and the connection with 60 Hz is hardly ever obvious, it is tempting to ignore it and try to explain the phenomenon as a "pure" magnetospheric effect. It is the author's opinion that the magnetospheric plasma has no well defined time constants in the millisecond range, and that any observed frequency difference of the order of tens of Hertz either comes from an external transmission or is due to PLR contamination, no matter what the phenomena displaying them look like on the surface. With this in mind, the following effects should be given a thorough investigation:

1. *Effect of PLR on triggered emissions.* A preliminary analysis made by the author indicates that triggered emission, as shown in the Siple data, is the last step of a process that starts with a sideband generating interaction between a carrier and PLR. If the sidebands grow sufficiently, their resonances overlap, creating chaotic electron motion. Such electrons are swept away from the wave by the inhomogeneity, creating the emission. It is possible that a PLR-free plasma will produce emissions, since wave growth is accompanied by a broadening that also generates electron chaotic motion, but the wave intensities required for such a process are expected to be higher than the ones found in the earth's magnetosphere.
2. *Effect of PLR on band limited impulses (BLI).* A preliminary observation of BLI's indicates that they are made up of broadened sidebands coming from the interaction between a transmitted carrier and PLR. When there are no other waves being transmitted in the same time and frequency interval, and triggered emissions produced by BLI's become entrained, the en-

trainment frequency is a possible sideband frequency (either from a carrier-PLR or a PLR-PLR interaction).

3. *Effect of PLR on suppression.* Supression effects, of the type observed in the CBVA experiment [*Helliwell*, 1986] and others, should be thoroughly analyzed, especially because they represent a tempting escape from the PLR issue. The amplitude minimum, frequently observed around 25 Hz, can be explained by PLR interactions, that at 23 Hz (the Golden Mean of 60 Hz) produce several overlapping resonances that eliminate wave growth and sideband production. The alternate explanation, that the minimum is a consequence of the overlap of the coherence bandwidths of each wave, does not seem consistent with known facts. Phase plot analyses show that the range of frequencies over which resonance overlap produces completely chaotic electron motion is approximately 10:1 [*Menyuk*, 1985]. If we assume that at 25 Hz the two carriers are separated by the carriers' trapping frequency, complete chaos will still be present at twice that separation (50 Hz). For smaller separations, chaos will be found even at one fifth of the trapping frequency (5 Hz). In other words, completely chaotic motion would be found over all frequency values of the CBVA experiment, little growth and sideband formation being possible. This is clearly not consistent with what is seen in the data.
4. *Effect of PLR on natural line formation.* Natural line formation effects pose a special problem because their line structures are not as clearly defined as the ones observed in controlled experiments. In the past, those lines were analyzed with fairly wideband filters (20 Hz), and PLR influence on them was looked for having in mind extremely simplified theories: natural lines, if created by PLR, would be nothing more than amplified PLR harmonics; if the line separations were not exactly 60 Hz or if the lines drifted, they could not be PLR related [*Paschal*, 1988]. The present work shows that in reality small line shifts should always be found in magnetospheric lines and that sideband formation is so complicated that frequently no direct evidence is found in them of the generating carrier frequency separations. Large line shifts, analyzed by tracking filters [*Paschal*, 1988], can be explained by variations in amplitude of two or more lines falling inside the same filter. The filter will be unable to separate them, indicating only the frequency drift of their weighted average. Amplitude variations can be explained by "weak" rising emissions of the type discussed by *Chang*, [1980], or by simpler variations in the electron density gradient.

As a last comment on methodology, it should be said that if a real scientific understanding of phenomena, such as the ones displayed in this work, is wanted, as much emphasis should be put on theoretical understanding as on data analysis. The unity and consistency of physics, present in all natural phenomena, is found only at an abstract level beyond the ones directly reachable by data analysis. A morphological and phenomenological analysis of the data does not make full use of the constraints imposed by those higher levels and runs the risk of either being inconsistent with the underlying physical reality, or of displaying a multiplicity of effects that exist only superficially, being in reality different manifestations of a same basic underlying process. Application of such ideas to research in the field would entail a complete reworking of all theoretical results obtained in the past, until they are either shown to be wrong or clearly consistent with the laws of physics.

7. References

Bell, T. F., and U. S. Inan, Transient nonlinear pitch angle scattering of energetic electrons by coherent VLF wave packets in the magnetosphere, *J. Geophys. Res., 86*, 9047, 1981.

Berry, M. V., Regular and irregular motion, in *Topics in Nonlinear Dynamics*, edited by S. Jorna, pp. 16-120, American Institute of Physics, New York, 1978.

Brinca, A. L., Whistler side-band growth due to nonlinear wave-particle interaction, *J. Geophys. Res., 77*, 3508, 1972.

Carlson, C. R., *Simulation and Modeling of Whistler Mode Wave Growth Through Cyclotron Resonance with Energetic Electrons in the Magnetosphere,* PhD Thesis, Stanford University, Stanford, CA, 1987.

Cary, J. R., Lie transform perturbation theory for Hamiltonian systems, *Phys. Rep., 79*, 129, 1981.

Chang, D. C. D., R. A. Helliwell, and T. F. Bell, Sideband mutual interactions in the magnetosphere, *J. Geophys. Res., 85*, 1703, 1980.

Chirikov, B. V., A universal instability of many-dimensional oscillator systems, *Phys. Rep., 52*, 263, 1979.

Das, A. C., A mechanism for VLF emissions, *J. Geophys. Res., 73*, 7457, 1968.

Dysthe, K. B., Some studies of triggered whistler emissions, *J. Geophys. Res., 76*, 6915, 1971.

Feynman, R. P., *The Feynman lectures on physics*, Addison-Wesley, Reading, Massachusetts, 1964.

Helliwell, R. A., and T. L. Crystal, A feedback model of cyclotron interaction between whistler-mode waves and energetic electrons in the magnetosphere, *J. Geophys. Res., 78*, 7357, 1973.

Helliwell, R. A., U. S. Inan, J. P. Katsufrakis, and D. L. Carpenter, Beat excitation of whistler mode sidebands using the Siple VLF transmitter, *J. Geophys. Res., 91*, 143, 1986.

Inan, U. S., T. F. Bell, and R. A. Helliwell, Nonlinear pitch angle scattering of energetic electrons by coherent VLF waves in the magnetosphere, *J. Geophys. Res., 83*, 3235, 1978.

Lichtenberg, A. J., and M. A. Lieberman, *Regular and stochastic motion*, Springer Verlag New York Inc., New York, 1983.

Littlejohn, R. G., *A pedestrian guide to Lie transforms: a new approach to perturbation theory in classical mechanics,* Lawrence Berkeley Laboratory, University of California, Berkeley, CA, 1978.

Menyuk, C. R., Particle motion in the field of a modulated wave, *Phys. Rev. A, 31*, 3282, 1985.

Nunn, D., The sideband instability of electrostatic waves in an inhomogeneous medium, *Planet. Space Sci., 21*, 67, 1973.

Nunn, D., A self-consistent theory of triggered VLF emissions, *Planet. Space Sci., 22*, 349, 1974.

Nunn, D., A nonlinear theory of sideband stability in ducted whistler mode waves, *Planet. Space Sci., 34*, 429, 1986.

Park, C. G., Generation of whistler mode sidebands in the magnetosphere, *J. Geophys. Res., 86*, 2286, 1981.

Paschal, E. W., *Phase measurements of very low frequency signals from the magnetosphere*, PhD Thesis, Stanford University, Stanford, CA, 1988.

Rasband, S. N., *Dynamics*, Wiley-Interscience, New York, 1983.

Sá, L. A. D., and R. A. Helliwell, Structure of VLF whistler mode sideband waves in the magnetosphere, *J. Geophys. Res., 93*, 1987, 1988.

Serra, F. M., VLF two-wave-electron interactions in the magnetosphere, *Planet. Space Sci., 32*, 985, 1984.

Smith, G. R., and N. R. Pereira, Phase-locked particle motion in a large-amplitude plasma wave, *Phys. Fluids, 21*, 2253, 1978.